Aus dem

Deutschen Herzzentrum Berlin

Klinik für Herz-, Thorax- und Gefäßchirurgie

Direktor: Prof. Dr. med. Volkmar Falk

Habilitationsschrift

Heart Valve Disease & Therapy – The Value of Translational Animal Models

zur Erlangung der Lehrbefähigung

für das Fach Experimentelle Herzchirurgie

vorgelegt dem Fakultätsrat der Medizinischen Fakultät Charité-

Universitätsmedizin Berlin

von

Dr.med.vet , Dr.sc.ETH Zürich Nikola Cesarovic

geboren in Belgrad, Serbien

Eingereicht: Januar 2022

Dekan: Prof. Dr. med. Axel R. Pries

1.Gutachter/in: Prof. Dr. Nikolaos Bonaros

2.Gutachter/in: Prof. Dr. Sabine Bleiziffer

Contents

Abbreviations

CVD	Cardiovascular Disease
VHD	Valvular Heart Disease
FEA	Finite Element Analysis
CFD	Computational Fluid Dynamics
FSI	Fluid–Structure Interaction
hiPSC	Human Induced Pluripotent Stem Cell
CT	Computer Tomography
MRI	Magnetic Resonance Imaging
TAVI/TAVR	Transcatheter Aortic Valve Interventions / Replacement
TMVR	Transcatheter Mitral Valve Replacement
4D MRI	Four Dimensional (3 space and 1 time dimension) Magnetic Resonance Imaging
LVEDV	Left Ventricular End Diastolic Volume
LVESV	Left Ventricular End Systolic Volume
TOE/TEE	Transesophageal echocardiography
AI	Aortic Valve Insufficiency
PVL	Paravalvular Leakage
RCC	Right Coronary Cusp of the Aortic Valve
NCC	Non Coronary Cusp of the Aortic Valve
EMD	Early Myocardial Damage
HFABP	Heart Fatty Acid Binding Protein
LVOT	Left Ventricular Outflow Tract

1. Introduction

1.1. Background

In late 2021, as the COVID-19 pandemic is still raging through the modern world, it is just so easy to forget about all other threats to human health. Threats like cardiovascular diseases (CVDs). The World Health Organisation (WHO) recently reported statistics showed that nearly 17.9 million deaths every year can be attributed to CVDs, along with the economic burden of billions of dollars spent on screening, diagnosis, and treatment related healthcare costs (1). Out of various CVDs, valvular heart disease (VHD), especially the one of the left ventricle, is one of the most prominent causes of cardiovascular morbidity and mortality worldwide (2-4). The aging population of the Western world is mostly affected by degenerative valve disease whereas in developing countries, rheumatic valve disease remains a public health problem affecting young adults (3, 5).

Cardiac health and normal function depend strongly on the functionality of all of its components, and vice versa. Hence, it would be wrong to observe cardiac valves as structures isolated in their morphology and function. Their anatomical position within the cardiac anatomy, their morphology as well as their cellular and sub-cellular structure are closely related to the fluid-dynamic characteristics of their surroundings. The normally developed human heart has four valves. All four valves are positioned in one plane, the so-called 'base of the heart', and are surrounded by a dense fibrinous tissue also known as the cardiac skeleton. The mitral and the tricuspid valve, also called atrioventricular valves, separate the left and the right atrium from their corresponding ventricles, whereas the aortic and the pulmonary valve lay between the left and the right ventricle and their respective large arteries.

1.1.1 Valvular Structure

Despite their unassuming appearance, cardiac valves represent highly complex tissue systems. This is particularly true for atrioventricular valves. The atrioventricular valves have three leaflets on the right side of the heart (tricuspid valve) and two leaflets on the left side (mitral valve). At its base, each leaflet is connected to its corresponding portion of the cardiac skeleton, ie. the valvular annulus. The annulus represents a connective tissue ring surrounding the valves perimeter. It is much more pronounced in the mitral than in the tricuspid valve, where it is dominated by fibrous and elastic collagen fibers (6). This fibrous 'skeleton' is fixed to the myocardium in a similar way as tendons are

attached to muscles and provides anchoring and hinge point for the valvular leaflets. On the other hand, at their free edge and along the ventricular side, the leaflets are connected to the papillary muscles in the corresponding ventricle via connective tissue cords called chordae tendineae. The chordae tendineae and papillary muscles prevent prolapse of the valves into the atria during cardiac contraction as the pressure inside the ventricles rises far above the one of its corresponding atrium. On the other hand, the aortic and pulmonary valves, also known as pocket valves due to their pocket-like appearance, consist of three crescent-shaped leaflets that are circumferentially attached to their corresponding valve annulus. It is important to note that in human aortic valves, the non-coronary cusp has the largest surface diameter and surface area, whereas in porcine aortic valves, the right-coronary cusp is the largest and the non-coronary cusp is the smallest. As a result, in humans, the central point of coaptation is skewed toward the left-coronary cusp, while in porcine valves, it tilts toward the non-coronary cusp.

Macroscopic appearance, as well as the microscopic structure of the four cardiac valves and their leaflets differ significantly from one another due to the different flow requirements and pressure gradients present at their place of action.

The two atrioventricular valves are similar in structure as the leaflets exhibit a typical four-layered arrangement: The atrialis, the uppermost layer facing the atrium, is covered by the endocardium's single-layered endothelium and consists of aligned elastic and collagen fibers. The adjacent lamina spongiosa consists mainly of extracellular matrix, proteoglycans and elastic fibers. Beneath the lamina spongiosa lies the lamina fibrosa, which bears most of the pressure of the ventricles. The layer closest to the ventricle, the ventricularis, is similar in structure to the atrialis and is also covered by endothelium (7). On the other hand, the aortic and pulmonary valves are connected to the anulus similarly to the leaflets of the atrioventricular valves and are both enclosed in single-layered endothelium. They exhibit comparable layering to the atrioventricular valves, namely a lamina ventricularis that faces the ventricle, a lamina radialis, the lamina spongiosa, lamina fibrosa and a lamina arterialis that faces the subsequent artery (6).

Within these layers, the connective tissue fibers display distinct arrangement and are mechanically coupled to each other. It has been suggested that this microarchitecture supports the transfer of force from the leaflets to the annulus when the valve is under pressure and helps maintain the leaflet geometry when external force is released (8). Despite the high structural similarity between porcine and human valves, studies have shown that aortic valve leaflets from aged humans are significantly less compliant than their porcine counterparts in bi-axial strain testing.

Another crucial component of cardiac valves, and in fact, the driver of many changes, is the cells residing within the three layers. The most notable cell population among them is the valvular endothelial (VECs) and interstitial cells (VICs). VICs are the dynamic, living components of heart valves

responsible for synthesizing the valve matrix and maintaining its composition. This, in turn, determines the valve's structural and mechanical properties as well as its functional abilities. A recent comparative analysis of human and porcine valvular endothelial and interstitial cells revealed that the cell types are quite comparable between the species, although there is slightly more pronounced cellular heterogeneity in VECs of porcine origin.

1.1.2 Determinants of valvular function and disease

The function of the cardiac valves is fairly simple but of great importance. They need to ensure that the blood flow propagated by cardiac contractions is unidirectional. As the atrioventricular valves (mitral and tricuspid) separate the atria from the ventricles, they need to open during diastole, allowing the blood accumulated in the atrias to fill the ventricles. During systole, they need to close the atrioventricular orifice, in order for the blood to be ejected into the systemic circulation. On the other hand, aortic and pulmonary valves are open during systole as blood travels from the ventricles to the corresponding large arteries and are closed during diastole to prevent already ejected blood flowing back into the ventricles. Besides providing the barrier for the back-flow, healthy heart valves should provide little resistance to the blood flowing in correct direction (9).

Disease-induced pathologic changes of the valvular tissue lead to either stenosis or regurgitation. Stenotic valves have restricted valve opening and provide large resistance to the forward flowing blood. On the other hand, regurgitant valves allow blood to flow back across the closed valve into the preceding chamber. Moreover, under certain conditions a particular valve can be stenotic and regurgitant at the same time. Regardless if stenotic or regurgitant, a heart bearing a diseased valve needs to apply more work to maintain the cardiac output necessary for the body to function normally.

Cardiac valve competence depends not only on proper function of its leaflets but also on supporting structures like annuli, chordae tendinae or papillary muscles, as well as the greater anatomical surrounding such as ventricular or aortic root geometry. Usually, abnormality in one of the component structures will induce further changes in other parts, perpetuating the disease further. If left untreated, in the vast majority of patients such a downwards spiral inevitably leads to heart failure with fatal consequences for the affected patients (10).

1.1.3 Therapy options

For patients suffering from heart valve disease, there are several treatment options (9, 10). Medical therapy with blood pressure lowering and heart rate controlling drugs, focusses on protecting the cardiac muscle from the secondary damage caused by the diseased valve, but does not address the root-cause of the disease. If the disease is recognized prior to development of explicit symptoms, a conservative therapeutic approach is often applied, comprising medical therapy and regular controls. On the other hand, in patients displaying clear symptoms, surgical or transcatheter

intervention is the only therapeutic approach targeting valvular function restauration. Cardiac surgeons successfully replaced the valve in the year 1952 for the first time (11). However, it was only in the 1960s and 70s that surgical valve replacement became the therapy of choice for the diseased valves (11). Nowadays, there is a whole spectrum of surgical and interventional techniques and implants to treat many different aspects of valvular disease complex. The most notable development in recent years was the introduction of self-anchoring valvular implants that are delivered via a minimally invasive (i.e. transcatheter) approach to the permanent residing place (12). Such methods do not rely on opening the chest nor placing the patient on external circulation (cardio-pulmonary bypass), hence enabling quicker recovery, less complications and increased patient comfort. Most importantly, transcatheter valve therapies can be safely performed in patients having high or even prohibitive surgical risk, having no other treatment possibility (12).

1.2 Heart valve models to study disease and develop new therapies

In order to better understand these thin tissue structures that are expected to flawlessly open and close 25 million times each year over the whole human lifetime, clinicians and scientists have been observing patients and healthy volunteers in numerous clinical trials for more than 70 years (10). However, ethical concerns, numbers of samples obtainable, therapy options applicable, patient comfort and compliance, as well as other obvious limitations in use of human subjects for scientific purposes, quickly prompted the need for models mimicking human valvular function and disease. At the present time, such models come in a large variety of shape and forms. Computational models can provide valuable information regarding material selection and implant behavior under conditions simulating target patient populations (13). Bench-top flow models and artificial heart simulators play an important role in the development process of novel valvular therapies as well as in education and training of medical practitioners (14). On the other hand, complex interactions and interplay between development, flow, function and immunology is best addressed in biological models such as cellular / microtissue assays or animal experiments.

Nevertheless, all in-silico, in-vitro and in-vivo models, regardless of their level of sophistication, are imperfect replicas of the human cardiovascular system and are burdened by their intrinsic flaws. However, the use of such models allowed researchers to understand molecular pathways and hemodynamic influences that lie in the root cause of the disease as well as to develop and test therapeutic strategies at the speed, precision and cost otherwise unattainable.

1.3 Small Animal Models of Valvular Disease

Small animal models such as amphibians or rodents represent the backbone of basic research, especially regarding molecular pathways and genetic contribution to the disease emergence and progression. This holds truth for investigation of mechanisms of valvular disease as well. In recent years much progress in understanding cardiac valve morphogenesis and development has been achieved by studying 2 chambered hearts of an amazing creature – the zebrafish (Danio rerio) (15).

Due to its small size (3-5 cm), high fertility and transparency of the embryo during its rapid development, the zebrafish was selected as one of the most promising model organisms for cardiovascular research (16). Non-invasive imaging can follow the entire phase of embryonic development while the embryo is kept in a petri dish, which allows cell biology to be performed in an intact organism (17). Studies of genetic mutations performed on zebrafish embryos have been instrumental in understanding the underlying genetic networks governing cardiac development. Such studies led to the identification of UDP-glucose dehydrogenase as well as the VEGF and WNT signaling pathways as crucial contributors in the development of heart valves in zebrafish as well as in humans (16).

Owing to the transparency of their externally developing embryos, high-resolution live imaging of intracardiac flow provided insight into necessity of proper trans-valvular and intra-ventricular flow dynamics for valve development (15, 18). Further, in contrast to most other vertebrates, zebrafish has large capacity of cardiac and valvular regeneration, rendering it one of the most interesting models for leaflet tissue remodeling (19). The use of decellularized tissue matrix as valve replacement material is a highly promising therapeutic development. However, in most translational in-vivo models (ie. large animals), the process of recellularization is slow and incomplete, hindering the translation of this technology into the clinic. However, by looking at the valve regeneration process naturally occurring in zebrafish, researchers were able to better understand the framework conditions necessary for long-term success of matrix valve replacement therapies in humans (19).

Thus, as an affordable and easy-to-use in vivo model, the zebrafish will continue to be used in cardiovascular research, especially in assessing the candidate gene for potential cardiac effect. However, the use of zebrafish as a translational model has its short comings. Its heart has only one atrium and one ventricle, it is much smaller and more simply constructed than the mammalian heart.

Corresponding valvular structures, although fully functional, are dealing with peek pressures around 3 mmHg, which is far less than the ones in the human heart (20).

Hence, despite sharing large blocks of chromosomal synteny with humans (70% of human genes has zebrafish orthologues), anatomy and function of teleost fish valves makes translation of research results still somewhat challenging (21).

On the other hand, heart valves of rodents and humans demonstrate great similarities during cardiac embryologic development as well as anatomical arrangement in adults (22). With mean aortic pressure of 100 mmHg, right atrial pressure between -2 and 8 mmHg and coronary perfusion pressure of approximately, not only cardiac anatomy but also cardiac physiology displays great similarities between mice and humans (23).

However, there are also some notable differences. For instance, the human heart weighs about 250–300 g and beats, on average, 60–70 times per minute. In contrast, the mouse heart weighs only about 0.2 g, and has a heartbeat of around 500–600 times per minute. Another striking difference is the overall ellipsoidal shape of the murine heart. Also, relatively large atria of the human heart are not so prominent features in mice (24). Furthermore, it is interesting to note that some of the developmental events that in the human are completed at birth are still in progress in the neonatal mouse (24).

On the other hand, the differences in valvular morphology and structure between mouse and man are quite subtle. Whereas the atrioventricular valves have the same basic layout, the chordae tendineae and the papillary muscles in mice are less numerous and less pronounced than in humans (24).

Because of the increasing availability of tools for genetic manipulation, the mouse is becoming the most popular animal model for studying normal and abnormal cardiac development as well as genetic contribution to cardiac disease. Bearing in mind that almost 99% of human genes have direct murine orthologs and due to their quick breeding rate, studies in mutant mice are uniquely positioned to produce rapid but translationally relevant results. Single-gene knockout mice, displaying precisely targeted loss of single gene function, have uncovered complex relationships in signaling pathways, such as VEGF, NFAT or Notch, necessary for proper development and function of cardiac valves (25).

Furthermore, genetically modified mouse strains have played an important role in exploration of chrondromodulin-I controlled leaflet angiogenesis, an important propagator of valvular disease, as well as in pointing to the first risk loci [tensin 1 (TNS1) and LIM and cysteine rich domains 1 (LMCD1)]

responsible for non-syndromic mitral valve prolapse (26, 27). Several mouse models of valvular disease have been described, however they all rely on either genetic deficits (hence model congenital disease) or display their phenotype in senile animals (28, 29). Although portraying well the target patient population, the use of such models turns animal trials into lengthy and costly endeavors, as the animals carrying specific gene modification often need to be created or bred in complex breeding systems. However, the recently established mouse model of rapidly developing inflammation/injury-induced calcific aortic valve stenosis could find broader acceptance in years to come (30).

Furthermore, the ability to precisely control the rodent immune system either by genetic manipulation or specific treatments made rodents a valuable tool for assessing tissue engineered valvular implants and graft materials. Although technically challenging, stented valve prosthesis have successfully been tested in rats (31).

Still, due to their small size and rapid cardiac action and metabolism, the use of human grade imaging and interventional technology is severely limited in rodents. Valvular implants can usually be implanted only in pulmonary valve position or as a heterotopic implant in the abdominal aorta (31). Researchers are forced to rely on specialized equipment (like high temporal resolution (40 MHz probes) echocardiography and MRI) or to develop unorthodox surgical techniques (like heterotopic heart transplantation with pulmonary valve matrix implant) to test valvular therapies (32, 33).

1.4 Translational Large Animal Models of Valvular Disease

To support knowledge transfer from researchers laboring away on bench-tops or animal experimentation units, to clinicians daily battling for lives of patients struck down by valvular disease, animal models should fulfill several criteria such as human-like anatomy and physiology, similar hemo-(fluid-) dynamic characteristics and good availability.

Fortunately, the structure of mammalian hearts is grossly invariant between the species. Nevertheless, the fact that heart dimensions closely correlate to the body size, puts large animals such as sheep and pigs on the center stage in translational model line-up (34). During the past decades, porcine models have found increasing interest in cardiovascular research.

As a large, omnivorous, diurnal animal, the pig closely resembles humans in many features of its anatomy, physiology, immunology, and even lifestyle, providing good basis for modeling valvular disease and testing novel therapies (35). The range of swine breeds used for research purposes can be

grossly subdivided into 2 categories: farm pigs (the most common breeds being the Yorkshire, Landrace, and Duroc as well as their crosses) and minipigs (such as Yucatan, Hanford, Göttingen, and Sinclair). One of the major advantages of minipigs over farm breeds is that for the same body weight, minipigs are more mature and do not experience intense growth as their farm breed relatives. Hence, minipigs are often used in studies requiring long follow-up times.

However, their smaller size makes them often challenging when testing of human-grade implants is intended. On the other hand, cardiac dimensions of farm pigs correlate well with such of adult humans. It is well known that the heart weight of juvenile (30 kg) farm pigs with 5 gr/kg body weight corresponds quite well to that of humans (36).

Despite some differences like slight skew of the coaptation central point towards the non-coronary cusp due to the larger right coronary and smaller non-coronary leaflet, porcine valves have been used as allografts for aortic valve replacement for decades (37, 38).

Then again, translational large animal models are not only useful as tissue donors or subjects of scientific studies. They also play a major role in teaching and training novel surgical procedures. The vast majority (more than 70%) of animals used for surgical training are porcine, as their size anatomy and physiology sufficiently resemble humans in surgically relevant aspects (39). This is especially true in the field of fast emerging novel transcatheter valvular repair and replacement interventions, where beside in-silico simulators work with large animal models represents the only possibility for the physicians to learn and practice.

Moreover, heavily reliant on pre- and intra-operative imaging for patient selection and procedural guidance, transcatheter valve procedures need to be developed and trained in models that allow the use of clinical grade imaging protocols and equipment. With some adaptations such protocols can be successfully applied in large animals like pigs or sheep (40). Moreover, sheep and pigs are still generally perceived as farm animals and producers of commodities such as meat, milk and wool. In the eyes of the wide public, this places them relatively low on the emotional value scale, which makes their use in research more socially acceptable than use of dogs or non-human primates (41). Although not best suited to study molecular mechanisms of disease, large animal models allow the use of clinical grade diagnostic equipment and therapeutic protocols hence enabling the researchers and clinicians to narrow down the translation gap.

1.5 Animal-free heart valve research

In-Silico and Computational Models

From the engineering perspective, heart valves are thin tissue structures that passively control blood flow and ensure forward cardiac output. Their action and performance is powered by pressure differences created by the heart's own contractions on one side and vascular resistance and compliance on the other. However, these thin pieces of tissue are highly complex biophysical systems, operating in a mechanically highly demanding environment (13). Recently, cardiovascular research has shown significant involvement in simulating cardiac behavior through in-silico and computational models (42). Raiding on favorable trend of rapid progress in computing power and technology, computational modeling and simulations like finite element analysis (FEA), computational fluid dynamics (CFD), and fluid–structure interaction (FSI) have become very effective tools for the engineering analysis of heart valve function in health and disease (13, 43). These technologies have found significant use in the studies of prosthetic valves, as they pose a relatively simple structure and are readily amenable to modeling (44, 45). Recently, another highly significant field of computer modeling application emerged, in support of tissue engineering and remodeling prediction (46, 47). Although coming in big strides, computational models are still not readily deployed in studying patient-specific fluid- and bio- mechanical questions. An immensely challenging task for the technology to match.

Cells, Cultures and Organoids

Innumerous cardiac conditions could trace their roots to changes at the cellular level. Hence, doubtlessly, narrow and specific scientific questions like expression of a particular gene or effects of a certain mechanical stimuli can be examined in-vitro using cell cultures (48). By using immortalized human cell-lines, problems of cross-species translation can be circumvented. Techniques of human-induced pluripotent stem cell (hiPSC) have enabled researchers to even conduct in-vitro studies with patient specific read-out. This astounding feat is made possible because hiPSC cells retain the genotype of the patient from whom they were derived (49). However, all of the above-mentioned experimental set-ups rely on 2-dimensional cell cultures, depriving the test object, namely cells, of their physiologic environment. In order to counter this key disadvantage, major efforts have been put to developments of 3D cell cultures containing most of the different cells types that could be found in the target organ. Strategy of bioengineering tissue-like constructs opened the door to engineering hiPSCs-based cardiac organoids on-a-chip, a promising approach for modeling human (or even patient specific) heart in vitro (50).

1.6. Goals of the current work

The following work intends to demonstrate the value of large animal models in translational research for understanding of heart valve disease and development novel of transcatheter therapeutic devices and concepts. First, this work evaluates the anatomical and fluid-dynamic properties of the porcine heart and its suitability to mimic the human heart. Next, aspects important to intra-procedural guidance will be elaborated. Finally, exemplary porcine models of mitral, tricuspid and aortic valve disease and interventions will be presented.

More specific, the following questions are addressed:

a) Is there a correlation between body weight and cardiac dimensions relevant for valvular interventions, and what weight group best represents adult patients suffering from heart valve disease?
b) Are blood flow patterns and fluid dynamic characteristics of porcine left ventricle in rest and during simulated exercise (domutamine stress) comparable to human?
c) How should intra-procedural echo guidance best be performed in porcine models for valvular interventions?
d) Porcine Model for Mitral Interventions: How could anatomic constrains of porcine models for mitral valve interventions be ameliorated?
e) Porcine Model of Tricuspid Disease: Is thoracic injury induced tricuspid regurgitation a reliable model?
f) Porcine Model of Aortic Regurgitation / Aortic Paravalvular Leakage: Reliability, Reproducibility and Fluid-dynamic Effect

2. Original contributions

2.1. Computed Tomography-based evaluation of porcine cardiac dimensions to assist in pre-study planning and optimized model selection for pre-clinical research

Lipiski M, Eberhard M, Fleischmann T, Halvachizadeh S, Kolb B, Maisano F, Sauer M, Falk V, Emmert MY, Alkadhi H, Cesarovic N. Computed Tomography-based evaluation of porcine cardiac dimensions to assist in pre-study planning and optimized model selection for pre-clinical research. Sci Rep. 2020 Apr 7;10(1):6020. doi: 10.1038/s41598-020-63044-1. PMID: 32265478; PMCID: PMC7138799.

At the turn of the millennium major progress has been achieved in development and quick clinical adoption of minimally invasive techniques such as trans-catheter valve therapies, driven by the need and expertise of cardiologists and cardiac surgeons (51). Now, 20 years later, such approaches have been fully integrated into the therapeutic portfolio for managing high risk patients suffering from cardio-vascular disease, thus leading to a high demand for development on novel trans-catheter implants and delivery systems (52). In the development process, translational large animal (pre-clinical) studies act as the last safety and efficacy 'filter' before such devices enter clinical trials (53). Amongst the plethora of animal models, domestic pig (Sus Scrofa Domestica) is a widely accepted and used species in preclinical evaluation of transcatheter cardiac implants (54). Similar to clinical practice, patient-prosthesis matching plays an immensely important role in preclinical testing. However, unlike in the human patient, where an implant of particular size and design is chosen to suite best the patient's annular size and geometry, in preclinical research a suitable animal is generally selected based on body weight for one particular valve size available for testing. Thus, the suitable animal must be large enough to accommodate human-grade devices, with the determining factors being the size of the target cardiac structure, as well as the diameter of the peripheral vessels used for vascular access (55). There are multiple studies describing correlation between body surface area and normal aortic and pulmonary valve diameter in humans. However, correlations of valvular size with easily measurable parameters and largely missing in pigs. Therefore, in this study, cardiac CT images of commercial farm pigs of the same breed but with different body weights were used to perform morphometric analyses of porcine cardiac structures. Twenty-four domestic pigs (Swiss large white, intact females and castrated males) that had undergone pre-operative cardiac CT for a variety of different projects approved by the local Committee for Experimental Animal Research (Cantonal Veterinary Office Zurich, Switzerland) under the License numbers 152/2013, 219/2016 and 138/2017 were included into this study. Animals were divided into the following weight groups: 50–60 kg (n = 8), 80–90 kg (n = 8), 100–110 (n = 8). Animal housing and all experimental procedures were in accordance

with Swiss animal welfare protection law and conform to European Directive 2010/63/EU of the European Parliament and the Council on the Protection of Animals used for Scientific Purposes, and to the Guide for the Care and Use of Laboratory Animals (56). Following CT acquisition under general anesthesia with a third-generation 192-slice dual-source CT machine, the data were reconstructed using a slice thickness of 0.6 mm and increment of 0.4 mm. Measurements were then performed using clinical grade 3mensio structural heart software. Relevant for TAVI procedures, a strong correlation was found between body weight and aortic valve diameter ($r = 0.83$, $p < 0.0001$) going from 23.5mm in 50-60kg group to 29.8mm in 100-110 kg group, as well as between body weight and length of the ascending aorta ($r = 0.72$, $p < 0.0001$) ranging from 38.9 mm in 50-60kg group to 49 mm in 100-110 kg group with intermedial weight group being in between in both cases. Surprisingly, the data revealed the left coronary ostia to be markedly lower in pigs than in humans (5.75 ± 1.33 mm vs. 13.4 ± 2.1 mm), but no increase of coronary ostia height could be found with advanced body weight (and age) of the animals. Similarly, mitro-aortic angle was constant in all study groups and averaged 120°. Relevant for TMVR procedures, left atrial height as well as T-T, S-L, C-C distances and mitral valve area in pigs has shown to be well correlating with pig's body weight being the greatest in 110kg animals with a height of 39.5mm, T-T of 33.6 mm, C-C 41.1 mm, S-L 33.8mm and mitral valve area of 1166 mm^2. These values, but especially the height of the left atrium is generally considered lower than in patients suffering from mitral regurgitation. Relevant for pulmonary valve / trunk procedures, a strong correlation was found between body weight and length of the pulmonary artery to bifurcation ($r = 0.81$, $p < 0.0001$) being longest in 100-110 kg group with 66.4 mm. Correlations between body weight and pulmonary artery diameter ($r = 0.55$, $p = 0.0059$), pulmonary valve diameter ($r = 0.61$, $p = 0.0019$), and pulmonary valve area ($r = 0.56$, $p = 0.0054$) were moderate, with maximal values of 26.9mm, 30.9 mm and 751 mm^2 in the heaviest animals respectively. Analysis of the tricuspid valve has been challenging as its perceived dimensions greatly depend on the contrast application route, hydration status, ventilation and the position of the animal in the CT scanner. However, it could be demonstrated that diameter of the tricuspid valve ranged between 41mm for the lightest and 49mm for the heaviest animals. In summary, valvular diameters and area sizes moderately to strongly correlate with pig's body weight of this particular swine breed and possibly of swine breeds with similar growth curve patterns. Hence certain weight-based animal selection could be made, however pre- procedural imaging for planning purposes is still highly advisable, as precise animal-prosthesis matching is crucial not only for successful implantation but also for ethical reasons.

SCIENTIFIC REPORTS
nature research

OPEN

Computed Tomography-based evaluation of porcine cardiac dimensions to assist in pre-study planning and optimized model selection for pre-clinical research

Miriam Lipiski[1*], Matthias Eberhard[2], Thea Fleischmann[1], Sascha Halvachizadeh[3], Beate Kolb[2], Francesco Maisano[4], Mareike Sauer[1], Volkmar Falk[5,6,7], Maximilian Y. Emmert[5,6], Hatem Alkadhi[2] & Nikola Cesarovic[1,7]

The pig (*Sus Scrofa Domestica*) is an accepted model for preclinical evaluation of prosthetic heart valves and trans-catheter implantation techniques. Understanding porcine cardiac dimensions through three-dimensional computed tomography (CT), increases preclinical study success, leading to higher cost efficiency and to the observance of the obligation to the 3 R principles. Cardiac CT images of twenty-four Swiss large white pigs were segmented; aortic root, mitral valve, pulmonary trunk, tricuspid valve, as well as the aorto-mitral angle and left atrial height were analyzed. Correlation coefficient (r) was calculated in relation to body weight. In Swiss large white pigs, valvular dimensions, length of the pulmonary artery and ascending aorta as well as left atrial height correlate with body weight. Coronary ostia heights and aorto-mitral angle size can be neglected in animal size selection; no changes were found for either of the two parameters with increasing body weight.

Driven by advancing technologies and skills, cardiology and cardiac surgery had been one of the medical fields quick to embrace minimally invasive techniques such as trans-catheter valve therapies in the early 2000s[1,2]. Minimally invasive techniques are generally accompanied by an improved patient satisfaction, a higher return to normality, a lesser requirement for post-rehabilitation services, and a marked reduction of costs[3]. Trans-catheter approaches have now been fully integrated into the therapeutic portfolio for managing patients suffering from cardiac disease with a risk too high for conventional surgery[4], thus, leading to a high demand in development of new trans-catheter devices and new types of delivery systems[5].

The use of large animal models in pre-clinical studies plays an important role in the initial evaluation of efficacy and safety of new medical devices before their use in human clinical trials[6–8]. The domestic pig (*Sus Scrofa Domestica*) is a widely accepted animal model of cardiovascular research and in particular for the preclinical evaluation of prosthetic heart valves and trans-catheter implantation techniques[9]. However, trans-catheter valve implantations in pigs, are often associated with the same complications as seen in humans, namely post-implantation para-valvular regurgitation, coronary occlusion and rupture of the aortic root or annulus due to oversizing of the valve[10,11]. Furthermore, left atrial volume and dimensions can be smaller in pigs for equivalent annulus size seen in humans[12], therefore high profile valves in pigs may lead to obstruction or reduction of the pulmonary vein inflow and in case of touching the left atrial roof causing complications such as tissue erosion or cardiac arrhythmias[13]. High profile valves may also cause obstruction of the left ventricular outflow tract due to the geometric relationship between the aortic and the mitral valve[13]. Pre-procedural planning with modern

[1]Division of Surgical Research, University Hospital Zurich, University of Zurich, Zurich, Switzerland. [2]Institute for Diagnostic and Interventional Radiology, University Hospital Zurich, Zurich, Switzerland. [3]Department of Trauma, University Hospital Zurich, Zurich, Switzerland. [4]Department of Cardiac Surgery, University Heart Center Zurich, Zurich, Switzerland. [5]Department of Cardiovascular Surgery, Charité Universitätsmedizin Berlin, Berlin, Germany. [6]Department of Cardiothoracic and Vascular Surgery, German Heart Institute Berlin, Berlin, Germany. [7]Department of Health Sciences and Technology, ETH Zurich, Zurich, Switzerland. *email: Miriam.Lipiski@usz.ch

imaging modalities such as trans-esophageal echocardiography and three-dimensional computed tomography (CT) have shown to lead to a better understanding of annular sizing and geometry and a reduction of these complications and have therefore become an integral part in the clinical assessment of patients[10,14–16].

Unlike in the human patient, where the valve is chosen based on the patient's annular size and geometry, in preclinical research a suitable animal is generally selected based on body weight for one particular valve size available for testing. Thus, the suitable animal must be large enough to accommodate human-grade devices, with the determining factors being the size of the target cardiac structure, as well as the diameter of the peripheral vessels used for vascular access[17].

Studies in humans described a strong correlation between body surface area to normal aortic and pulmonary valve diameter. Other strong predictors of valve diameter include the patient's age and body height[18]. Body weight and Body Mass Index (BMI) on the other hand are rather poor indicators of valve size in humans[18]. As for the pig, Allan *et al*. could also find a positive correlation between the body length and the aortic annulus and root diameter in the miniature swine[19]. Although miniature swine have become increasingly popular in research, the purchase price is markedly higher than for commercially raised farm breeds, which makes the latter more popular for acute and short term studies[20]. Additionally, most of miniature swine breeds will not reach the heart and blood vessel size which most closely approximates that of humans, precluding them from testing human-size implants[21].

Implementing CT as an integral part of animal selection would be ideal however, although non-invasive imaging procedures are of low severity grade based on the severity classification of the EU Directive 2010/63[22], they do require adequate sedation or general anesthesia and therefore an additional authorization from the competent authorities.

Therefore, in this study, cardiac CT images of commercial farm pigs of the same breed but with different body weights were used to perform morphometric analyses of porcine cardiac structures. The goal was to assess correlation between the pig's body weight and the (intra) cardiac dimensions with the ultimate goal to allow for an accurate prediction of which animal would be the best weight-matched to test a particular size of cardiac implant. Thus, leading to an improved animal selection and enhanced preclinical study success.

Methods

Animal Study. Twenty-four domestic pigs (Swiss large white, intact females and castrated males) that had undergone pre-operative cardiac CT for a variety of different projects approved by the local Committee for Experimental Animal Research (Cantonal Veterinary Office Zurich, Switzerland) under the License numbers 152/2013, 219/2016 and 138/2017 were included into this study. Animal housing and all experimental procedures were in accordance with Swiss animal welfare protection law, and conform to European Directive 2010/63/EU of the European Parliament and the Council on the Protection of Animals used for Scientific Purposes, and to the Guide for the Care and Use of Laboratory Animals[23].

Images were selected randomly and animals assigned to one of the following weight groups: 50–60 kg (n = 8), 80–90 kg (n = 8), 100–110 (n = 8).

Animal Preparation. All pigs were sedated with an intramuscular injection of ketamine (Ketasol®-100 ad us.vet.; Dr. E. Graeub AG, Berne, Switzerland; 15 mg/kg body weight), azaperone (Stresnil® ad us.vet.; Elanco Tiergesundheit AG, Basel, Switzerland; 2 mg/kg body weight) and atropine (Atropinsulfat KA vet 0.1%; Kantonsapotheke, Switzerland; 0.05 mg/kg body weight). Anesthesia was induced by an intravenous administration of propofol (Propofol ®- Lipuro 1%, B. Braun Medical AG; Sempach, Switzerland; 1-2 mg/kg body weight) to achieve relaxation and swallow-reflex diminishment sufficient for intubation. Anesthesia was maintained during the duration of the study with propofol (5-10 mg/kg/h). For pain medication buprenorphine (Temgesic®; Indivior Schweiz AG, Baar, Switzerland; 0.01 mg/kg) was administered.

Animals were equipped with a 5 F sheath (Cordis AVANTI® + Introducer; Cardinal Health, USA) in the femoral vein or an 18 G auricular vein catheter (B. Braun Medical AG; Sempach, Switzerland) for contrast agent injection.

CT imaging protocol and data reconstruction. Animals were scanned under general anesthesia with a third-generation 192-slice dual-source CT machine (SOMATOM Definition Flash, Siemens Healthineers, Forchheim, Germany). The data acquisition was synchronized with the electrocardiogram (ECG) of the animals using retrospective ECG-gating and using the following scan parameters: detector collimation $2 \times 0.6 \times 96$, slice acquisition $2 \times 0.6 \times 192$ by means of a z-flying focal spot, gantry rotation time 0.25 s, tube current–time product 380 mAs/rotation, and tube voltage 120 kVp. A total of 0.5–1 ml/kg BW iodinated contrast media (iopromide, Ultravist 370, Bayer Healthcare, Berlin, Germany) was administered intravenously at a flow-rate of 5 ml/s followed by 30 ml of saline chaser at a flow-rate of 3.5 ml/s.. Bolus tracking was performed in the ascending aorta. The contrast-enhanced CT scan was initiated after an attenuation threshold of 120 Hounsfield units [HU] at 100 kV was reached. Mean attenuation of the ascending aorta, left ventricle and right ventricle was 375 ± 130 HU, 368 ± 124 HU, and 367 ± 156 HU, respectively.

All CT data was reconstructed using a slice thickness of 0.6 mm and increment of 0.4 mm using advanced modeled iterative reconstructions (ADMIRE) at a strength level of 4. The reconstruction field-of-view (FoV) was set to 200 mm with a pixel matrix of 512×512. Images were reconstructed in 10% steps of the RR-interval.

Data Analysis. All measurements were performed using 3mensio structural heart software Version 9.1 (3mensio Medical Imaging BV; Bilthoven; the Netherlands) (Figs. 1 and 2).

Aortic Root. Aortic root measurements were performed in diastole, following manual segmentation of the ascending aorta. The following measurements were acquired: diameter by area derived and perimeter derived

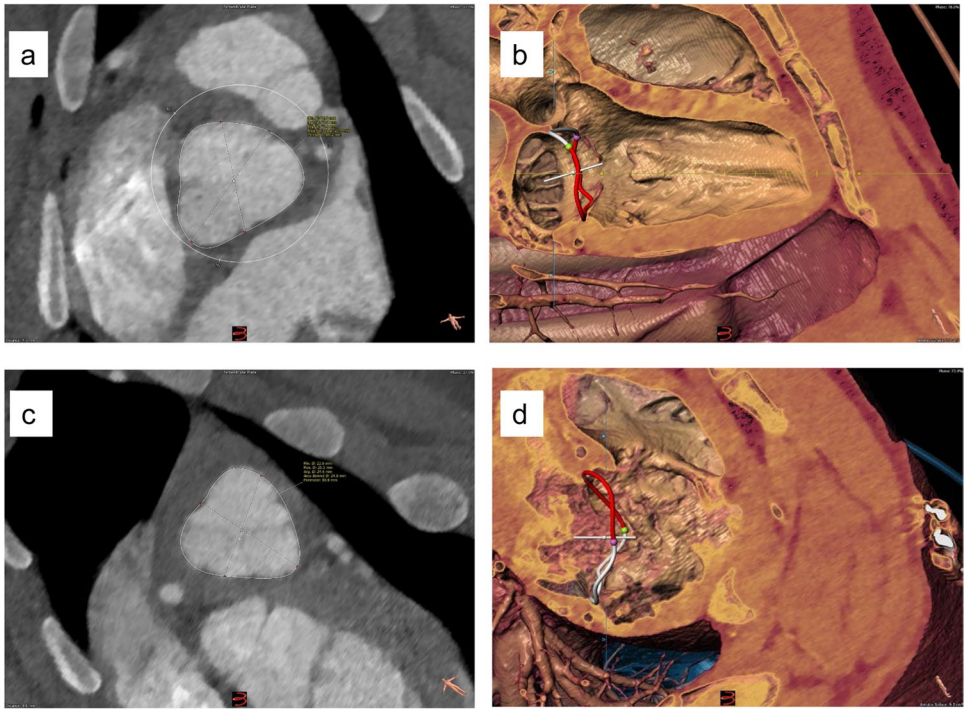

Figure 1. Representative Segmentation examples: Aortic Valve (**a**), Mitral Valve (**b**), Pulmonary Valve (**c**) and Tricuspid Valve (**d**).

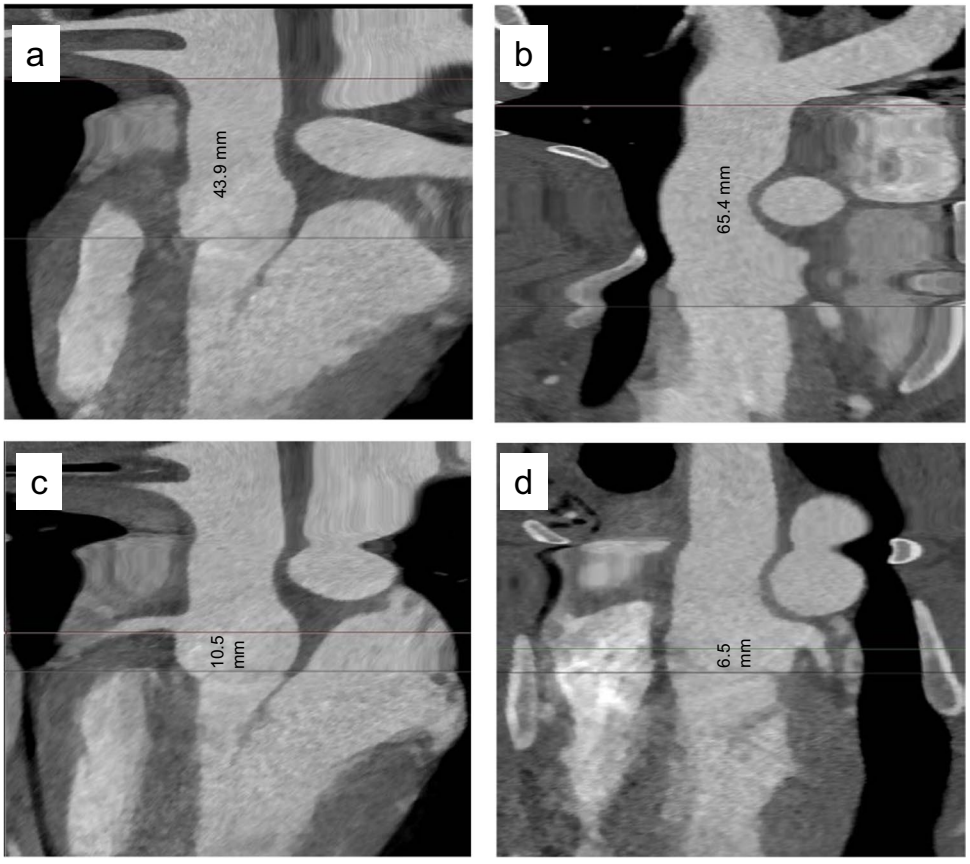

Figure 2. Representative Segmentation example: Length of ascending aorta (**a**), length of pulmonary trunk to bifurcation (**b**), RCA Ostium height (**c**) and LCA Ostium height (**d**).

annulus size; size of the left ventricular outflow tract (LVOT; 5 mm below the annulus plane). Length measurements were performed on the stretched vessel view, namely, length from annulus to the left coronary artery (LCA) ostia and the right coronary artery (RCA) ostia; length of the ascending aorta from annulus to the branch-off of the brachiocephalic trunk.

Mitral Valve. The following annulus dimensions were acquired in systole: Area; perimeter - in particular posterior perimeter, trigone-to-trigone (T-T) distance, septo-lateral (S-L) and commissure-to-commissure (C-C) distance.

Aortic-Mitral Angle. Aortic-Mitral Angle was measured in systole.

Pulmonary Trunk. Pulmonary trunk measurements were performed in diastole, following manual segmentation of the pulmonary artery. The following measurements were acquired: diameter by area derived and perimeter derived pulmonary annulus size; area and diameter of the pulmonary artery (20 mm above the annulus plane). Length measurements were performed on the stretched vessel view, namely, length from annulus to the bifurcation.

Tricuspid Valve. The following annulus dimensions were acquired in systole: area, perimeter, septo-lateral (S-L) distance, maximum diameter.

Left atrial height. left atrial height was measured in both systole and diastole.

Statistical analyses. All analyses were performed with GraphPad Prism software version 8.0.0. Correlation coefficients (r) were computed using Spearman nonparametric correlation. Strength of association was defined as very weak correlation (positive and negative 0.01 to 0.19), weak correlation (positive and negative 0.20 to 0.39), moderate correlation (positive and negative 0.40 to 0.69), strong correlation (positive and negative 0.70 to 0.89) and very strong correlation (positive and negative 0.90 to 1.00). A two-tailed P value was computed, significance for all statistical tests was established at $p \leq 0.05$. Correlation was determined between each column versus body weight. Columns assed were: all measurements acquired under aortic root, pulmonary trunk, mitral valve, tricuspid valve and left atrial height.

Additionally, a correlation matrix was created between all valve area sizes, LCA and RCA ostia height, coronary heights and length of ascending aorta.

Results

Aortic Root. A strong correlation was found between body weight and aortic valve diameter ($r = 0.83$, $p < 0.0001$) and aortic valve area, respectively ($r = 0.84$, $p < 0.0001$), as well as between body weight and length of the ascending aorta ($r = 0.72$, $p < 0.0001$) (Fig. 3). A moderate correlation was found between the body weight and LVOT diameter ($r = 0.64$, $p = 0.0007$). Correlation between body weight and LCA ostium was not significant ($r = 0.32$, $p = 0.123$), while the same correlation with the RCA ostium height was moderate ($r = 0.52$, $p = 0.0095$). Correlation between RCA ostium height and length of ascending aorta ($r = 0.38$, $p = 0.066$; $r = 0.32$) was not significant, similar to the correlation between LCA ostium height and length of the ascending aorta ($r = 0.07$, $p = 0.757$). Correlation between RCA and LCA ostia height was found to be moderate ($r = 0.50$, $p = 0.014$).

Aortic-Mitral Angle. There was no significant correlation between body weight and aortic-mitral angle ($r = 0.09$, $p = 0.66$).

Mitral Valve. A strong correlation was found between body weight and T-T distance ($r = 0.73$, $p < 0.0001$) as well as between body weight and left atrial height ($r = 0.76$, $p < 0.0001$) (Fig. 4). Correlations between body weight and mitral valve area, body weight and C-C distance, body weight and S-L distance as well as body weight to posterior perimeter was moderate ($r = 0.56$, $p = 0.0037$; $r = 0.44$, $p = 0.0297$; $r = 0.49$, $p = 0.0143$; $r = 0.43$, $p = 0.0338$).

Pulmonary Trunk. A strong correlation was found between body weight and length of the pulmonary artery to bifurcation ($r = 0.81$, $p < 0.0001$) (Fig. 5). Correlations between body weight and pulmonary artery diameter ($r = 0.55$, $p = 0.0059$), pulmonary valve diameter ($r = 0.61$, $p = 0.0019$), and pulmonary valve area ($r = 0.56$, $p = 0.0054$) were moderate.

Tricuspid Valve. A moderate correlation was found between body weight and maximum tricuspid valve diameter ($r = 0.46$, $p = 0.027$) (Fig. 6). There was no significant correlation between body weight and tricuspid valve area, and between body weight S-L distance ($r = 0.19$, $p = 0.3913$; $r = 0.04$, $p = 0.8520$).

Valve area sizes. Correlation matrix for all valve areas revealed the following correlations: A strong positive correlation was found between aortic valve area and mitral valve area ($r = 0.70$, $p < 0.0001$), correlation between aortic valve area and pulmonary valve area was moderate ($r = 0.51$, $p = 0.014$). A moderate correlation was also found between mitral valve area and tricuspid valve area ($r = 0.59$, $p = 0.004$). No significant correlation was found between aortic valve area and tricuspid valve area ($r = 0.38$, $p = 0.081$), between mitral valve area and pulmonary valve area ($r = 0.15$, $p = 0.498$), and between tricuspid valve area and pulmonary valve area ($r = -0.12$, $p = 0.617$).

a

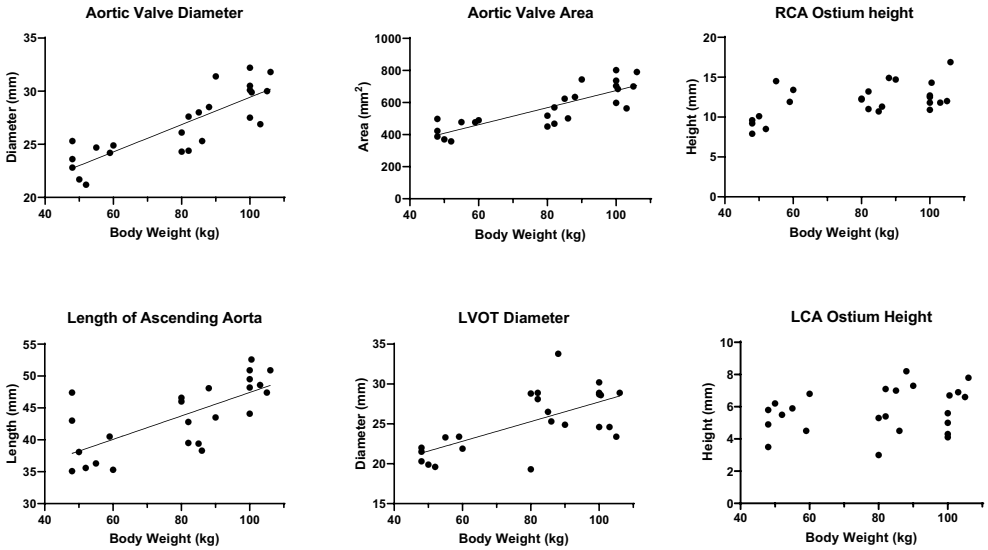

b

Body Weight	Diameter (mm)	Area (mm²)	LCA Ostium Height (mm)	RCA Ostium Height (mm)	Length of ascending aorta (mm)	Diameter LVOT (mm)
52.5 ± 4.67	23.55 ± 1.42	435.34 ± 53.55	5.39 ± 0.98	10.64 ± 2.23	38.91 ± 4.14	21.49 ± 1.36
84.13 ± 3.48	26.95 ± 2.26	563.64 ± 92.98	5.98 ± 1.61	12.54 ± 1.51	43.03 ± 3.46	26.95 ± 3.89
101.81± 2.34	29.86 ± 1.73	697.3 ± 78.40	5.88 ± 1.25	12.86 ± 1.78	49.03 ± 2.44	27.24 ± 2.42

Figure 3. Aortic Root; a. Aortic Valve Diameter, Aortic Valve Area, RCA/LCA Ostium height, Length of Ascending Aorta, LVOT Diameter: Each parameter is correlated to body weight; each dot represents a single value. A linear regression line was fitted for parameters with moderate to strong correlation. (**b**) Values for the measured parameters are shown as Mean ± SD; Values are grouped in three groups of different body weights (50–60 kg (n = 8), 80–90 kg (n = 8), 100–110 (n = 8)).

Discussion

Heart valve prosthesis are designated as high-risk medical devices, requiring rigorous *in-vitro* and *in-vivo* safety, efficacy and/or performance studies[24]. The use of standardized animal models for preclinical testing is thereby essential to provide invaluable information on the device safety. Choosing a suitable animal model for a particular experiment is of great importance and can significantly affect the outcome of a study[25,26]. Over the last decades, public concern about animal welfare in biomedical research has evolved markedly resulting in the 3R principles (i.e. replace, reduce, refine) being established worldwide as the ethical approach in regulating the use of animals for scientific purposes[27]. The aim of the refine-principle requires the use of improved experimental techniques particularly when testing new medical devices and biomaterials in animal models.

The pig has been widely used as a model in cardiovascular research[9] with a broad acceptance in the literature that the anatomy of the pig's heart is nearly identical to that of man[28–30]. In fact, trans-catheter valve implantations in pigs used for pre-clinical studies are often associated with the same complications as seen in humans[10,11]. However, unlike in humans, complications in pigs are often a consequence of a size mismatch, as preclinical studies are mostly performed with prototype devices of limited size variations[31,32]. While undersizing of prosthetic valves leads to para-valvular leakage and dislodgment of the prosthesis[33] oversizing significantly impairs hemodynamic performance[34]. As both scenarios have a negative impact on the informative value of the preclinical study results, appropriate annular measurements and prosthesis sizing are considered critical. A better understanding of cardiac morphometries, including the inter-species differences and intra-species anatomical variabilities, is thereby essential to improve safety and efficacy in non-clinical device evaluation[14–16] and to concurrently reduce the possibility of misleading and meaningless study results lacking transferability[35].

Adequate pre-procedural planning with modern imaging modalities such as three-dimensional CT is successfully used in clinical patients to ensure appropriate prosthesis-patient size matching and should therefore also be used for the pre-selection of study animals. In previous publications, detailed analysis of porcine cardiac anatomy was mainly achieved by gross examination and dissection[12,36]. However, a study in human patients has shown, that measurements acquired by CT are significantly more precise than intraoperative direct measurements. *In-situ* measurements appear to be highly influenced by the unphysiological state the cardiac structures

a

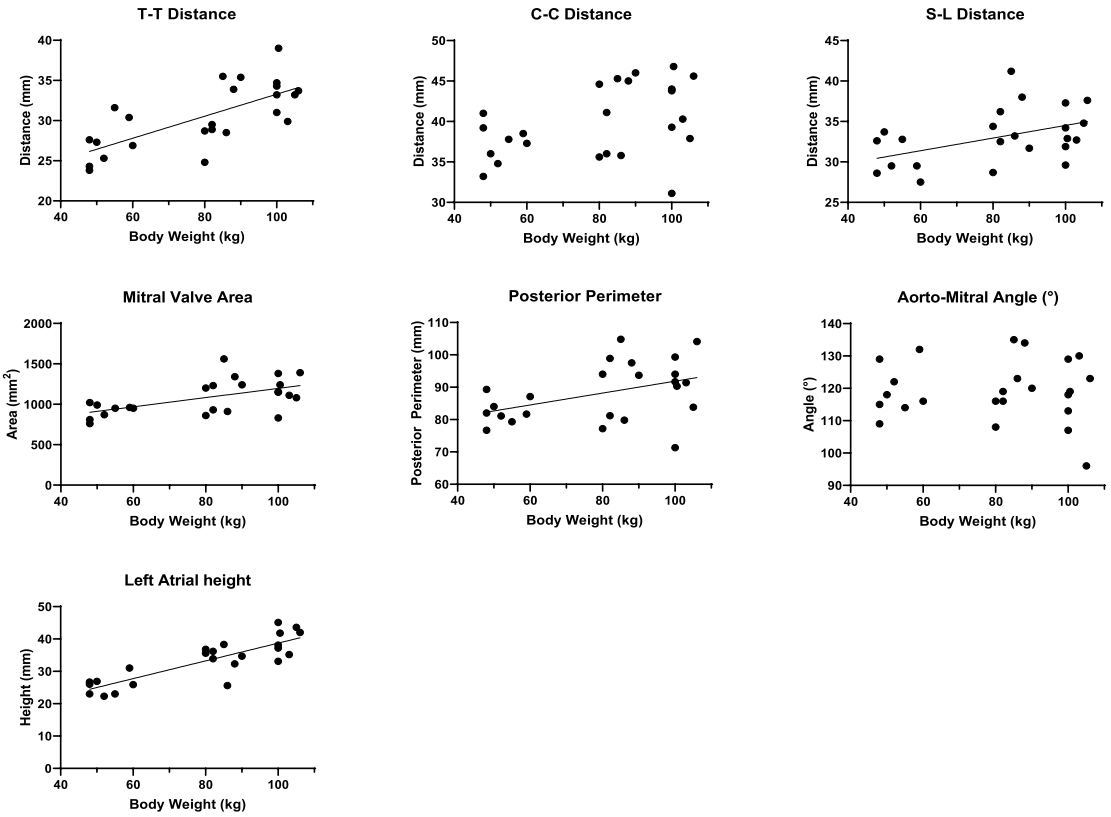

b

Body Weight	T-T (mm)	C-C (mm)	S-L (mm)	Area (mm2)	Posterior Perimeter (mm)	Aorto-Mitral Angle (°)	Left Atrial height (mm)
52.5 ± 4.67	27.15± 2.58	37.23 ±2.34	30.36 ± 2.17	913.75± 85.28	82.65± 3.81	119.38± 7.31	25.6± 2.66
84.13 ± 3.48	30.65 ± 3.6	41.18± 4.38	34.49± 3.66	1158.75± 226.57	90.89± 9.51	121.38± 8.60	34.18± 3.66
101.81 ± 2.34	33.63± 2.54	41.1± 4.78	33.88± 2.53	1166.25± 167.85	90.74± 9.29	116.88± 10.67	39.51± 3.98

Figure 4. Mitral Valve; a. T-T Distance, C-C Distance, S-L Distance, Mitral Valve Area, Posterior Perimeter, Aorto-Mitral Angle and Left Atrial Height: Each parameter is correlated to body weight; each dot represents a single value. A linear regression line was fitted for parameters with moderate to strong correlation. (**b**) Values for the measured parameters are shown as Mean ± SD; Values are grouped in three groups of different body weights (50–60 kg (n = 8), 80–90 kg (n = 8), 100–110 (n = 8)).

are assessed in as well as numerous structural conditions including angle of the great heart vessels and compliance of the valvular annulus[37].

Three-dimensional evaluation of coronary ostia height by CT is especially fundamental when planning transcatheter aortic valve implantation (TAVI). In human patients, ostia heights greater than 12 mm from the annulus are commonly considered safe for TAVI procedures[38]. This study however, not only showed the left coronary ostia to be markedly lower in pigs than in humans (5.75 ± 1.33 mm vs. 13.4 ± 2.1 mm), but no increase of coronary ostia height could be found with advanced body weight of the animals. Low coronary ostia are associated with a higher risk for post-implant coronary obstruction, depending on the type of implanted prosthesis, resulting in myocardial ischemia and infarction[39]. The question whether the lower coronary ostia height in pigs makes them unsuitable in the testing of TAVI procedures or enhances the development of novel TAVI strategies for intermediate-risk patients (coronary ostia height <7 mm), remains open.

Transcatheter mitral valve replacement (TMVR) is mainly challenged by high-profile delivery systems accommodating large valve prosthesis, having to overcome an extreme angle within a relatively small space, when approaching transseptally via the atrium to reach the mitral valve[40]. Left atrial height in pigs has shown to be strongly correlating with pig's body weight in this study. However, in pigs, the orientation of the heart along the cranio-caudal axes of the body resulting in a non-human cavo-apical angle poses an additional challenge on delivery devices[41]. Therefore, the transapical approach is a common alternative in TMVR procedures in pigs, making left ventricular dimension important factors to be considered in pre-surgical planning. Ventricular length

a

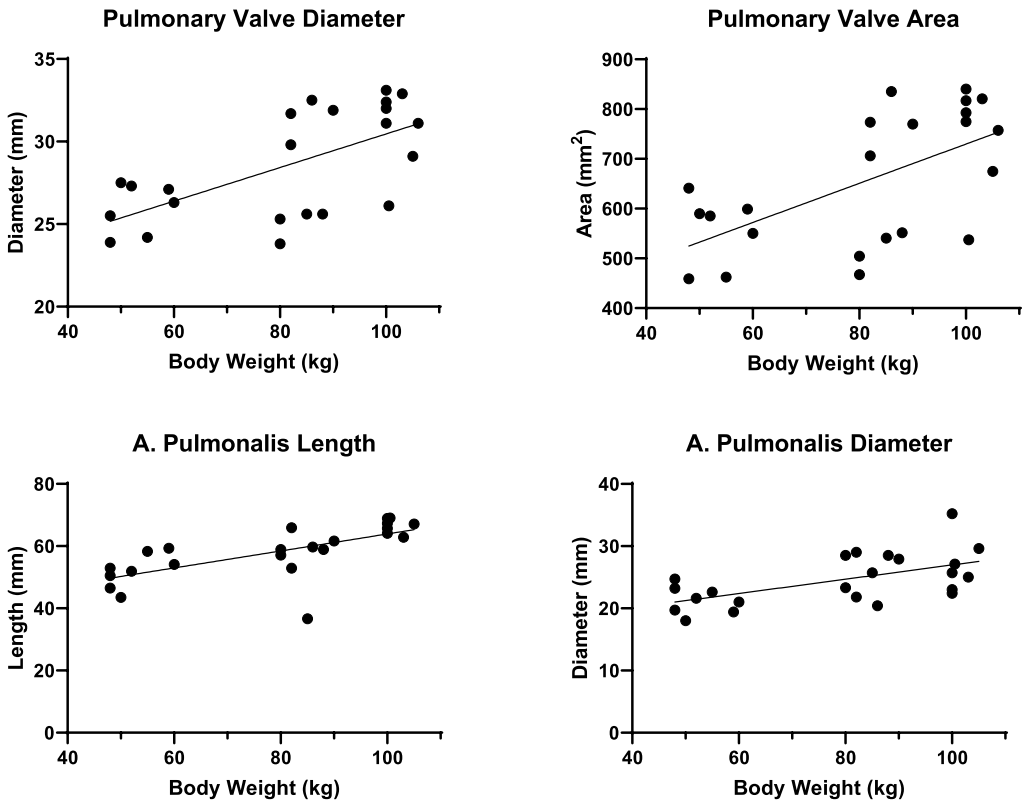

b

Body Weight	Valve Diameter (mm)	Valve Area (mm²)	Length to Bifurcation (mm)	A. Pulmonalis Diameter (mm)
52.5 ± 4.67	25.97± 1.37	555.14± 64.74	52.13± 5.04	21.28± 2.06
84.13 ± 3.48	28.28± 3.32	643.49± 133.67	56.45± 8.28	25.64± 3.17
101.81± 2.34	30.98± 2.20	751.76± 94.22	66.41± 2.17	26.86± 4.08

Figure 5. Pulmonary Trunk; (**a**) Pulmonary Valve Diameter, Pulmonary Valve Area, A.Pulmonalis Diameter, Length of A. Pulmonalis: Each parameter is correlated to body weight; each dot represents a single value. A linear regression line was fitted for parameters with moderate to strong correlation. (**b**) Values for the measured parameters are shown as Mean ± SD; Values are grouped in three groups of different body weights (50–60 kg (n = 8), 80–90 kg (n = 8), 100–110 (n = 8)).

shows no significant change with increased body weight in the animals included in this study (data not shown). Heart weight in modern farm pigs is thought to scale proportionally with body weight until the animals reach sexual maturity at the age of 4-5 months in males and 5-6 months in females[42], corresponding to an approximate body weight of 80-90 kg. The relative heart weight later decreases as the animals continue to grow[36]; leading to the assumption that measurements determining size of intra-cardiac structures reflect the above-mentioned flattening of the curve with increased body weight. Previous studies have shown a positive correlation between the body length and the aortic annulus and root diameter in the miniature swine[19]. In the presented study a positive correlation between body weight and aortic valve diameter, aortic valve area and the length of the ascending aorta could be confirmed in Swiss large white pigs. Furthermore, a strong positive correlation between body weight and the length of the pulmonary artery to bifurcation was observed. However, most of the intra-cardiac dimensions assessed in this study appear to fail in complying or only moderately comply with natural scaling laws.

A few hypothesis for this non-compliance can be proposed: Firstly, in commercially bred farm pigs the rate of fat deposition increases during the growth stages, leading to an inaccurate reflection of body weight[43]. Prediction equations for estimating lean body mass in farm pigs are available, however, they are not well established and were therefore not applied in the presented study[44]. Secondly, deviations in measurements due to selected cardiac phases. As the software used for analysis was unable to perform the automatic segmentation of the ascending aorta in pigs, all measurements of the aortic root were performed with the valve closed to facilitate accurate

a

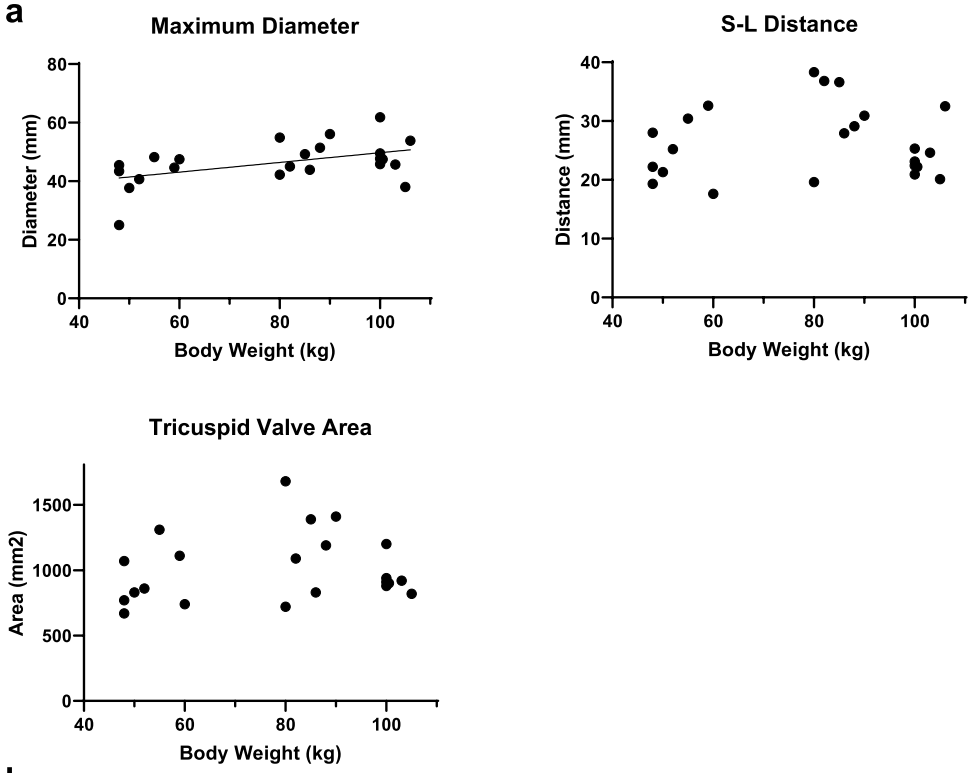

b

Body Weight	max. Diameter (mm)	Area (mm²)	S-L (mm)
52.5 ± 4.67	41.58 ± 7.09	920 ± 206.09	24.58 ± 5.04
84.13 ± 3.48	48.96 ± 5.06	1187.14 ± 313.72	31.31 ± 6.10
101.81± 2.34	48.76 ± 6.45	938.57 ± 112.43	23.89 ± 3.63

Figure 6. Tricuspid Valve; (**a**) Maximum Valve Diameter, S-L Distance, Tricuspid Valve Area: Each parameter is correlated to body weight; each dot represents a single value. A linear regression line was fitted for parameters with moderate to strong correlation. (**b**) Values for the measured parameters are shown as Mean ± SD; Values are grouped in three groups of different body weights (50–60 kg (n = 8), 80-90 kg (n = 8), 100–110 (n = 8)).

manual identification of the most basal attachment points of the three aortic valve cusps needed for quantitative assessment of the annulus plane[45]. All other valves were subsequently also measured in the closed position although intra-cardiac cycle variations are known to have a marked influence on cardiac dimensions and indices of cardiac functions in humans[46] with differences of up to 15% expected when using different cardiac phases[47]. Best correlation has shown to be achieved when measurements are done in mid-systole in 25–35% of the heart cycle[48]. Data on the amount of cyclical changes on annular dimensions in pigs, including cross-sectional area, perimeter and subsequently derived diameters however is more conflicting[34]. A dynamic geometry, mainly affecting the maximal diameter but not the minimal diameter, throughout the cardiac cycle is described for the left ventricular outflow tract and the mitral valve in pigs[35,36]. Possible further deviations in the measurements might be caused by high variations in heart rate between the animals, causing the respective cardiac phases, namely best systole and best diastole, to be defined at different percentiles of the RR interval.

Due to its retrospective nature, a further flaw in this presented study was the application of the contrast. A biphasic contrast injection protocols (80% high flow, 20% low flow) allowing for improved contrast in the right heart, while keeping the image of the left heart structures high and diagnostic[49,50] was applied for all recordings of porcine cardiac CT scans. However, as the contrast was given over either the auricular vein or the femoral vein, inhomogeneity of contrast in the right ventricle was greater in the animals with auricular vein access due to the larger amount of non-contrasted blood mixing in from the inferior vena cava. The resulting reduction in image quality of the right heart partially hampered the accurate reconstruction of the anatomy and dimensions of the tricuspid valve and the pulmonary valve respectively.

The most common breeds of domestic swine used in biomedical research found in the literature are Yorkshire, Landrace, Duroc, Pietrain and crossbreeds such as the Swiss Large White used in this study[51]. Landrace, Duroc, Pietrain and crossbreeds appear to have a similar linear growth curve[52,53],while Yorkshire pigs are described to significantly differ by having a curvilinear growth pattern[54]. The breed difference in rate of growth of heart relative to total muscle mass has been found to be not significant in Pietrain and Large White Pigs[53]. Although the current study included castrated males and intact females of only Swiss Large White Pigs, potentially neglecting an influence of sex and breed, similar data in pigs of breeds with similar growth patterns might be speculated.

Last, pre-procedure planning for trans-catheter implantation studies requires thorough knowledge of cardiac dimensions to pick a suitable study animal size. However, vascular access route, including aorto-iliac vessel assessment (angulation, luminal size) and length and diameter of the abdominal aorta for delivery system length and diameter suitability is equally crucial for animal selection[48]. Further studies are needed to complete these missing parameters.

In conclusion, blindly correlating the body weight of a domestic swine breed, to all intra-cardiac structures leading to an accurate prediction of which pig would be the best size-matched to test a particular cardiac implant, appears unfeasible based on the acquired data. However, there are a few statements that can be made: Firstly, valvular diameters and area sizes moderately to strongly correlate with pig's body weight of this particular swine breed and possibly of swine breeds with similar growth curve patterns. The here collected data can therefore serve as a future guide in prosthetic valve size selection. Secondly, coronary ostia height and aorto-mitral angle size can be neglected in animal size selection as no change was found for either of the two parameters with increasing body weight. Lastly, length of the pulmonary artery to bifurcation as well as length of the ascending aorta can be well correlated with body weight.

Received: 9 October 2019; Accepted: 24 March 2020;
Published online: 07 April 2020

References

1. Sierra, J., Lahlaidi Sierra, N., Bednarkiewicz, M. & Montessuit, M. [Minimal invasive cardiac surgery]. *Revue medicale suisse* **11**, 543–545 (2015).
2. Bohula May, E. A. & Faxon, D. Transcatheter aortic valve replacement: history and current status. *Trends in cardiovascular medicine* **23**, 172–178, https://doi.org/10.1016/j.tcm.2012.11.001 (2013).
3. Cohn, L. H. *et al*. Minimally invasive cardiac valve surgery improves patient satisfaction while reducing costs of cardiac valve replacement and repair. *Annals of surgery* 226, 421–426; discussion 427–428 (1997).
4. Vahl, T. P., Kodali, S. K. & Leon, M. B. Transcatheter Aortic Valve Replacement 2016: A Modern-Day "Through the Looking-Glass" Adventure. *Journal of the American College of Cardiology* **67**, 1472–1487, https://doi.org/10.1016/j.jacc.2015.12.059 (2016).
5. Salenger, R., Gammie, J. S. & Collins, J. A. Minimally Invasive Aortic Valve Replacement. *Journal of cardiac surgery* **31**, 38–50, https://doi.org/10.1111/jocs.12652 (2016).
6. Koruth, J. S. *et al*. Pre-Clinical Investigation of a Low-Intensity Collimated Ultrasound System for Pulmonary Vein Isolation in a Porcine Model. *JACC. Clinical electrophysiology* **1**, 306–314, https://doi.org/10.1016/j.jacep.2015.04.011 (2015).
7. Yi, G. H. *et al*. Safety and feasibility of percutaneous delivery of a novel circulatory assist device (CircuLite(R) SYNERGY(R)) in the swine model. *EuroIntervention: journal of EuroPCR in collaboration with the Working Group on Interventional Cardiology of the European Society of Cardiology* **9**, 259–268, https://doi.org/10.4244/eijv9i2a42 (2013).
8. Monreal, G. *et al*. Large animal models for left ventricular assist device research and development. *ASAIO journal (American Society for Artificial Internal Organs: 1992)* **60**, 2–8, https://doi.org/10.1097/mat.0000000000000005 (2014).
9. Smerup, M. *et al*. A long-term porcine model for evaluation of prosthetic heart valves. *The heart surgery forum* **7**, E259–264, https://doi.org/10.1532/hsf98.20041015 (2004).
10. Barbanti, M. *et al*. Anatomical and procedural features associated with aortic root rupture during balloon-expandable transcatheter aortic valve replacement. *Circulation* **128**, 244–253, https://doi.org/10.1161/circulationaha.113.002947 (2013).
11. Ribeiro, H. B. *et al*. Coronary obstruction following transcatheter aortic valve implantation: a systematic review. *JACC. Cardiovascular interventions* **6**, 452–461, https://doi.org/10.1016/j.jcin.2012.11.014 (2013).
12. Crick, S. J., Sheppard, M. N., Ho, S. Y., Gebstein, L. & Anderson, R. H. Anatomy of the pig heart: comparisons with normal human cardiac structure. *Journal of anatomy* **193**(Pt 1), 105–119 (1998).
13. Ma, L. *et al*. Double-crowned valved stents for off-pump mitral valve replacement. *European journal of cardio-thoracic surgery: official journal of the European Association for Cardio-thoracic Surgery* 28, 194–198; discussion 198–199, https://doi.org/10.1016/j.ejcts.2004.12.068 (2005).
14. Willson, A. B. *et al*. Computed tomography-based sizing recommendations for transcatheter aortic valve replacement with balloon-expandable valves: Comparison with transesophageal echocardiography and rationale for implementation in a prospective trial. *Journal of cardiovascular computed tomography* **6**, 406–414, https://doi.org/10.1016/j.jcct.2012.10.002 (2012).
15. Santos, A. *et al*. Cardiovascular imaging: what have we learned from animal models? *Frontiers in pharmacology* **6**, 227, https://doi.org/10.3389/fphar.2015.00227 (2015).
16. Sundermann, S. H. *et al*. Computed tomography for planning and postoperative imaging of transvenous mitral annuloplasty: first experience in an animal model. *The international journal of cardiovascular imaging* **31**, 135–142, https://doi.org/10.1007/s10554-014-0516-7 (2015).
17. Choo, S. J. *et al*. Development of an animal experimental model for a bileaflet mechanical heart valve prosthesis. *Journal of Korean medical science* **19**, 37–41, https://doi.org/10.3346/jkms.2004.19.1.37 (2004).
18. Capps, S. B., Elkins, R. C. & Fronk, D. M. Body surface area as a predictor of aortic and pulmonary valve diameter. *The Journal of thoracic and cardiovascular surgery* **119**, 975–982, https://doi.org/10.1016/s0022-5223(00)70092-4 (2000).
19. Allan, J. S. *et al*. Morphometric analysis of miniature swine hearts as potential human xenografts. *Xenotransplantation* **8**, 90–93 (2001).
20. Gutierrez, K., Dicks, N., Glanzner, W. G., Agellon, L. B. & Bordignon, V. Efficacy of the porcine species in biomedical research. *Frontiers in genetics* **6**, 293, https://doi.org/10.3389/fgene.2015.00293 (2015).
21. Swindle, M. M., Smith, A. C. & Helke, K. Recommendations for Medical Device Implantation in Swine. *Isr J Vet Med* **68**, 3–11 (2013).
22. Smith, D. *et al*. Classification and reporting of severity experienced by animals used in scientific procedures: FELASA/ECLAM/ESLAV Working Group report. *Lab Anim* **52**, 5–57, https://doi.org/10.1177/0023677217744587 (2018).
23. Worlein, J. M., Baker, K., Bloomsmith, M., Coleman, K. & Koban, T. L. The Eighth Edition of the Guide for the Care and Use of Laboratory Animals (2011); Implications for Behavioral Management. *Am J Primatol* **73**, 98–98 (2011).

24. Zhang, B. L., Bianco, R. W. & Schoen, F. J. Preclinical Assessment of Cardiac Valve Substitutes: Current Status and Considerations for Engineered Tissue Heart Valves. *Frontiers in cardiovascular medicine* **6**, 72, https://doi.org/10.3389/fcvm.2019.00072 (2019).
25. IOo, S. (ISO).
26. Kheradvar, A., Zareian, R., Kawauchi, S., Goodwin, R. L. & Rugonyi, S. Animal Models for Heart Valve Research and Development. *Drug Discov Today Dis Models* **24**, 55–62, https://doi.org/10.1016/j.ddmod.2018.04.001 (2017).
27. Kirk, R. G. W. Recovering The Principles of Humane Experimental Technique: The 3Rs and the Human Essence of Animal Research. *Sci Technol Human Values* **43**, 622–648, https://doi.org/10.1177/0162243917726579 (2018).
28. White, D. & Wallwork, J. Xenografting: probability, possibility, or pipe dream? *Lancet (London, England)* **342**, 879–880, https://doi.org/10.1016/0140-6736(93)91939-j (1993).
29. Niekrasz, M., Ye, Y., Rolf, L. L., Zuhdi, N. & Cooper, D. K. The pig as organ donor for man. *Transplantation proceedings* **24**, 625–626 (1992).
30. Douglas, W. R. Of pigs and men and research: a review of applications and analogies of the pig, sus scrofa, in human medical research. *Space life sciences* **3**, 226–234, https://doi.org/10.1007/bf00928167 (1972).
31. Berreklouw, E. *et al*. Sutureless replacement of aortic valves with St Jude Medical mechanical valve prostheses and Nitinol attachment rings: feasibility in long-term (90-day) pig experiments. *J Thorac Cardiovasc Surg* **141**, 1231–1237 e1231, https://doi.org/10.1016/j.jtcvs.2010.07.014 (2011).
32. Banai, S. *et al*. Transapical mitral implantation of the Tiara bioprosthesis: pre-clinical results. *JACC Cardiovasc Interv* **7**, 154–162, https://doi.org/10.1016/j.jcin.2013.10.009 (2014).
33. Dasi, L. P. *et al*. On the Mechanics of Transcatheter Aortic Valve Replacement. *Ann Biomed Eng* **45**, 310–331, https://doi.org/10.1007/s10439-016-1759-3 (2017).
34. Cleveland, J. D. *et al*. Evaluation of Hemodynamic Performance of Aortic Valve Bioprostheses in a Model of Oversizing. *Ann Thorac Surg* **103**, 1866–1876, https://doi.org/10.1016/j.athoracsur.2016.10.019 (2017).
35. Bergsland, J., Elle, O. J. & Fosse, E. Barriers to medical device innovation. *Med Devices (Auckl)* **7**, 205–209, https://doi.org/10.2147/MDER.S43369 (2014).
36. Lelovas, P. P., Kostomitsopoulos, N. G. & Xanthos, T. T. A comparative anatomic and physiologic overview of the porcine heart. *Journal of the American Association for Laboratory Animal Science: JAALAS* **53**, 432–438 (2014).
37. George, I. *et al*. Aortic Valve Annular Sizing: Intraoperative Assessment Versus Preoperative Multidetector Computed Tomography. *Circ Cardiovasc Imaging* **10**, 10.1161/CIRCIMAGING.116.005968 (2017).
38. Ribeiro, H. B. *et al*. Predictive factors, management, and clinical outcomes of coronary obstruction following transcatheter aortic valve implantation: insights from a large multicenter registry. *Journal of the American College of Cardiology* **62**, 1552–1562, https://doi.org/10.1016/j.jacc.2013.07.040 (2013).
39. Falk, V. *et al*. ESC/EACTS Guidelines for the management of valvular heart disease. *European journal of cardio-thoracic surgery: official journal of the European Association for Cardio-thoracic Surgery* **52**, 616–664, https://doi.org/10.1093/ejcts/ezx324 (2017).
40. Regueiro, A., Granada, J. F., Dagenais, F. & Rodes-Cabau, J. Transcatheter Mitral Valve Replacement: Insights From Early Clinical Experience and Future Challenges. *Journal of the American College of Cardiology* **69**, 2175–2192, https://doi.org/10.1016/j.jacc.2017.02.045 (2017).
41. Maisano, F. *et al*. A translational "humanised" porcine model for transcatheter mitral valve interventions: the neo inferior vena cava approach. *EuroIntervention: journal of EuroPCR in collaboration with the Working Group on Interventional Cardiology of the European Society of Cardiology* **11**, 92–95, https://doi.org/10.4244/eijy15m02_04 (2015).
42. van Essen, G. J. *et al*. Cardiovascular Function of Modern Pigs Does not Comply with Allometric Scaling Laws. *Scientific reports* **8**, 792, https://doi.org/10.1038/s41598-017-18775-z (2018).
43. Shields, R. G. Jr., Mahan, D. C. & Graham, P. L. Changes in swine body composition from birth to 145 kg. *Journal of animal science* **57**, 43–54 (1983).
44. Swantek, P. M., Marchello, M. J., Tilton, J. E. & Crenshaw, J. D. Prediction of fat-free mass of pigs from 50 to 130 kilograms live weight. *Journal of animal science* **77**, 893–897 (1999).
45. Blanke, P. *et al*. Computed tomography imaging in the context of transcatheter aortic valve implantation (TAVI)/transcatheter aortic valve replacement (TAVR): An expert consensus document of the Society of Cardiovascular Computed Tomography. *Journal of cardiovascular computed tomography* **13**, 1–20, https://doi.org/10.1016/j.jcct.2018.11.008 (2019).
46. DeMaria, A. N., Neumann, A., Schubart, P. J., Lee, G. & Mason, D. T. Systematic correlation of cardiac chamber size and ventricular performance determined with echocardiography and alterations in heart rate in normal persons. *The American journal of cardiology* **43**, 1–9 (1979).
47. Holmes, D. R. Jr. & Mack, M. J. Transcatheter valve therapy: a professional society overview from the American College of Cardiology Foundation and the Society of Thoracic Surgeons. *The Annals of thoracic surgery* **92**, 380–389, https://doi.org/10.1016/j.athoracsur.2011.05.067 (2011).
48. Feuchtner, G. Imaging of cardiac valves by computed tomography. *Scientifica* **2013**, 270579, https://doi.org/10.1155/2013/270579 (2013).
49. Hinzpeter, R. *et al*. Computed tomography in patients with tricuspid regurgitation prior to transcatheter valve repair: dynamic analysis of the annulus with an individually tailored contrast media protocol. *EuroIntervention: journal of EuroPCR in collaboration with the Working Group on Interventional Cardiology of the European Society of Cardiology* **12**, e1828–e1836, https://doi.org/10.4244/eij-d-16-00891 (2017).
50. Vrachliotis, T. G. *et al*. Atypical chest pain: coronary, aortic, and pulmonary vasculature enhancement at biphasic single-injection 64-section CT angiography. *Radiology* **243**, 368–376, https://doi.org/10.1148/radiol.2432060447 (2007).
51. Swindle, M. M., Makin, A., Herron, A. J., Clubb, F. J. Jr. & Frazier, K. S. Swine as models in biomedical research and toxicology testing. *Veterinary pathology* **49**, 344–356, https://doi.org/10.1177/0300985811402846 (2012).
52. Wetten, M., Odegard, J., Vangen, O. & Meuwissen, T. H. Simultaneous estimation of daily weight and feed intake curves for growing pigs by random regression. *Animal* **6**, 433–439, https://doi.org/10.1017/S1751731111001832 (2012).
53. Davies, A. S. A comparison of tissue development in Pietrain and Large White pigs from birth to 64 kg live weight 2. Growth changes in muscle distribution. *Animal Science* **19**, 377–387, https://doi.org/10.1017/S0003356100022959 (1974).
54. Quijandria, B. Jr., Woodard, J. R. & Robison, O. W. Genetic and environmental effects on live and carcass traits at the North Carolina swine evaluation station. *J Anim Sci* **31**, 652–655, https://doi.org/10.2527/jas1970.314652x (1970).

Acknowledgements

The authors would like to thank Flora Nicholls for helping in the preparation of the pigs for the CT scans, Robin Schneider, Dr. Hugo Battaglia, Prof. Margarete Arras and the animal caretakers of the Central Biological Laboratory for their valuable support in housing the pigs.

Author contributions

M.L. wrote the main manuscript text. M.L. and N.C. analyzed the C.T. scans. M.L., N.C., T.F. and M.S. were involved in data acquisition and in animal care. M.E., B.K., H.A. did the C.T. scans for all animals, M.E. was involved in the C.T. analyzes. M.Y.E., S.H., V.F. and F.M. provided C.T. data from previous projects. All authors read and approved the manuscript.

Competing interests

The authors declare no competing interests.

Additional information

Correspondence and requests for materials should be addressed to M.L.

Reprints and permissions information is available at www.nature.com/reprints.

Publisher's note Springer Nature remains neutral with regard to jurisdictional claims in published maps and institutional affiliations.

2.2 Left ventricular blood flow patterns at rest and under dobutamine stress in healthy pigs

Cesarovic N, Busch J, Lipiski M, Fuetterer M, Fleischmann T, Born S, von Deuster C, Sauer M, Maisano F, Kozerke S, Stoeck CT. Left ventricular blood flow patterns at rest and under dobutamine stress in healthy pigs. NMR Biomed. 2019 Jan;32(1):e4022. doi: 10.1002/nbm.4022. Epub 2018 Nov 7. PMID: 30403426.

In order to closely mimic human valvular function and disease, a translational animal model does not only need to comply with anatomical determinants but also to simulate complex fluid movement that occurs during every heartbeat. Swirling flow patterns in aortic sinuses have been postulated as early as 15th century by Leonardo da Vinci (57). Modern imaging modalities subsequently demonstrated that vortical flow patterns are a common feature in the human heart, where vortices appear during diastole and are associated with a smooth redirection of flow from the inflow to the outflow tract (58). It has been shown that such vortices are disturbed in patients with myocardial infarction, dilated cardiomyopathy or heart failure as well as after surgical valve interventions (59). Hence, left ventricular diastolic vortices have been recently suggested as a novel biomarker of cardiac health and valvular function (60). However, properties of diastolic blood flow patterns in rest and under stress in healthy porcine have largely been unexplored. The objective of this study was to assess the feasibility of 4D MRI flow measurements under conditions of increased heart rate and to record changes in intraventricular blood flow patterns during a high demand state (such as physical exercise) mimicked by dobutamine-induced stress, relative to the resting condition, in a healthy pig animal model. Twelve juvenile domestic pigs with a median weight of 30.5 kg (29–31.5 kg) were included in the study and split into a dobutamine stress and a control group (N = 6 each). The animal housing and experimental protocols were approved by the Cantonal Veterinary Office, Zurich, Switzerland, under License ZH 152/2013, and were performed in accordance with Swiss animal protection law and ordinance as well as the European Directive 2010/63/EU on the Protection of Animals Used for Scientific Purposes and the Guide for the Care and Use of Laboratory Animals (56). In brief, magnetic resonance phase contrast imaging was performed under general anesthesia on a clinical grade 3 T Philips Ingenia system equipped with a 28-channel cardiac coil. Cardiac stress was pharmacologically induced by intravenous administration of dobutamine until the target heart rate of 120 bpm was reached. Four dimensional velocity vector field data have reformatted and analysed at 7 time-points during diastole (3 in E wave, 3 in A wave and 1 in diastasis) using GTVolume and GTFlow (GyroTools) software. The study demonstrated that in general anesthesia under resting (no-stress) conditions healthy pigs display large similarities to healthy humans regarding parameters such as mitral inflow pattern (E and A wave) and velocity. Direct and retained flow volume, where 43 ± 6% of the blood entering the left ventricle during

diastole is ejected within the next heartbeat (direct flow) and 57 ± 6% remains inside the left ventricle. Further, under such conditions the mitral valve directed the diastolic inflow towards the antero-septal segment of the ventricle with inflow angles of 15 ± 2° to the central long axis of the heart. In this group vortex could develop early (during E-wave acceleration phase) and persisted largely until late diastole (A-wave deceleration phase) with cross-sectional size (max 529 ± 98 mm^2), vorticity (and rotations center point that closely corresponds to healthy human volunteers. Further, the septaly oriented inflow trajectory and the reduced LVEDV under dobutamine infusion influenced the vortical flow patterns towards a later development, earlier disappearance and generally smaller vortices, a situation also observed in humans during high demand states (61). These results led to the conclusion that left ventricular blood flow patterns in rest and under pharmacologicaly induced stress can be well assessed in pigs using clinical grade MRI equipment. Further, despite certain anatomical differences, intra-ventricular flow patterns in pigs correspond well to the ones observed in healthy humans. However, physiological left ventricular hypertrophy in pigs might be a confounding factor in translation of porcine-derived fluid dynamic data to humans. In this aspect more research is merited.

Full article can be found under the following link: https://doi.org/10.1002/nbm.4022

2.3 Two- and three-dimensional transoesophageal echocardiography in large swine used as model for transcatheter heart valve therapies: standard planes and values

Sündermann SH, Cesarovic N, Falk V, Bettex D. Two- and three-dimensional transoesophageal echocardiography in large swine used as model for transcatheter heart valve therapies: standard planes and values. Interact Cardiovasc Thorac Surg. 2016 May;22(5):580-6. doi: 10.1093/icvts/ivv381. Epub 2016 Jan 31. PMID: 26831678; PMCID: PMC6716457.

Large animal models, especially domestic pigs, are widely used in preclinical investigation and evaluation of novel heart valve implants. Due to large similarities with human anatomy and physiology, but also good availability these models are widely used to train physicians in new valvular trans-catheter interventions (62). Transoesophageal echocardiography (TOE) plays an important role in intra-procedural guidance and result evaluation in such procedures. The use of TOE for aortic and mitral trans-catheter interventions is well established in the clinic, however it seems not to be the case in large animal preclinical trails where this imaging technique needs to be modified for use in pigs. An exemplary issue is the anatomy of the bronchial system, where the main bronchus is often located between the oesophagus and the heart, hence hampering TOE along its course. The aim of this study was to show the feasibility of TOE in swine and to establish standard projections and values for a large swine animal model that can be routinely used during transcatheter heart valve procedures. Following the ethical approval (licence no. ZH 152/13), twenty domestic pigs with a median weight of 92.5 kg (56–106 kg) were included in the study. After the induction of general anaesthesia, real-time 2D and 3D TOE was performed using a standard adult matrix array TOE probe X7-2t (Philips Medical Systems). We could demonstrate that TOE examination was possible in all animals. The main TOE imaging window was found to be at 53 ± 5 cm from the front incisor teeth, but to avoid the bronchus shadowing, the probe needed strong ante- and latero-flexion. After adjusting the transducer rotation, at this position modified 4-chamber, 3-chamber and left ventricular 2-chamber views could be readily obtained. The mitral and aortic valve as well as aortic annulus, sinus of Valsalva, sinotubular junction and ascending aorta could be visualized both in 2- and 3D when the TOE probes flexion and rotation was attuned (rotation 40-70°), whereas the tricuspid valve was often partially obscured by the bronchus. For imaging of the pulmonary valve as well as aortic and pulmonary valve Doppler echocardiography, the probe needed to be pulled back approx. 10 cm, retroflexed and transducer angle rotated to 0-60°. Cardiac functional parameters (such as stroke volume, ejection fraction, LVESV, LVEDV) as well as valvular dimension and function obtained by using this TOE method in large domestic porcine, were strongly comparable with corresponding values in humans (63, 64). Such results led to conclusion that standardized TOE is possible during preclinical investigations of novel valvular therapies, and that by modification of clinical (human) TOE technique almost all cardiac structures could readily be visualized.

These cardiac structures bare close resemblance and share the dimensional similarities between humans and large domestic pigs used in this study.

Interactive CardioVascular and Thoracic Surgery 22 (2016) 580–586
doi:10.1093/icvts/ivv381 Advance Access publication 31 January 2016

Cite this article as: Sündermann SH, Cesarovic N, Falk V, Bettex D. Two- and three-dimensional transoesophageal echocardiography in large swine used as model for transcatheter heart valve therapies: standard planes and values. Interact CardioVasc Thorac Surg 2016;22:580–6.

Two- and three-dimensional transoesophageal echocardiography in large swine used as model for transcatheter heart valve therapies: standard planes and values

Simon H. Sündermann[a,*], Nikola Cesarovic[b], Volkmar Falk[a] and Dominique Bettex[c]

[a] Department of Cardiothoracic and Vascular Surgery, Deutsches Herzzentrum Berlin, Berlin, Germany
[b] Department of Surgical Research, University Hospital Zurich, University of Zurich, Zurich, Switzerland
[c] Institute of Anesthesiology, University Hospital Zurich, University of Zurich, Zurich, Switzerland

* Corresponding author. Department of Cardiothoracic and Vascular Surgery, Deutsches Herzzentrum Berlin, Augustenburger Platz 1, 13353 Berlin, Germany. Tel: +49-30-45932086; fax: +49-30-45932100; e-mail: suendermann@dhzb.de (S.H. Sündermann).

Received 14 July 2015; received in revised form 13 November 2015; accepted 26 November 2015

Abstract

OBJECTIVES: Swine models are widely used to develop new techniques and materials for the treatment of heart valve disease like aortic valve and mitral valve transcatheter interventions and to train physicians in these techniques. Transoesophageal echocardiography (TOE) is crucial in these models. We defined standard planes of 2D and 3D TOE in healthy pigs undergoing transcatheter heart valve interventions.

METHODS: Twenty healthy pigs (weight 56–106 kg) underwent different mitral and aortic valve interventions (transcatheter aortic valve implantations, implantations of a mitral band, bicuspidization of the aortic valve, trans-septal punctures). For image guidance of the procedures, an adult TOE probe was introduced under direct vision in the oesophagus. Before the procedure itself was performed, a standardized protocol was used to determine normal values for anatomical and functional echocardiographic parameters.

RESULTS: Positioning of the probe was possible in all animals and ideal when achieving a distance from the front teeth (incisors) of 40–60 cm. Anteflexion and lateroflexion of the probe was necessary to achieve optimal imaging quality. 2D visualization of all relevant cardiac structures was possible. The aortic annulus diameter was 24.1 ± 2.5 mm, the sinus of valsalva diameter was 30.6 ± 4 mm and the sinotubular junction diameter was 25.2 ± 4 mm. The ascending aorta had a diameter of 24 ± 4 mm and the descending aorta a diameter of 16 ± 5 mm. The mitral valve anterior–posterior diameter was 31.8 ± 4 mm and the commissure to commissure diameter was 40.5 ± 5 mm resulting in a mitral valve area of 10.7 ± 1.5 cm^2. 3D visualization was possible for the aortic and the mitral valve. None of the animals showed any pathology except one that had a dilated left ventricle and moderate mitral valve insufficiency. Left and right ventricular dimensions and the anatomy of the aortic-, mitral-, tricuspid and pulmonary valve as well as of the aorta were comparable with those of the human anatomy.

CONCLUSIONS: 2D and 3D TOE can be routinely applied as image guidance in pigs used as a model for the development and training of new techniques to treat heart valve disease.

Keywords: Animal model • Transoesophageal echocardiography • Minimally invasive surgery • Transcatheter valve therapy

INTRODUCTION

Domestic pigs (Sus Scrofa) are used as an animal model for preclinical evaluation and investigation of new heart valve prostheses and therapies due to their similarities to the human physiology and anatomy of the heart and vessels, and their good availability [1–3]. Furthermore, good correlation between weight and sizes of the valvular annuli, short but well-defined ascending aorta and aortic arch curvature stronger than the ones found in cloven-footed animals have been described in pigs [4, 5]. These models are also widely used to train physicians in these new techniques. Important imaging modality for aortic valve and mitral valve interventions is transoesophageal echocardiography (TOE). The use of TOE in transcatheter aortic valve implantation (TAVI) procedures and transcatheter mitral valve interventions (i.e. the MitraClip procedure) is extensively described in the literature [6–9]. For the use of TOE in large swine models, the literature is very limited [10]. For the development and the training of new transcatheter techniques in large swine models, TOE for image guidance of the procedure is crucial as well.

The aim of this study was to show the feasibility of TOE in swine to develop a TOE approach and establish standard values for a large swine animal model that can be used during the development and training of transcatheter heart valve therapies.

METHODS

The animal housing and experimental protocols were approved by the Cantonal Veterinary Department, Zurich, Switzerland, under

licence no. ZH 152/2013, and were in accordance with Swiss Animal Protection Law. Housing and experimental procedures were also conforming to the European Directive 2010/63/EU of the European Parliament and of the Council on the protection of animals used for scientific purposes and to the Guide for the Care and Use of Laboratory Animals (Institute of Laboratory Animal Resources, National Research Council, National Academy of Sciences, 2011).

The animals were included in different projects within the licence covering transcatheter aortic valve replacement with standard transcatheter heart valve prosthesis (i.e. Symetis ACURATE TA Aortic prosthesis) and transcatheter mitral valve repair techniques (Valtech Cardioband [11], Cardiosolutions Mitra-Spacer [12]).

TOE was part of the study protocols. The examinations were performed in the operating room before the interventions were started; no additional animals were needed for this study.

Twenty domestic pigs with a median weight of 92.5 kg (56–106 kg) were included in the study. All animals received premedication with ketamine (20 mg/kg), azaperone (1.5 mg/kg) and atropine (0.75 mg) intramuscularly. After the loss of postural reflexes, the animals were transported to the surgical preparation room. The anaesthesia was deepened by a bolus injection of propofol (1–2 mg/kg) and the trachea of the animal was intubated. Anaesthesia was then maintained with 2–3% of isoflurane in 1 : 1 oxygen/air mixture (4–5 l/min). Amiodarone (2–3 mg/kg bolus i.v.) was administered to stabilize the heart rhythm. Animals were placed on the operating table in dorsal recumbence.

After the induction of anaesthesia, real-time 3D TOE Philips iE33 (Philips Medical Systems, Andover, MA, USA) was performed using a standard adult matrix array TOE probe X7-2t (Philips Medical Systems). The probe was covered with a latex coat that was floated with ultrasonic gel (Skintact, Leonhard Lang Gmbh, Innsbruck, Austria) and was introduced under laryngoscopic sight, lifting the tongue and the lower jaw with the spatula. The TOE probe was introduced from the right side of the pig's pharynx to find the oesophagus below the trachea. For introduction, the probe was kept unblocked in neutral position.

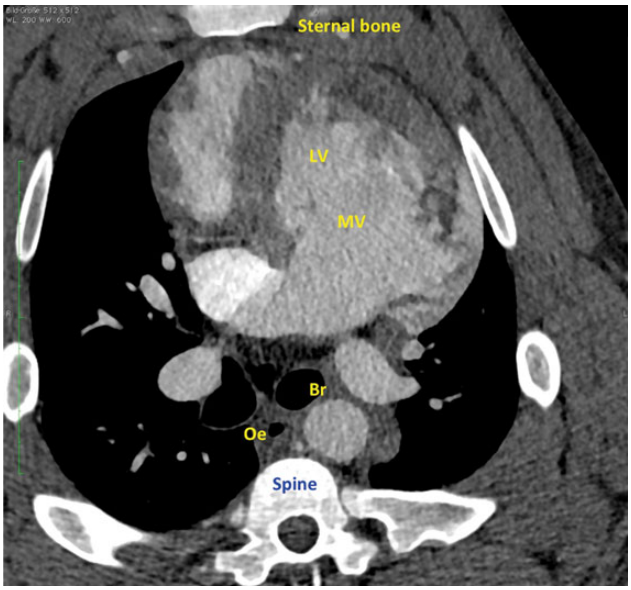

Figure 1: Computed tomography of n pig. MV: mitral valve; LV: left ventricle; Oe: oesophagus; Br: bronchus.

Two-dimensional transoesophageal echocardiography

The examination was started at around 55 cm from the incisors. The exact depth of the probe, the flexion of the tip of the probe and the rotation of the transducer were adapted for optimal imaging. An issue of TOE in pigs is the anatomy of the bronchial system. The main bronchus is located between oesophagus and the heart (Fig. 1). Therefore, strong anteflexion and lateroflexion with the tip of the probe is needed to avoid the interferences with the bronchus. After anteflexion and lateroflexion of the tip of the probe and forward rotation of the transducer between 0 and 20° or 160 and 180° (Fig. 2), a modified four-chamber view was generated. Although the left cavities were well visualized in this view, the right heart structures, particularly the triscuspid valve and the right ventricle could be partially hidden behind the main bronchus. Systolic and diastolic wall thickness of the free walls of the left and the right ventricle as well as of the septal wall was measured. Further anteflexion and lateroflexion of the tip of the probe at this level allowed the visualization of a short-axis view of the aortic valve and an inflow–outflow view of the right ventricle (Fig. 3). To assess mitral valve function and anatomy in a two-chamber view, a rotation of the transducer angle to 40–60° was used and transmitral Doppler obtained (Fig. 4). The probe was left at the same level in the oesophagus, and the transducer was rotated between 50 and 70° to achieve a mid-oesophageal long-axis view (Fig. 5). The diameters of the aortic annulus, sinus of Valsalva, sinotubular junction and ascending aorta were measured

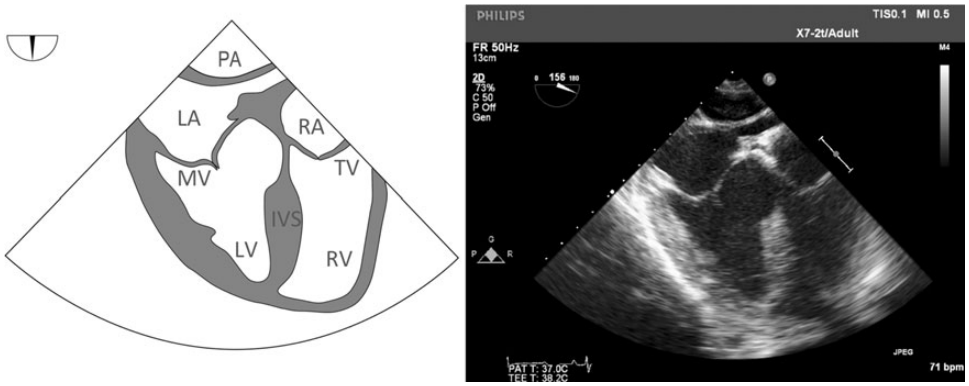

Figure 2: Four-chamber view. Left side shows a schematic. Right side shows an exemplary image. MV: mitral valve; TV: tricuspid valve; IVS: inter-ventricular septum; LV: left ventricle; RV: right ventricle; LA: left atrium; RA: right atrium; PA: pulmonary artery.

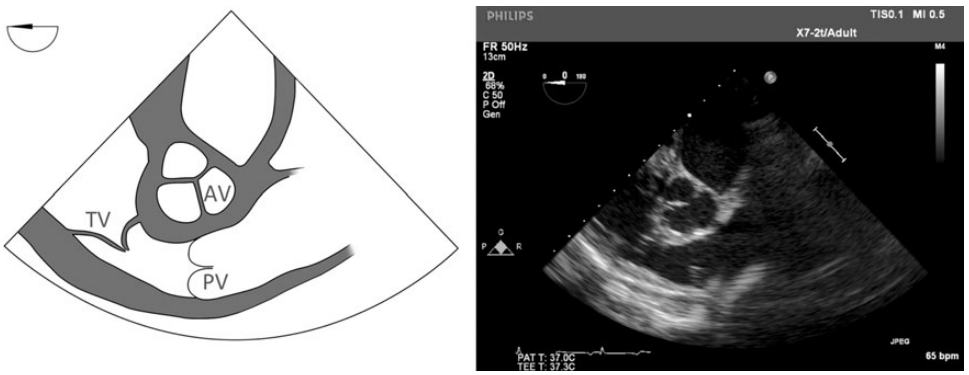

Figure 3: Aortic valve in SAX and right ventricular inflow–outflow view. AV: aortic valve; TV: tricuspid valve; PV: pulmonary valve; SAX: short-axis.

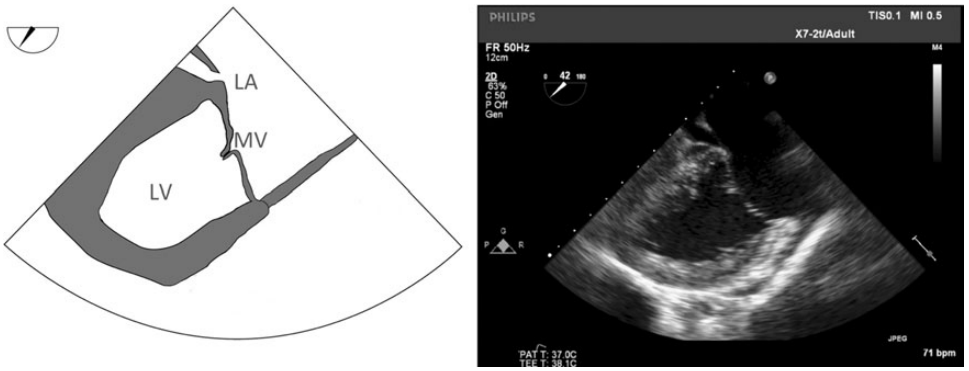

Figure 4: Mitral valve in a two-chamber view. MV: mitral valve; LV: left ventricle; LA: left atrium.

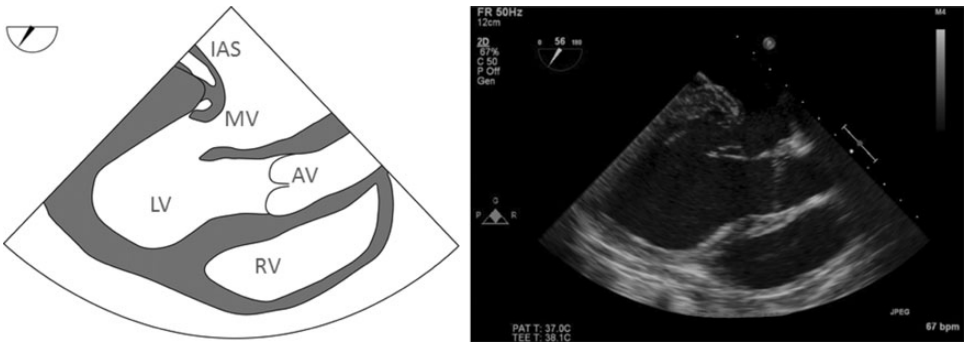

Figure 5: Mid-oesophageal LAX view. Left side shows a schematic. Right side shows an exemplary image. LAX: long-axis; IAS: interatrial septum; MV: mitral valve; AV: aortic valve; LV: left ventricle; RV: right ventricle.

in this view. The left ventricular mid-papillary end-systolic and end-diastolic diameters (LVESD and LVEDD) and the left ventricular end-systolic and end-diastolic volumes (LVESV and LVEDV) using Simpson's rule were assessed and the left ventricular ejection fraction (LVEF) was calculated. Cardiac output was obtained from the multiplication of the ejection volume and the heart rate. Using the 3D software X-Plane on the aortic valve in long-axis, a short-axis of the aortic valve was obtained, with the inflow–outflow view of the right ventricle. From this position, the probe was then pulled back of 10 cm and the transducer angle rotated between 0 and 60°. The aortic and the pulmonary valve could then be seen in long-axis view, parallel to each other and parallel to the probe. Small rotations of the probe were necessary to focus on each valve separately. In this position, Doppler echocardiography was performed to measure the peak and the mean gradient, the peak and the mean jet velocity and the velocity time integral through the aortic and the pulmonary valve (Fig. 6).

Three-dimensional transoesophageal echocardiography

3D imaging of aortic, pulmonary and mitral valves was always possible; 3D imaging of the tricuspid valve was generally more difficult to obtain because of its anterior position and the extremely fine quality of its leaflets. Main focus was laid on the aortic and the mitral valve. Examples are shown in Videos 1 and 2. 3D views of the mitral and the aortic valve were obtained from the long-axis bidimensional imaging (rotation of the probe between 50 and 70° as shown in Fig. 5). For 3D measurement of the mitral valve

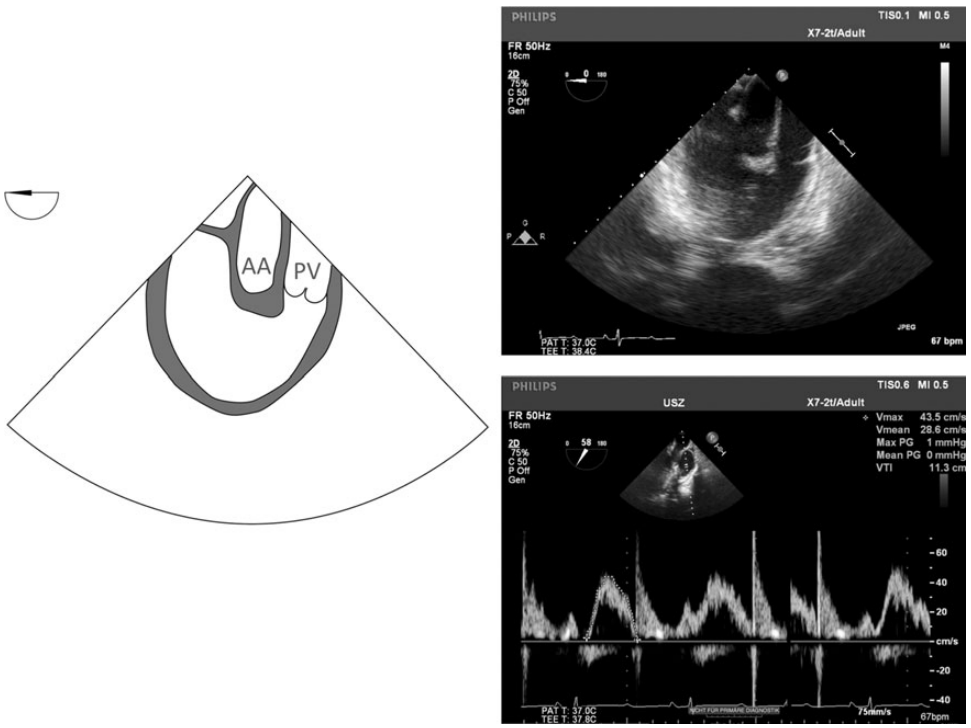

Figure 6: Aorta and pulmonary valve shown in parallel. Left image shows a schematic. Right image shows an exemplary TOE image and the Doppler measurement in the pulmonary valve. AA: ascending aorta; PV: pulmonary valve; TOE: transoesophageal echocardiography.

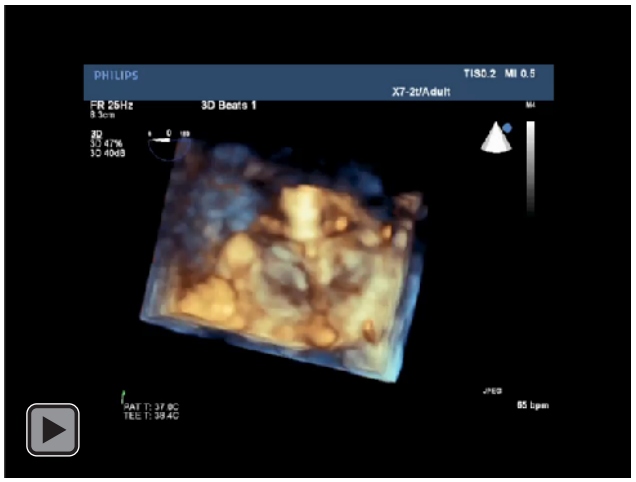

Video 1: 3D Transoesophageal echocardiography of the aortic valve.

Video 2: 3D Transoesophageal echocardiography of the mitral valve.

opening area, we used the 3D quantification software (3DQ–QLab) by Philips Medical Systems. 3DQ is widely used for quantification in 3D. The mitral valve was displayed in three orthogonally orientated planes and the plane in which the measurement was performed was orientated perpendicularly to the valve leaflets. An example of these measurements is shown in Fig. 7.

Statistics

All variables were tested for normal distribution with the Kolmogorow–Smirnow and the Shapiro–Wilk test. If normal distribution was present, the mean with standard deviation was calculated. In all other cases, the median with the range was calculated. To test the correlation of weight and cardiac dimensions, Pearson's *R* was calculated. A *P*-value of <0.05 was defined as high enough to decline the null hypothesis.

RESULTS

Insertion of the TOE probe was possible in all animals. The depth of insertion from the front teeth (incisors) row varied from 40 to 60 cm. The mean depth for visualization of the aortic, the mitral and the tricuspid valves was 53 ± 5 cm. To visualize the pulmonary valve, the probe had to be pulled back ∼10 cm to a mean depth of 45 ± 4 cm (range from 35 to 55 cm). Mean heart rate during the examinations was 67 ± 8 beats per minute. Except in one animal, which had a dilated left ventricle with consecutive mitral valve insufficiency, no pathologies were found. Values for left ventricular dimensions and

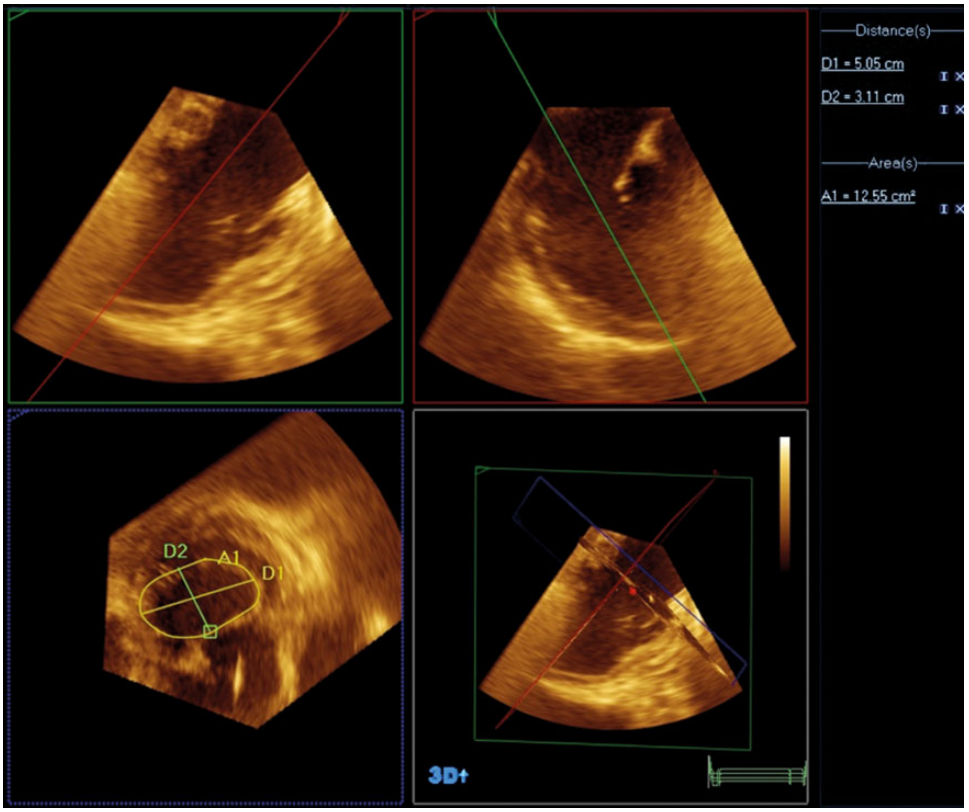

Figure 7: Measurement of the mitral valve dimensions with Philips' QLab. D1: commissure-to-commissure diameter; D2: antero-posterior diameter; A1: mitral valve area.

function, aortic root and aortic dimensions as well as functional parameters for the aortic and the mitral valve are presented in Table 1. With more experience, the pulmonary valve was assessed as well. Results are available for 13 animals.

There was a significant correlation of body weight with the diameters of the aortic annulus ($R = 0.6$; $P < 0.01$), left ventricular outflow tract ($R = 0.7$; $P < 0.001$), sinus of Valsalva ($R = 0.6$; $P < 0.01$) and sinotubular junction ($R = 0.7$; $P < 0.001$). Animals with a body weight of 56–65 kg had annulus diameters of 20–24 mm. All animals with a body weight of >100 kg had annulus diameters of at least 25 mm (up to 30 mm) except one animal with an annulus diameter of 24.4 mm. There was also a correlation of the body weight with the mitral valve annulus area ($R = 0.6$; $P < 0.01$), the antero-posterior ($R = 0.5$; $P < 0.05$) and inter-commissural diameters ($R = 0.7$; $P < 0.001$) of the mitral valve. Animals with a body weight of >95 kg had a mitral valve annulus area of >10.5 cm^2.

DISCUSSION

In this study, we demonstrate feasibility, show landmark data and suggest a method, closely resembling actual TOE standard in humans that can be used as the imaging modality in large porcine model for preclinical testing and training of transcatheter heart valve therapies.

2D and 3D TOE in experimental, closed chest porcine models is feasible. To the best of our knowledge, there is only one study available that systematically describes transoesophageal echocardiographic findings in pigs [11]. At this time, 3D echocardiography was not yet available. In that publication, TOE and intracardiac ultrasound were used to describe cardiac dimensions. Left ventricular diameters and wall thickness were comparable with those of our findings. In contrast, end-systolic and end-diastolic volumes were found to be lower in our study. Consequently, we also found a lower stroke volume but the same LVEF. We used Simpson's rules to measure the ventricular volumes whereas the biplane area-length formula was used previously by Ren *et al*. The use of the modified Simpson's rules to assess left ventricle volume has been shown to be reliable in humans [15]. The ventricular volume might be underestimated because of the foreshortening of the apex in TOE.

Ascending and descending aortic dimensions were similar in both studies. Aortic root dimensions as well as mitral valve dimensions were not published previously in [11]. However, these parameters are important nowadays for the planning of animal experiments. Porcine models play an important role in the development of transcatheter heart valve therapies. The first implantation of a valve in a stent for closed chest aortic valve implantation in a pig model was described in 1992 [16]. In 2002, the first human case of a balloon expandable stent-valve implantation was described [17]. The first human implantation of a CoreValve prosthesis was performed in 2004 [18] after extensive testing in a porcine model [19]. Since then, TAVI grew rapidly and numerous new prostheses appeared on the market. In this setting, acute porcine experiments played and still play an important role. One major topic is the development of new prosthesis. Another main issue is the need for training of the physicians performing the procedures. Many companies request an animal training before the first human implantations for new implanters.

After the rise of TAVI, the mitral valve is the next target for transcatheter therapies. Different devices are under preclinical and clinical testing. Among others, a transcatheter mitral annuloplasty band has been developed and tested heavily in a porcine model [11].

Table 1: Echocardiographic findings in pigs

	Study values pig (n = 20)	Normal values human
Heart rate (bpm)	67 ± 8 [55–81]	
Left ventricular dimensions and function		1.
LVESD (mm)	34 ± 4 [27–41]	22–35[a]
LVEDD (mm)	49.6 ± 4.7 [39–59]	38–52[a]
LVESV (ml)	37.1 ± 10 [22–62]	14–42[a]
LVEDV (ml)	88.4 ± 21.5 [61–147]	46–106[a]
LVEF (%)	58.1 ± 7.4 [47–71]	≥55[a]
BV (ml)	51.9 ± 15 [30–85]	
CO (ml/min)	3421 ± 815.7 [2040–5346]	
CI (ml/min/kg)	43.4 ± 11.5 [19–65]	
IVS wall thickness syst. (mm)	15.5 ± 0.7 [10–21]	6–9[a]
IVS wall thickness diast. (mm)	10.9 [7–13]	6–9[a]
Aortic root and aorta		
Aortic annulus diameter (mm)	24.1 ± 2.5 [20–30]	20–31[b]
Sinus of Valsalva diameter (mm)	30.6 ± 4 [24–39]	29–45[b]
Sinotubular junction diameter (mm)	25.2 ± 4 [20–33]	22–36[b]
Ascending aorta diameter (mm)	24 ± 4 [19–33]	22–36[b]
Descending aorta diameter (mm)	16 ± 5	20–30[b]
Max. jet velocity aortic valve (m/s)	0.75 ± 0.2 [44–128]	
Mean jet velocity aortic valve (m/s)	0.5 ± 0.1 [19–87]	
Max. gradient aortic valve (mmHg)	2 [1–6]	
Mean gradient aortic valve (mmHg)	1 [0–4]	
Mitral valve		
Mitral valve diameter ap (mm)	31.8 ± 4 [25–38]	
Mitral valve diameter cc (mm)	40.5 ± 5 [32–51]	
Mitral valve area (cm^2)	10.7 ± 1.5 [8–13]	
Max. jet velocity mitral valve (cm/s)	57.6 ± 12 [39–83]	
Mean jet velocity mitral valve (cm/s)	29.4 ± 5.5 [20–41]	
Max. gradient mitral valve (mmHg)	1 [1–3]	
Mean gradient mitral valve (mmHg)	0 [0–1]	
Pulmonary valve		
Max. jet velocity pulmonary valve (cm/s)	45 ± 8	
Mean jet velocity pulmonary valve (cm/s)	30 ± 5	
Max. gradient pulmonary valve (mmHg)	0 [0–1]	
Mean gradient pulmonary valve (mmHg)	0 [0–1]	
RV wall thickness systole	8.5 ± 2.1	
RV wall thickness diastole	4.6 ± 1.7	

LVESD: left ventricular end-systolic diameter; LVEDD: left ventricular end-diastolic diameter; LVESV: left ventricular end-systolic volume; LVEDV: left ventricular end-diastolic volume; LVEF: left ventricular ejection fraction; BV: beating volume; CO: cardiac output; CI: cardiac index; IVS: inter-ventricular septum; syst.: in systole; diast.: in diastole; Max.: maximum; ap: anterior–posterior; cc: commissure-to-commissure. RV: right ventricular. All animals and the animal with the pathologic mitral valve are included in Table 1.
[a]Lang *et al*. [13].
[b]Evangelista *et al*. [14].

Transcatheter mitral valve replacement is on the rise. For these therapies, preclinical testing [20, 21] and training are crucial as well. Especially for these new mitral valve therapies, echocardiography is indispensable and has to be started in the preclinical phase. The advantage of TOE in pig models is that, compared with human anatomy, several similarities can be found: the aortic valve is tricuspid and the aortic root dimensions are comparable with the human anatomy as well as cardiac chamber dimensions and the mitral valve anatomy. The mitral valve has an anterior and a posterior leaflet and the annulus has a similar shape. These findings underline that 2D and 3D TOE in animal experiments with pigs represents a useful tool for preclinical testing of transcatheter valve therapies under 'human-like' conditions. Beating heart mitral valve repair procedures, TAVI, as well as atrial and ventricular septal defect device closure all rely on limited intraprocedural visualization that could be enhanced with this guide.

In the present study, we demonstrate feasibility, show landmark data and suggest a method, closely resembling actual TOE standard in humans that can be used in large porcine model for preclinical testing of devices and training of clinicians.

Conflict of interest: none declared.

REFERENCES

[1] http://pubs.nal.usda.gov/sites/pubs.nal.usda.gov/files/srb94-01.html (27 November 2015, date last accessed).
[2] Gallegos RP, Nockel PJ, Rivard AL, Bianco RW. The current state of in-vivo pre-clinical animal models for heart valve evaluation. J Heart Valve Dis 2005;14:423–32.
[3] Kleine P, Abdel-Rahman U, Klesius AA, Scherer M, Simon A, Moritz A. Comparison of hemodynamic performance of Medtronic Hall 21 mm versus St. Jude Medical 23 mm prostheses in pigs. J Heart Valve Dis 2002;11:857–63.
[4] Allan JS, Rose GA, Choo JK, Arn JS, Vesga L, Mawulawde K *et al*. Morphometric analysis of miniature swine hearts as potential human xenografts. Xenotransplantation 2001;8:90–3.

[5] How T. Advances in Hemodynamics and Hemorheology. Elsevier Science, Philadelphia, 1996, 328.
[6] Patel PA, Fassl J, Thompson A, Augoustides JG. Transcatheter aortic valve replacement—part 3: the central role of perioperative transesophageal echocardiography. J Cardiothorac Vasc Anesth 2012;26:698–710.
[7] Zamorano JL, Badano LP, Bruce C, Chan KL, Gonçalves A, Hahn RT *et al.* EAE/ASE recommendations for the use of echocardiography in new transcatheter interventions for valvular heart disease. Eur Heart J 2011;32:2189–214.
[8] Biaggi P, Felix C, Gruner C, Herzog BA, Hohlfeld S, Gaemperli O *et al.* Assessment of mitral valve area during percutaneous mitral valve repair using the MitraClip system: comparison of different echocardiographic methods. Circ Cardiovasc Imaging 2013;6:1032–40.
[9] Flachskampf FA, Wouters PF, Edvardsen T, Evangelista A, Habib G, Hoffman P *et al.* Recommendations for transoesophageal echocardiography: EACVI update 2014. Eur Heart J Cardiovasc Imaging 2014;15:353–65.
[10] Ren JF, Schwartzman D, Lighty GW Jr, Menz V, Michele JJ, Li KS *et al.* Multiplane transesophageal and intracardiac echocardiography in large swine: imaging technique, normal values, and research applications. Echocardiography 1997;14:135–48.
[11] Maisano F, Vanermen H, Seeburger J, Mack M, Falk V, Denti P *et al.* Access transcatheter mitral annuloplasty with a sutureless and adjustable device: preclinical experience. Eur J Cardiothorac Surg 2012;42:524–9.
[12] Svensson LG, Ye J, Piemonte TC, Kirker-Head C, Leon MB, Webb JG. Mitral valve regurgitation and left ventricular dysfunction treatment with an intravalvular spacer. J Card Surg 2015;30:53–4.
[13] Lang RM, Bierig M, Devereux RB, Flachskampf FA, Foster E, Pellikka PA *et al.* Recommendations for chamber quantification. Eur J Echocardiogr 2006;7:79–108.
[14] Evangelista A, Flachskampf FA, Erbel R, Antonini-Canterin F, Vlachopoulos C, Rocchi G *et al.* Echocardiography in aortic diseases: EAE recommendations for clinical practice. Eur J Echocardiogr 2010;11:645–58.
[15] Tortoledo FA, Quiaones MA, Fernandez GC, Waggoner AD, Winters WL. Quantification of left ventricular volumes by two-dimensional echocardiography: simplified and accurate approach. Circulation 1983;67:579–84.
[16] Andersen HR, Knudsen LL, Hasenkam JM. Transluminal implantation of artificial heart valves: description of a new expandable aortic valve and initial results with implantation by catheter technique in closed chest pigs. Eur Heart J 1992;13:704–8.
[17] Cribier A, Eltchaninoff H, Bash A, Borenstein N, Tron C, Bauer F *et al.* Percutaneous transcatheter implantation of an aortic valve prosthesis for calcific aortic stenosis: first human case description. Circulation 2002;106:3006–8.
[18] Grube E, Laborde JC, Zickmann B, Gerckens U, Felderhoff T, Sauren B *et al.* First report on a human percutaneous transluminal implantation of a self-expanding valve prosthesis for interventional treatment of aortic valve stenosis. Catheter Cardiovasc Interv 2005;66:465–9.
[19] Ferrari M, Figulla HR, Schlosser M, Tenner I, Frerichs I, Damm C *et al.* Transarterial aortic valve replacement with a self-expanding stent in pigs. Heart 2004;90:1326–31.
[20] Banai S, Verheye S, Cheung A, Schwartz M, Marko A, Lane R *et al.* Transapical mitral implantation of the Tiara bioprosthesis: pre-clinical results. JACC Cardiovasc Interv 2014;7:154–62.
[21] Iino K, Boldt J, Lozonschi L, Metzner A, Schoettler J, Petzina R *et al.* Off-pump transapical mitral valve replacement: evaluation after one month. Eur J Cardiothorac Surg 2012;41:512–7.

2.4 A translational “humanised” porcine model for transcatheter mitral valve interventions: the neo inferior vena cava approach

Maisano F, Reser D, Pavicevic J, Guidotti A, Denti P, Taramasso M, Addis A, Cesarovic N, Emmert MY, Nietlispach F, Swain J, Falk V, Leon M. A translational "humanised" porcine model for transcatheter mitral valve interventions: the neo inferior vena cava approach. EuroIntervention. 2015 May;11(1):92-5. doi: 10.4244/EIJY15M02_04. PMID: 25671425.

Despite the fact that human and porcine cardiovascular system bare strong resemblance, there are certain differences that could hamper preclinical trials of valvular therapies. In contrast to humans , pigs have anteriorly positioned heart that oriented along the cranio-caudal axes (65). Such anatomical constellation dictates angles between the inferior- / superior vena cava and the central long axis of the heart, that are quite dissimilar to human and can largely influence delivery of devices that rely on transvenous approach. To overcome the dissimilarities, we developed a model that “humanises” porcine anatomy by relocating the access route of inferior vena cava. After right lateral thoracotomy a 10 mm Dacron tube was grafted to the right atrium hence creating a neo-cava approach. This access route was then tested for delivery of an investigational, human-grade transcatheter mitral annuloplasty device. Fluoroscopy time, procedural duration, and procedural success rate were compared to standard trans-femoral approach. Following the ethical approval of Italian Ministry of Health and Swiss Cantonal Veterinary Office (license ZH-138/10), fifty female farm pigs were used (n=15 in trans femoral / transseptal approach and n=35 in neo-cava / transseptal approach). The novel, “humanised” neo-cava approach greatly improved the procedural success rate (97% compared to 0% in standard approach) and reduces procedural as well as fluoroscopic time almost by half. Implanters reported improved device steerability and deployment. Although being more invasive (thoracothomy vs. per cutaneous) neo-cava approach enabled the researchers to reach the mitral annulus in all animals and dramatically increased successful implantation rate. Hence demonstrating large potential not only in improving device testing but also in reducing the number of animals needed. Therefore, such access route should be considered for acute testing of implant that strongly depend on the access through the great veins.

EuroIntervention 2015;11:92-95 published online ahead of print February 2015

A translational "humanised" porcine model for transcatheter mitral valve interventions: the neo inferior vena cava approach

Francesco Maisano[1]*, MD; Diana Reser[1], MD; Jovana Pavicevic[1], MD; Andrea Guidotti[1]; Paolo Denti[2], MD; Maurizio Taramasso[1], MD; Alessandro Addis[3], DMV; Nikola Cesarovic[4], DMV, PhD; Maximilian Y. Emmert[1], MD, PhD; Fabian Nietlispach[5], MD; Julie Swain[6], MD; Volkmar Falk[1], MD; Martin Leon[7], MD

1. Cardiovascular Surgery Department. University Hospital of Zurich, Zurich, Switzerland; 2. Cardiovascular Surgery Unit, San Raffaele Hospital, Milan, Italy; 3. Biotech Research Centre for Cardiothoracic Applications CRABCC, Rivolta d'Adda, Italy; 4. Department of Surgical Research, University Hospital of Zurich, Zurich, Switzerland; 5. Cardiology Department, University Hospital of Zurich, Zurich, Switzerland; 6. Department of Cardiothoracic Surgery, Mount Sinai School of Medicine, New York, NY, USA; 7. Center for Interventional Vascular Therapy, Columbia University Medical Center, New York, NY, USA

KEYWORDS

- animal model
- animal testing
- mitral interventions
- transcatheter annuloplasty

Abstract

Aims: Preclinical studies and translational animal models are fundamental for the development of new clinical interventions. Compared to human anatomy, pigs present a more anterior heart position in the chest which may jeopardise the imaging and testing of devices designed to be delivered to the human mitral valve. To imitate human anatomy, we developed a novel model to "humanise" a pig heart.

Methods and results: The creation of a neo inferior vena cava with a Dacron tube grafted to the right atrium was tested for transseptal delivery of an experimental mitral annuloplasty device in 35 animals. In 15 animals with native anatomy a conventional right transfemoral access was used. Imaging guidance was achieved with intracardiac or epicardial echocardiography. In all transfemoral approaches (n=15), the delivery of the device was unsuccessful and the handling was dissimilar to a human implant. In all neo-cava approaches (n=35), the handling and manoeuvring were as expected in humans, the targets were reached as intended and all procedures but one were successful.

Conclusions: A translational "humanised" animal model with the creation of a neo cava eliminates the differences between pig and human anatomy and is suitable for testing human grade devices.

**Corresponding author: Klinik für Herz- und Gefässchirurgie, UniversitätsSpital Zürich, Rämistrasse 100, CH-8091 Zürich, Switzerland. E-mail: francesco.maisano@usz.ch*

SUBMITTED ON 06/07/2014 - REVISION RECEIVED ON 1st 14/10/2014 / 2nd 05/11/2014 - ACCEPTED ON 14/11/2014

DOI: 10.4244/EIJY15M02_04

Introduction

Reliable translational animal models are necessary to demonstrate proof-of-concept of new interventions and devices. Most preclinical studies are based on either sheep or pig models[1,2]. Despite the similarities with human anatomy, pigs have a more anterior heart position in the chest compared to humans[3], resulting in challenging imaging and device delivery **(Figure 1)**. To overcome the dissimilarities, we developed a model that "humanises" porcine anatomy: the inferior vena cava is relocated creating the same angle to the mitral annulus as seen in humans to facilitate deliverability of mitral valve devices.

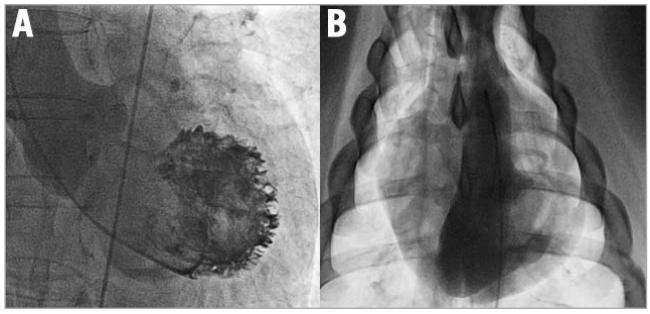

Figure 1. *Different orientation of human and pig left ventricle. A) Anteroposterior view: long axis of the human heart pointing to the left, caudal. B) Anteroposterior view: long axis of the pig heart pointing to the right, caudal.*

Methods

The animal studies were conducted in two facilities in compliance with Italian Ministry of Health national law (116/92), European Union guideline (86/609/EEC) and Swiss Federal animal protection law and ordinance (licence 138/2010 issued by Zürich Cantonal Veterinary Office).

Fifty female farm pigs were used and prepared using standardised protocols. Monitoring known from human cardiac surgery was applied. All animals underwent the same interventional procedure (endovascular implantation of an annuloplasty ring intended to treat mitral regurgitation: Cardioband; Valtech Cardio, Or Yehuda, Israel), but were divided into two groups with different access: group one (n=15) with right transfemoral/transseptal approach (conventional) and group two (n=35) with the novel approach through a right lateral thoracotomy creating a neo cava with a 10 mm Dacron tube grafted to the right atrium **(Figure 2)**. The graft was connected to a custom-made haemostatic valve and oriented with a 45° angle to the midline of the animal to reproduce a "human-like" angulation between the vena cava and the mitral annulus **(Figure 3)**.

To overcome the limitation of transoesophageal echocardiography due to minimal contact of the pig oesophagus with the left atrium, we used intracardiac echocardiography (ICE). To provide concomitant short- and long-axis views of the annulus, we modified the standard approach[4] and used two probes instead of one **(Figure 3)**: femoral vein for transseptal puncture and mitral short-axis view **(Figure 4A, Figure 4D)**, and transapical access for detailed posterior annulus long-axis view **(Figure 4B, Figure 4C)**.

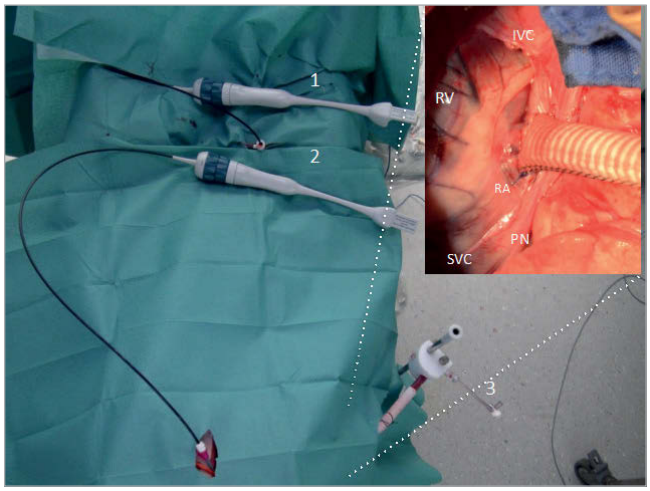

Figure 2. *Set-up. 1) Intracardiac echo probe through right femoral vein. 2) Intracardiac echo probe through apical approach. 3) Neo-cava graft with approximately 45° orientation. The inset picture shows the neo-cava graft. IVC: inferior vena cava; PN: phrenic nerve; RA: right atrium; RV: right ventricle; SVC: superior vena cava*

Due to the different orientation of the heart relative to the chest cavity in the animal model **(Figure 5A)**, a caudal anteroposterior projection **(Figure 5B, Figure 5C)** corresponds to left anterior oblique projection in humans **(Figure 5D)**. The aim of the study was to analyse deliverability of the implant. Success was defined as full deployment along the posterior annulus. Unsuccessful implant was defined as a gap >1 cm between the implant and the commissures.

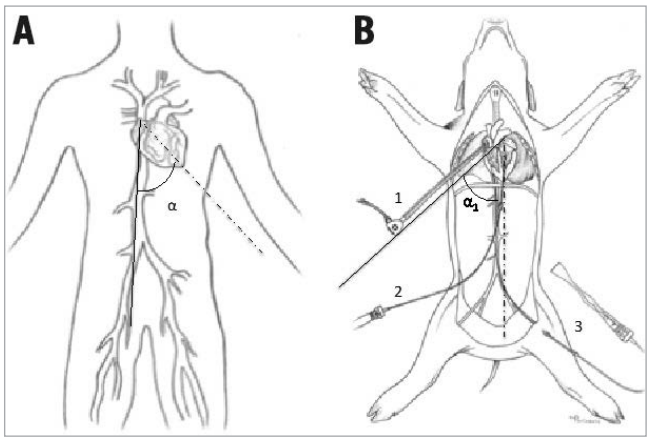

Figure 3. *The different anatomy of human and pig hearts. A) Human: the angle (α) between the axis of the IVC (continuous line) and the long axis of the heart (dotted line) is greater than 45°. B) Pig: the axis of the native IVC and the long axis of the heart (dotted line) are parallel. With the Dacron neo cava (continuous line), the new angle (α_1) is similar to humans. 1: neo cava; 2: transapical ICE; 3: transfemoral ICE*

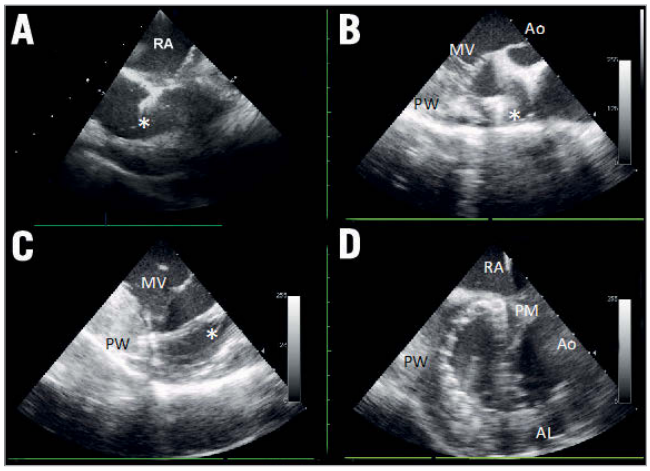

Figure 4. *Intracardiac echo. A) Short axis from transfemoral to guide transseptal puncture: fossa ovalis is tented by the needle (asterisk). B) Long axis from transapical: aortic valve (Ao), mitral valve (MV), left ventricle posterior wall (PW). Asterisk showing the implant pointing towards the target in the anterolateral commissure. C) Long axis from transapical: mitral leaflets (MV). Asterisk indicates the implant connected to the target in the annulus. D) Short axis from transfemoral: implant situated on the entire posterior annulus from the posteromedial commissure (PM) to the anterolateral commissure (AL). RA: right atrium*

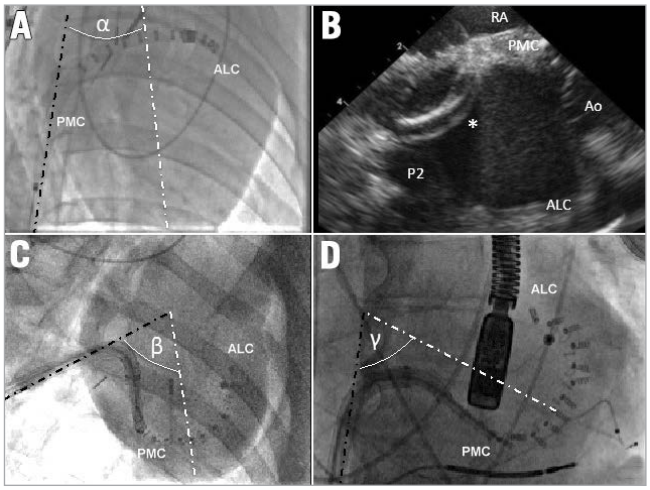

Figure 5. *Effect of neo cava on device delivery. A) Conventional animal approach: the angle (α) between the IVC (dark dotted line) and the left ventricle (white dotted line) is very narrow. B) Although the delivery system (asterisk) is fully steered, its tip does not reach the posteromedial commissure (PMC), and barely touches the posterior annulus (P2). C) & D) Delivering the final anchors of the implant into the PMC: anteroposterior caudal view in the neo-cava approach (C), and left anterior oblique view in a human using the same device (D). With the neo-cava approach (C), the IVC (dark dotted line) and the left ventricular long axis (white dotted line) angle (β) is similar to the angle (γ) observed in humans. The curves on the delivery system at the same stage of implant are comparable in (C) and (D), demonstrating the reproducibility of the animal delivery in humans. ALC: anterolateral commissure; Ao: aortic valve; RA: right atrium*

Results

Procedural timing is shown in **Table 1**. Operators assessed ease-of-use of the delivery system with a subjective usability score **(Table 2)**. In the conventional approach, the manoeuvrability of the device was unlike in humans (tight angle between native vena cava and the heart) and the implant was never successful due to the limited steering of the system to target the posteromedial annulus **(Figure 6A, Figure 6B)**. Through the neo-cava approach, the delivery was successful in all but one animal because the handling and manoeuvring were as in humans. All targets were reached without need for excessive steering **(Figure 6C, Figure 6D)**. The neo-cava approach **(Figure 5C)** increased the angle between the inferior vena cava and the left heart long axis **(Figure 5B)**, reproducing human anatomy **(Figure 5D)**.

Table 1. Procedural data.

	Conventional N=15	Neo cava N=35
Procedure time (minutes)	112±14	72±21
Fluoroscopic time (minutes)	51±12	27±9
Successful implant	0/15 (0%)	34/35 (97%)
Usability score	2.9±0.6	4.8±0.1
Usability score=subjective evaluation of device performance by the operator: 1 (impossible to perform) to 5 (very easy to perform).		

Table 2. Comparison between conventional and neo-cava model.

	Transfemoral	Neo cava
Set-up	Groin access	Right atrial exposure
Deliverability of catheters	Needs proper sheath (limited to max. size) Challenging: – tortuous vessels – large catheters	Any size and length usable
Angulation	Acute angle needs additional steering	Similar to humans
Device deployment	Limited navigation in the left atrium. Excessive steering	Easy navigation and steering

Discussion

Our study shows that a translational "humanised" animal model for transcatheter mitral therapies enables improved deliverability of an annuloplasty device using a "human grade" delivery system. It eliminates the differences between human and animal anatomy resulting in near 100% successful implants while using systems designed for humans in an animal model that would otherwise result in unsuccessful delivery (conventional group) due to technical difficulties caused by different animal anatomy. It also allows for a device insertion in a straight line, as opposed to the tortuous access of the animal femoral veins in the conventional approach.

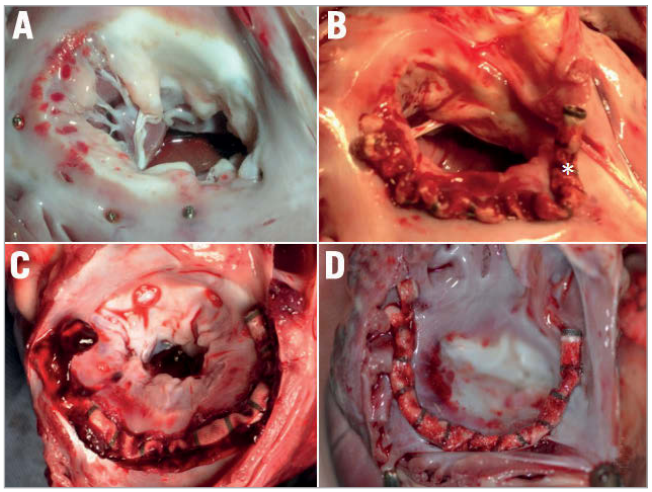

Figure 6. *Post-mortem study following annuloplasty in conventional (A & B) vs. neo-cava animals (C & D). A) Simple anchoring (without device) into the annulus with anchors located distally to the commissures. B) Unsuccessful implant with asterisk indicating the last anchor. The anchors are far away from the commissures. C) & D) Successful implants: anchors located correctly at the level of the commissures.*

When the "human grade" device was delivered by standard transfemoral access in the animal model, the implant was never successful because the posteromedial commissure was not reachable. The handling of the device was neither predictable nor comparable to standard human manoeuvring for other mitral delivery systems.

The limitations of this model are the need for a surgical vascular access requiring a multidisciplinary experimental "Heart Team", and the fact that the two groups were used in sequence. Therefore, the effect of the learning curve cannot be excluded.

In conclusion, although heart anatomy is very similar among mammals, the great vessel anatomy and heart orientation differ between humans and quadrupeds. Such differences may jeopardise animal testing of devices designed to be delivered in humans. A "humanised" animal model involving the creation of a neo inferior vena cava to reproduce the same angle of approach to the heart as in humans is an efficient method to test deliverability of "human grade" devices for mitral valve transcatheter interventions. In addition, multiple ICE catheters can provide ideal imaging to guide experimental interventions.

Impact on daily practice

Preclinical translational animal models are fundamental for the development of new clinical interventions. Compared to human anatomy, pigs have a different heart position which may jeopardise testing of devices designed for human hearts. To imitate human anatomy, we developed a novel model to "humanise" a pig heart: we created a neo inferior vena cava with a Dacron tube grafted to the right atrium for transseptal delivery of an experimental mitral annuloplasty device. In all neo-cava animals (n=35) the handling and manoeuvring was as expected in humans, the targets were reached and all procedures but one were successful. Our "humanised" animal model with a neo cava eliminates the differences between pig and human anatomy and is suitable to test human grade devices.

Conflict of interest statement

F. Maisano, V. Falk, P. Denti, A. Addis and A. Guidotti are consultants for or have received research grants from Valtech Cardio or Abbott Vascular. The other authors have no conflicts of interest to declare.

References

1. Konerding MA, Simpanen J, Ihlberg L, Aittomaki J, Werkkala K, Delventhal V, Ackermann M. Comparison of the novel Medtentia double helix mitral annuloplasty system with the Carpentier-Edwards Physio annuloplasty ring: morphological and functional long-term outcome in a mitral valve insufficiency sheep model. *J Cardiothorac Surg.* 2013;8:70.

2. Kimblad PO, Harnek J, Roijer A, Meurling C, Brandt J, Solem JO. Percutaneous Transvenous Mitral Annuloplasty (PTMA) with the Viking device reduces pacing-induced mitral regurgitation. *EuroIntervention.* 2005;1:346-51.

3. Crick SJ, Sheppard MN, Ho SY, Gebstein L, Anderson RH. Anatomy of the pig heart: comparisons with normal human cardiac structure. *J Anat.* 1998;193:105-19.

4. Webb JG, Maisano F, Vahanian A, Munt B, Naqvi TZ, Bonan R, Zarbatany D, Buchbinder M. Percutaneous suture edge-to-edge repair of the mitral valve. *EuroIntervention.* 2009;5:86-9.

2.5 Septaly Oriented Mild Aortic Regurgitant Jets Negatively Influence Left Ventricular Blood Flow—Insights From 4D Flow MRI Animal Study

Cesarovic N, Weisskopf M, Kron M, Glaus L, Peper ES, Buoso S, Suendermann S, Canic M, Falk V, Kozerke S, Emmert MY, Stoeck CT. Septaly Oriented Mild Aortic Regurgitant Jets Negatively Influence Left Ventricular Blood Flow-Insights From 4D Flow MRI Animal Study. Front Cardiovasc Med. 2021 Aug 9;8:711099. doi: 10.3389/fcvm.2021.711099. PMID: 34434980; PMCID: PMC8380779.

In cases of severe aortic insufficiency (AI) and/or paravalvular leakage, clinical guidelines give clear indication for surgical or interventional treatment. However, in patients suffering from mild-to-moderate AI therapeutic strategy is less clear, as this patient population may display wide variety of symptoms raging from almost none to rapidly developing heart failure. Intrigued by this variety of clinical manifestations caused by similar and relatively small amounts of regurgitant flow, we wondered if the location of the eccentric AI jet, it's trajectory within the left ventricle and subsequent disturbances of the diastolic blood flow patterns could be the catalyst for such different outcomes. Due to the need for close control of parameters such as blood pressure and heart rate, as well as significant patient discomfort related to prolonged MRI examinations, a highly reproducible large animal model was deemed necessary for the purpose of this study. Following ethical approval by the cantonal veterinary office (ZH 213/2019 and ZH 219/2016), 14 animals with a median weight of 65kg were included in the study. A small defect at the leaflet hinge point in either non coronary (NCC) (N=6) or right coronary cusp (RCC) (N=6) of the aortic valve was created by pierce-and-dilate technique in a complete transcatheter fashion, using a steerable sheet, coronary guide wire and a 5mm balloon. Subsequently, blood flow dynamics were investigated by the means of phase contrast (4D Flow) magnetic resonance imaging. Mild aortic insufficiency ie. 14% of stroke volume, was successfully created in 93% of study animals. The origin and trajectory of otherwise comparable mild aortic regurgitant jets, induced different effects on left ventricular blood flow patterns. While regurgitant blood originating from NCC jets got well integrated into the diastolic vortex and was largely contained within the left ventricular outflow tract, blood from the RCC jet firstly collided with the diastolic vortex, markedly reducing its size and finally reached the apical region of left ventricle where it resided over the consequent heartbeat. These findings suggest that aortic insufficiency jets originating from the RCC region have potentially stronger negative effects on the on the left ventricular homeostasis and could potentially lead to more adverse remodeling, as compared to their NCC analogues. Moreover, this study demonstrates the usefulness of porcine model to reliably produce mild aortic insufficiency, by using transcatheter pierce-and-dilate technique. Additionally, with the use of general anesthesia, detailed and prolonged 4D flow MRI examinations with stable hemodynamic conditions (ie. heart rate and blood pressure) could be performed, what is otherwise immensely challenging in human trials.

frontiers in Cardiovascular Medicine

ORIGINAL RESEARCH
published: 09 August 2021
doi: 10.3389/fcvm.2021.711099

Septaly Oriented Mild Aortic Regurgitant Jets Negatively Influence Left Ventricular Blood Flow—Insights From 4D Flow MRI Animal Study

Nikola Cesarovic[1,2], Miriam Weisskopf[3], Mareike Kron[3], Lukas Glaus[1], Eva S. Peper[4], Stefano Buoso[4], Simon Suendermann[2,5], Marko Canic[3], Volkmar Falk[1,2,5], Sebastian Kozerke[4], Maximilian Y. Emmert[2,5,6] and Christian T. Stoeck[4]*

[1] Department of Health Sciences and Technology, Swiss Federal Institute of Technology, Zurich, Switzerland, [2] Department of Cardiothoracic and Vascular Surgery, German Heart Center Berlin, Berlin, Germany, [3] Division of Surgical Research, University Hospital Zurich, University of Zurich, Zurich, Switzerland, [4] Institute for Biomedical Engineering, University and ETH Zürich, Zurich, Switzerland, [5] Department of Cardiovascular Surgery, Charité-Universitätsmedizin Berlin, Berlin, Germany, [6] Institute for Regenerative Medicine, University of Zurich, Zurich, Switzerland

Objectives: Paravalvular leakage (PVL) and eccentric aortic regurgitation remain a major clinical concern in patients receiving transcatheter aortic valve replacement (TAVR), and regurgitant volume remains the main readout parameter in clinical assessment. In this work we investigate the effect of jet origin and trajectory of mild aortic regurgitation on left ventricular hemodynamics in a porcine model.

Methods: A pig model of mild aortic regurgitation/PVL was established by transcatheter piercing and dilating the non-coronary (NCC) or right coronary cusp (RCC) of the aortic valve close to the valve annulus. The interaction between regurgitant blood and LV hemodynamics was assessed by 4D flow cardiovascular MRI.

Results: Six RCC, six NCC, and two control animals were included in the study and with one dropout in the NCC group, the success rate of model creation was 93%. Regurgitant jets originating from NCC were directed along the ventricular side of the anterior mitral leaflet and integrated well into the diastolic vortex forming in the left ventricular outflow tract. However, jets from the RCC were orientated along the septum colliding with flow within the vortex, and progressing down to the apex. As a consequence, the presence as well as the area of the vortex was reduced at the site of impact compared to the NCC group. Impairment of vortex formation was localized to the area of impact and not the entire vortex ring. Blood from the NCC jet was largely ejected during the following systole, whereas ejection of large portion of RCC blood was protracted.

Conclusions: Even for mild regurgitation, origin and trajectory of the regurgitant jet does cause a different effect on LV hemodynamics. Septaly oriented jets originating from RCC collide with the diastolic vortex, reduce its size, and reach the apical region of the left ventricle where blood resides extendedly. Hence, RCC jets display hemodynamic features which may have a potential negative impact on the long-term burden to the heart.

Keywords: paravalvular leakage, 4D flow MRI, vortex formation, intraventricular hemodynamics, aortic regurgitation, mild regurgitation, translational large animal model

OPEN ACCESS

Edited by:
Ali Yilmaz,
University Hospital Münster, Germany

Reviewed by:
Polydoros Kampaktsis,
New York University, United States
Florian Bönner,
Heinrich Heine University of Düsseldorf, Germany

****Correspondence:***
Nikola Cesarovic
nikola.cesarovic@hest.ethz.ch

Specialty section:
This article was submitted to Cardiovascular Imaging, a section of the journal Frontiers in Cardiovascular Medicine

Received: *17 May 2021*
Accepted: *06 July 2021*
Published: *09 August 2021*

Citation:
Cesarovic N, Weisskopf M, Kron M, Glaus L, Peper ES, Buoso S, Suendermann S, Canic M, Falk V, Kozerke S, Emmert MY and Stoeck CT (2021) Septaly Oriented Mild Aortic Regurgitant Jets Negatively Influence Left Ventricular Blood Flow—Insights From 4D Flow MRI Animal Study. Front. Cardiovasc. Med. 8:711099. doi: 10.3389/fcvm.2021.711099

INTRODUCTION

Beside aortic leaflet prolapse and perforation, eccentric aortic valve regurgitation could be caused by paravalvular leakage (PVL) following surgical but more often transcatheter aortic valve replacement. PVL remains a major concern with TAVR and is associated with post-procedural complication created by insufficient sealing between prosthetic valve and the aortic wall. In the past it has been reported that up to 60% of the patients receiving TAVR displayed signs of at least mild aortic regurgitation caused by post-procedural PVL (1). While clinical outcomes and procedural success steadily improved over recent years, still significant regurgitation is observed in more than 17% of cases (2). Presence of moderate/severe aortic regurgitation following TAVR is associated with worse long-term outcomes, impeded reverse remodeling, increased morbidity, and mortality (2–5). Although recent procedural efforts, such as improved prosthesis alignment and commissural overlap (6) as well as adapted implant designs (7), might reduce the likelihood of PVL, the patient pool requiring TAVR has increased considerably, leaving a significant number of patients with this problematic issue (1, 8).

In clinical assessment, regurgitant volume remains the main reference value to determine prognosis and guide therapy in patients with incompetent aortic valve. In cases of severe regurgitation, guidelines give clear therapeutic recommendations (9). However, for mild-to-moderate aortic insufficiency and/or PVL, the situation is less clear. Although it has been shown that moderate or greater PVL induced volume overload following TAVR in patients with hypertrophic left ventricle is one of the causes for increased long-term mortality (2, 4, 10, 11), the effects of the jets origin and trajectory on left ventricular (LV) hemodynamics have not been investigated yet.

Diastolic filling of the left ventricle (LV) is associated with characteristic, vorticial patterns of blood flow (12). These patterns are closely dependent on pressure differences between the cardiac chambers, as well as on the shape and motion of the ventricular walls, valves, and great vessels. Therefore, blood flow patterns have been proposed as a sensitive marker of cardiac health and as a key component of the function itself (13). In pathologies such as myocardial infarction, dilated cardiomyopathy, heart failure, or aortic regurgitations, vortices are disturbed (14–16). Deviations from physiologic diastolic blood flow have also been observed after surgical interventions, creating regurgitant jets at the outer bound of implanted artificial valve (17, 18). In the presence of aortic PVL, turbulent blood flow is reported due to the regurgitant jet, resulting in an increased energy dissipation within the LV (17). As a consequence, the LV not only needs to overcome the volume overload but also requires it to produce additional work (14). Studies employing mathematical models, *in-silico* ventricular models, as well as isolated beating heart experiments clearly demonstrated the effects of significant aortic regurgitant flow on LV energy loss and diastolic vortex formation, highlighting the importance of a more in-depth understanding of its impact on LV myocardial remodeling (18–20).

We hypothesize that in the setting of eccentric mild aortic regurgitation/PVL, not the regurgitant volume *per se*, but rather the regurgitant jet origin and its path within the ventricle affects the diastolic intra-ventricular blood flow with the potential of becoming a predictor or even a catalyst for adverse remodeling and poor clinical outcome.

In this study, we aim to investigate the effects of mild aortic regurgitant/PVL jets originating either from the annular region of either the non-coronary (NCC) or the right coronary cusp (RCC), on diastolic vortex parameters, kinetic energy, and blood residence time. For this purpose, we developed a translational large animal model of mild aortic regurgitation by minimally invasive (transcatheter) piercing of the aortic valve annulus/leaflets and subsequent state of the art cardiovascular magnetic resonance four-dimensional phase contrast flow imaging (4D-flow MRI).

MATERIALS AND METHODS

Animal Protocol

The animal housing and experimental protocols were approved by the Cantonal Veterinary Office, Zurich, Switzerland, under License ZH 213/2019 and ZH 219/2016, and were performed in accordance with Swiss animal protection law and ordinance. Animal housing and experimental procedures also conformed to the European Directive 2010/63/EU of the European Parliament and the Council of September 22, 2010, on the Protection of Animals Used for Scientific Purposes and to the Guide for the Care and Use of Laboratory Animals. A total of 14 female animals (Swiss large white race, 65 $\pm$ 5 kg) were included in this study and split into the following groups: NCC PVL $N = 6$, RCC PVL $N = 6$, and Control $N = 2$. Procedure of PVL creation failed in 1 animal in the NCC group, and hence this animal was excluded from the study.

At the beginning of the experiment, all animals received premedication with ketamine (20 mg/kg), azaperone (1.5 mg/kg), and atropine (0.75 mg) intramuscularly. After loss of postural reflexes, the anesthesia was deepened by a bolus injection of propofol (1–2 mg/kg) to facilitate intubation. Anesthesia maintained with 2–3% isoflurane and propofol (2–5 mg/kg/h) for the remainder of the experiment. Amiodarone (2–3 mg/kg bolus iv) was administered to stabilize the heart rhythm. Pain management included fentanyl infusion (0.02 mg/kg/h) for the duration of the procedure. Aortic valve defects were induced with transcatheter approach by a pierce and dilate technique at the hinge points of the NCC or the RCC, respectively. Due to its symmetrical position as NCC in respect to the mitral valve, close proximity of the orifice of the left coronary artery and potential life threatening complications if partially occluded during the intervention, left coronary cusp (LCC) defect was omitted in this study. In brief, the target point in the NCC or RCC was reached under Echo and Fluoroscopy guidance by using a steerable sheet (Agilis™ EPI Steerable Sheath, 8.5F, St. Jude Medical, Minnetonka, MN, USA). The annulus/leaflet hinge was pierced with a stiff-end of a coronary guide-wire (IRON MAN Guide Wire, 0.014″ 190 cm, Abbott Vascular, Santa Clara CA, USA). The puncture was then dilated with a 5 mm PTCA balloon (NC Emerge MONORAIL™ PTCA Dilation Balloon 5 x 12 mm, Boston Scientific Corporation, Marlborough, MA,

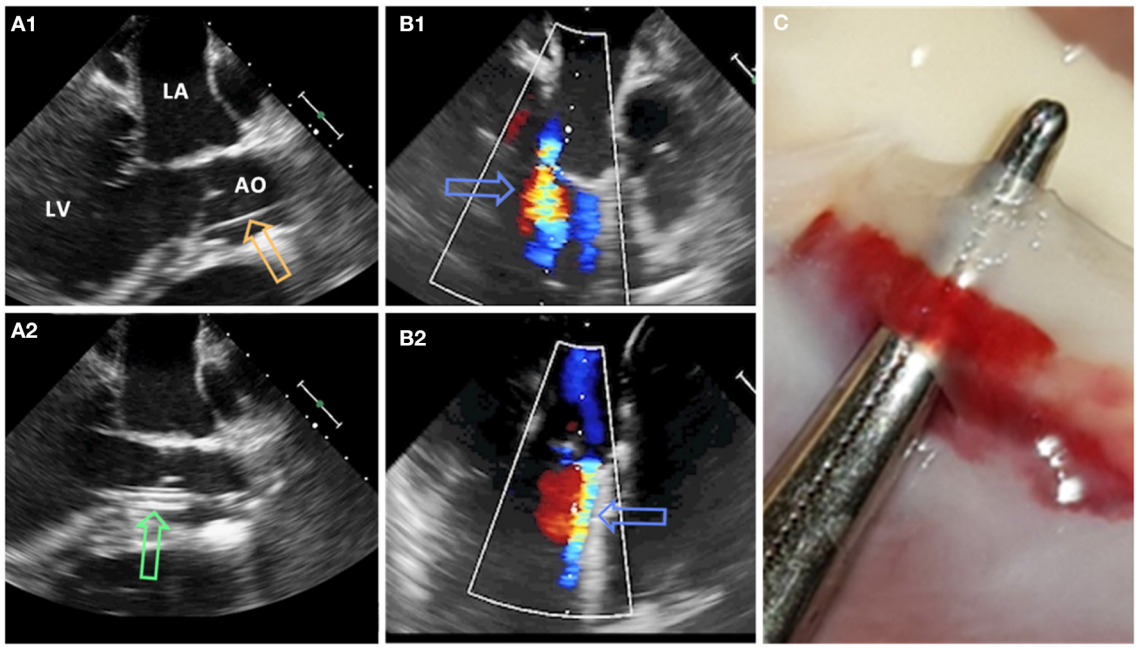

FIGURE 1 | Pierce and dilate technique used to create the model of mild eccentric aortic regurgitation/para valvular leakage (AO, aorta; LA, left atrium; LV, left ventricle). **(A1)** Coronary guide wire (orange arrow) is used to pierce the leaflet/annulus at the hinge point. **(A2)** Standard PTCA 5 mm balloon (green arrow) is positioned across the defect and inflated. **(B1,B2)** Aortic regurgitant jet (blue arrows) originating from NCC and RCC region, respectively. **(C)** Defect of the aortic valve at the hinge point of the leaflet.

USA) (**Figure 1**). Due to the elasticity of non-calcified annular and leaflet tissue, defects have been expected to reduce the size uniformly in all animals. Hence, the effective regurgitant orifice was expected to be smaller than the 5 mm balloon used for dilatation.

After echocardiographic confirmation of the aortic valve defect, animals were transferred to the in-house MR facility where anesthesia was maintained by mechanical ventilation with 2–3% of isoflurane in a 1:1 oxygen/air mixture (4–5 L/min) for the duration of the imaging procedure. On the completion of the study procedure (∼6–8 h long), all animals were euthanized by the administration of an overdose of pentobarbital while still under general anesthesia according to the animal study protocol.

Imaging Protocol

All experiments were performed on a 3 T Philips Ingenia (Philips Healthcare, Best, The Netherlands) system equipped with a 28-channel receiver coil. The imaging protocol was adopted from (21) and in brief consisted firstly of clinical cine sequences for acquisition of the anatomical reference and functional imaging in four-chamber, two chamber, and short axis orientation: field of view (FOV) 281–360 × 198–291 mm^2, slice thickness 8 mm, in-plane resolution 1.9 × 1.9 mm^2, echo time (TE) 1.3–1.4 ms, repetition time (TR) 2.6–2.8 ms, flip angle (FA) 45°, cardiac phases 60. Secondly, 4D-flow MRI with 40 to 50 slices covering the whole heart in four-chamber orientation was acquired: spatial resolution of 2.6 × 2.6 × 2.6 mm^3, FOV of 300 × 197–237 × 80–100 mm^3, flip angle of 7°, TE/TR 2.2–2.3 ms/4.6–4.7 ms, and an isotropic encoding velocity of 160 cm/s. The acquisition was synchronized with the electrocardiogram (ECG) or pulse-oximetry signal, and was retrospectively binned to 18–25 heart phases. Imaging was performed during ventilated breathing, with a total scan duration of ∼45 min.

Data were reconstructed and corrected for concomitant fields using the MRecon software package (GyroTools, Winthertur, Switzerland). Linear eddy-current-induced background phase errors were corrected for by referencing through stationary tissue (22) implemented in GTFlow (GyroTools, Winthertur, Switzerland).

Data Analysis

Data analysis was performed using GTFlow (GyroTools, Winthertur, Switzerland). Four-dimensional flow MRI data were reformatted to identify the mitral valve c in short axis view. In early diastole a region of interest (ROI) was placed by manually drawing a contour at the inner edge of the valve. For vortex analysis, the three-chamber slice orientation was chosen, as it halves the anterior and posterior leaflets of the mitral valve, providing a good view for measuring vortex ring dimensions. For standardization, the three-chamber orientation was aligned to be a long axis view of the heart, including the left ventricular outflow tract showing the branch of the right coronary artery. Mitral valve inflow velocities averages across the mitral valve ROI were measured at defined time points during diastole (TP1, E-wave acceleration; TP2, peak E-wave; TP3, E-wave deceleration; TP4, diastasis; TP5, A-wave acceleration; TP6,

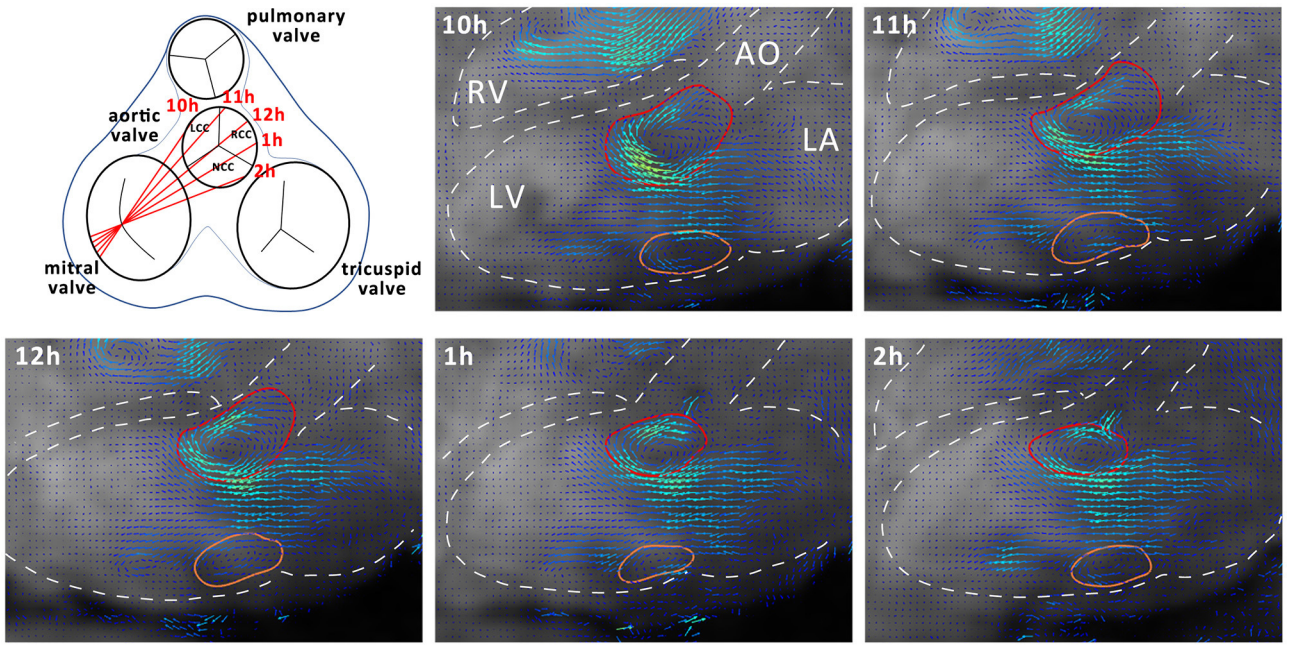

FIGURE 2 | Schematic representation of different observation planes annotated as 10–2 h and example images for vortex cross sectional area estimation. Dashed white lines represent outline of anatomical structures of interest. AO, Aorta; LA, Left Atrium; LV, Left Ventricle; RV, Right Ventricle. Anterior cross section of the vortex is delineated in red and the posterior in orange.

peak A-wave; TP7, A-wave deceleration phase) (21). Blood flow through the left ventricle was visualized using two-dimensional vector field representations in the three-chamber orientation and three-dimensional streamline and path line calculations. By streamline tracking of NCC and RCC jets, the interaction with the mitral valve inflow and diastolic vortices was visualized. To evaluate the effects of different aortic regurgitant jet trajectories on the diastolic vortex, four additional long-axis observational planes were defined as illustrated in **Figure 2**. These long-axis observational cut planes were prescribed rotating the three chamber view around the long axis defined by the center point of the mitral valve in short axis view and the apex covering the width of the aortic valve from the left fibrous trigone to the right fibrous trigone. In this orientation, the 3-dimensional vortex ring was presented as two separate vortices forming behind the anterior and posterior leaflets of the mitral valve (**Figure 2**). Cross-sectional dimensions of the anterior and posterior vortex defined as the largest closed loop of non-zero velocities were measured in each animal. Additionally, the vortex index, defined as the Euclidean norm of the curl of the velocity vector field at each voxel (23) averaged over the vortex cross-sections, was computed and vortex development/change was tracked during E- and A-wave in diastole. Using particle trace counts initialized at the orifice of the PVL jet over diastole, the fraction of the regurgitant blood volume ejected from the left ventricle during the next R-R interval referred to as direct flow was compared for both NCC and RCC PVL groups. Particle tracking analysis failed in one animal in the RCC group.

Ventricular lumen, mitral, and aortic planes were manually segmented at the end systolic frame and tracked over the cardiac cycle using finite element image registration on short axis cine images (24). The tracked mesh was consequently used to mask 4D flow data. The specific energy per voxel was computed as $\frac{1}{2}\rho u^2$ with ρ being the blood density: 1.05 g/cm^3 and u the voxel velocity magnitude. Total specific kinetic energy in the lumen was obtained by summation averaging of the specific kinetic energy of the voxels within the tracked lumen. The inflow and outflow of kinetic energy through the mitral and the aortic valves were computed from the weighted average of the specific kinetic energy of the voxels within the corresponding valve planes.

Statistic

Data on mitral inflow, aortic stroke volume, and regurgitant volume as well as cardiac output and heart rate were reported as mean and min/max values. All data on vortex analysis were presented as mean values and corresponding standard deviation across the individual cohort.

RESULTS

Transcatheter Mild Aortic Regurgitation/PVL Model Creation—Procedural Success 93%

Procedure of model creation (i.e., mild eccentric aortic regurgitation/PVL originating from either NCC or RCC annular region) was successful in 93% of study animals. In one animal (NCC group), a severe regurgitation was introduced and the

TABLE 1 | Hemodynamic values of animals used.

Group	*N*	Heart rate (bpm)	Mitral inflow volume (ml/stroke)	Aortic stroke volume (ml/stroke)	Cardiac output (L/min)	Regurgitant volume (ml/stroke)	Regurgitant fraction %
NCC anterior	5	66 (60–78)	66 (61–80)	71 (55–88)	4.7 (3.7–5.3)	10 (8–14)	14 (10–18)
RCC posterior	6	69 (66–75)	59 (51–66)	71 (61–78)	4.8 (4.2–5.5)	10 (8–13)	14 (11–17)
Control	2	69 (66–71)	74 (69–80)	72 (69–74)	4.8	-	-

No statistically significant difference in heart rate, aortic stroke, and mitral inflow volume as well as in cardiac output could be observed between any of the study groups. PVL/AI regurgitant volume and regurgitant fraction were comparable between the NCC and RCC group.

animal was excluded from the study. Heart rate, mitral inflow, as well as aortic stroke volume and cardiac output were comparable between the groups and averaged at 68 bpm, 64 ml, 71 ml, and 4.8 L/min, respectively (**Table 1**). With a regurgitant fraction of 14% for both NCC and RCC the assessment of the aortic regurgitant volume demonstrated a mild aortic regurgitation as defined by the European Association of Echocardiography (25). However, considering VARC 3 criteria, such regurgitation (RF 14%) would be regarded as trace (26). There was no significant difference between NCC, RCC, and control groups in any parameter. Peak inflow velocities averaged across the mitral valve orifice at peak E-wave (i.e., TP2) were 30 ± 7 cm/s and 33 ± 12 cm/s for the NCC and RCC group, respectively. Mitral inflow velocities were not influenced by the origin and trajectory of the mild aortic regurgitant jet and were comparable to controls at all time points during diastole (NCC/RCC/control: TP1: 19.6 ± 6/20.8 ± 8/20.5 ± 5 cm/s; TP2: 30.6 ± 7/33.8 ± 12 30.5 ± 2 cm/s; TP3 18.7 ± 5/22.7 ± 7/20.8 ± 9 cm/s; TP4: 0.8 ± 2/0.8 ± ¼ ± 6 cm/s; TP5: 14.6 ± 7/10.7 ± 4/14.3 ± 4 cm/s; TP6: 19.4 ± 2/19.5 ± 13/19.2 ± 1 cm/s; TP7: 4.5 ± 3/1.8 ± 4/4.5 ± 7 cm/s).

NCC Jet Did, but RCC Jet Did Not Integrate into the Diastolic Vortex

Streamline tracking (**Figure 3**) revealed that the NCC regurgitant jet got predominantly integrated into the diastolic vortex forming in the left ventricular outflow track and the inflow jet of the mitral valve during the filling phase (E and A phase). Consequently the regurgitant blood was largely contained within the basal segments of the LV. In contrast, the RCC jets were directed along the septum and collided with the anterior vortex in the area of opposing flow direction during both filling phases (E and A phase). During diastasis, the RCC jets reached to the apical region of the LV (**Figure 3**).

RCC Jet Negatively Influenced Timely Development of the Vortex

Additionally, the presence of eccentric mild aortic regurgitation/PVL was found to negatively affect the temporal development of the vortex. A distinct reduction of vortex presence during E-wave was found for the jets originating from RCC, while for the NCC jet the vortex was visible for all timepoints during E-wave except one case during E-wave acceleration (**Table 2**) in the three-chamber view cut plane. Mild aortic regurgitation/PVL induced absence of anterior vortex formation was also found during early A-wave, where 20% of NCC and 0% RCC animals displayed a vortex in the LVOT. The vortex was visible in all control subjects at that timepoint (**Table 2**). During peak A-wave and A-wave deceleration phase, the vortex was visible in all subjects. The presence of the vortex behind the posterior leaflet of the mitral valve was comparable for all animals in this study.

RCC Jet Locally Induced Reduction in Vortex Size

By using multiple cut planes as described in **Figure 2**, assessment of vortex cross sectional areas was performed. In control animals the cross-sectional size of the diastolic vortex was comparable between the observation cut planes at the same heart phase (**Figure 4**). Mild aortic regurgitant jets tended to affect the parts of the vortex ring differently depending on the jets' origins. In the NCC group the vortex size as function of cut plane positions followed the trend of the control animals. The largest cross-sectional area of the anterior diastolic vortex in the direct path of the PVL jet (NCC) was observed during the E-Wave deceleration phase (TP3), which amounted to an average across all NCC animals of 573 mm^2 (range 253–680 mm^2). In contrast, the anterior vortex size was found to be on average 183 mm^2 (range 0–344 mm^2) in the RCC group during the same heart phase. It was noted that the reduction of vortex cross sectional area in the RCC group was found to be localized predominantly in the cut planes around 12 and 1 h as defined in **Figure 2**. For the area of the posterior vortex no differences were found across groups. No differences in average and maximal vorticity index between NCC and RCC PVL animals were found when a vortex was still present.

RCC Regurgitant Blood Displayed Prolonged LV Residence Time

The origin of the mild eccentric regurgitant/PVL jet (either NCC or RCC) and its trajectory within the left ventricle had a profound effect on the residence of the regurgitant blood within the LV lumen across consecutive heart beats. Whereas most of the NCC regurgitant blood volume remained in the basal segments of the LV, RCC regurgitant blood reached further to the apex of the LV and remained within the ventricle during the next ejection phase. Subsequently, the direct flow fraction was calculated to be on average 60% (43–76%) for all NCC subjects and 21% (12–33%) for all RCC subjects (**Figure 5**). Particle tracking illustrated the mixing of the NCC regurgitant blood with the mitral inflow and ejection from the LV cavity in the consecutive heart beat (**Figure 5**).

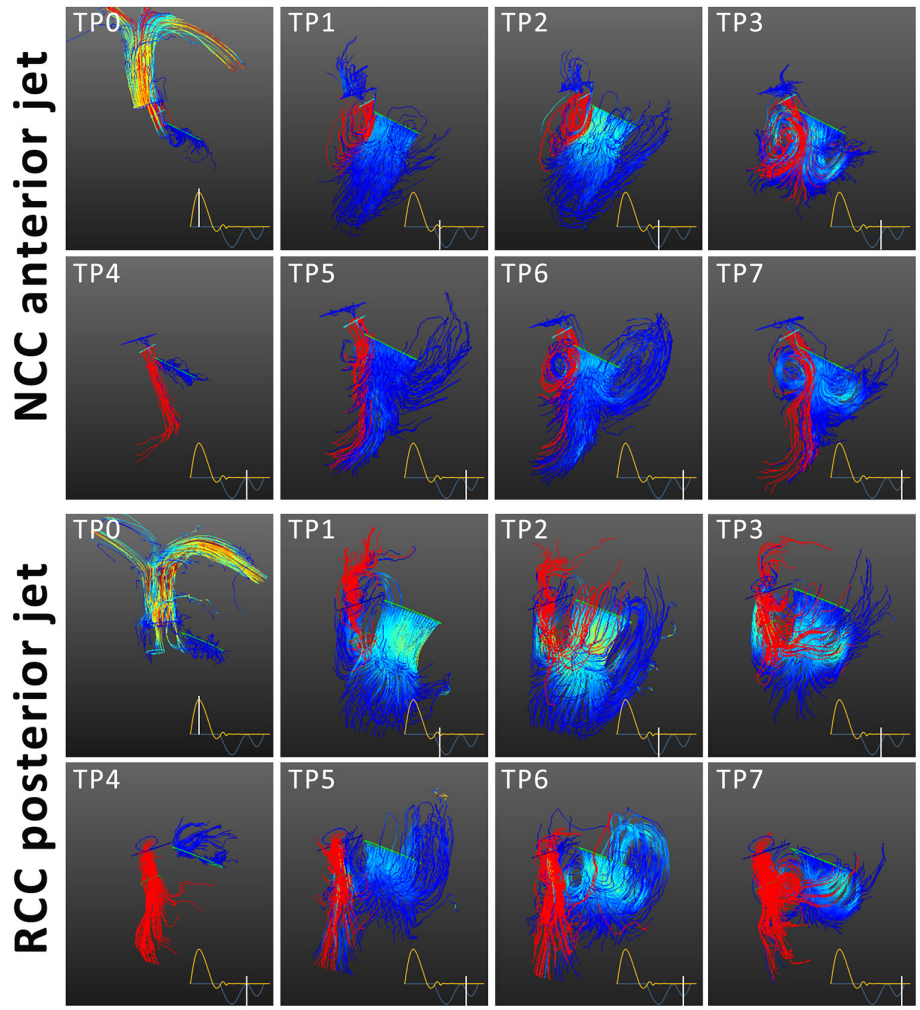

FIGURE 3 | Streamline tracing of blood flow for NCC and RCC paravalvular leakage. Mitral inflow in blue and aortic regurgitant jet in red. The time points correspond to ejection (TP0), E-wave acceleration (TP1) peak E-wave (TP2) E-wave deceleration (TP3), diastasis (TP4), A-wave acceleration (TP5), peak A-wave (TP6), A-wave deceleration phase (TP7). The mitral and aortic streamlines are color coded according to the flow velocities. The regurgitant jet is depicted in red. The NCC jet integrated into the anterior vortex and the mitral inflow jet, while the RCC jet is directed along the septum and collides with the anterior vortex during filling.

TABLE 2 | Presence of anterior and posterior vortex for each time point (TP) at the site of PVL jet impact.

	Group	TP1	TP2	TP3	TP4	TP5	TP6	TP7
		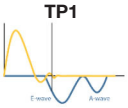	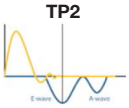	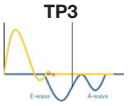	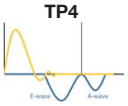	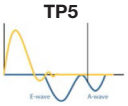	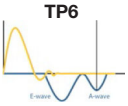	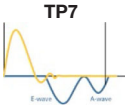
Anterior vortex	NCC	4/5	5/5	5/5	0/5	1/5	5/5	5/5
	RCC	3/6	4/6	4/6	1/6	0/6	6/6	6/6
	Control	2/2	2/2	2/2	1/2	2/2	2/2	2/2
Posterior vortex	NCC	5/5	5/5	5/5	0/5	2/5	5/5	5/5
	RCC	5/6	5/6	5/6	0/6	1/6	5/6	4/6
	Control	2/2	2/2	2/2	1/2	2/2	2/2	2/2

Data presented as fraction of animals where vortex was observed and all animals in the corresponding group. TP1, E-wave acceleration; TP2, peak E-wave; TP3, E-wave deceleration; TP4, diastasis; TP5, A-wave acceleration; TP6, peak A-wave; TP7, A-wave deceleration phase.

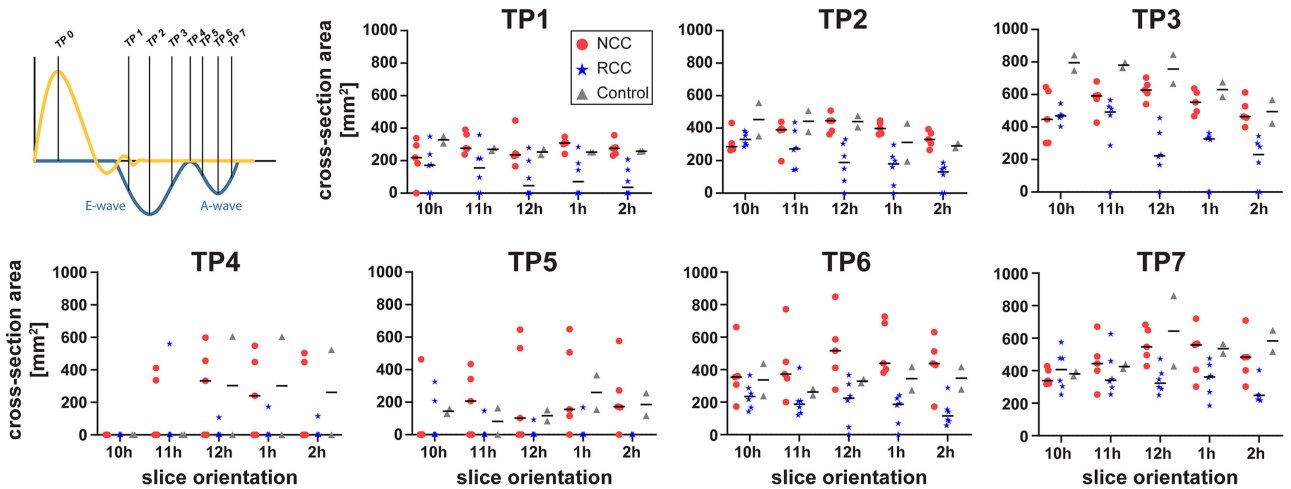

FIGURE 4 | Cross-sectional area of the anterior vortex for different long axis cut planes (according to **Figure 2**) for NCC (red circles), RCC (blue stars), and control (grey triangles) animals.

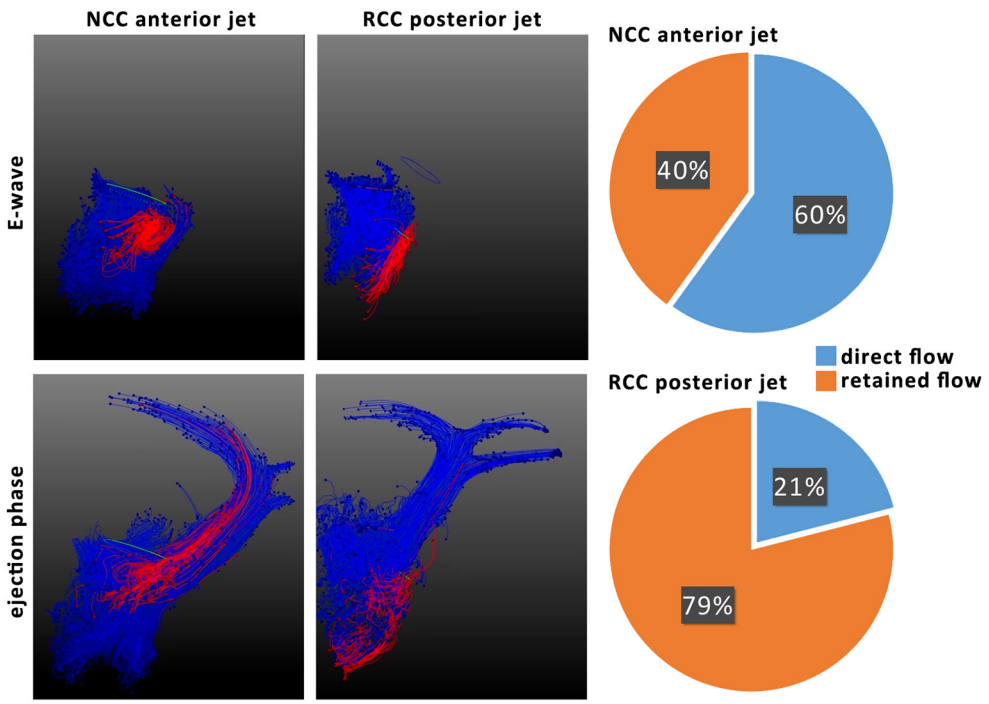

FIGURE 5 | Particle tracking of NCC and RCC regurgitant jets to illustrate residence time of regurgitant blood (left). Particles originating from mitral valve inflow are colored in blue and particles from the regurgitant jet red. Ratios of direct and retained flow of the regurgitant blood volume are shown on the right. Direct flow is the part of diastolic inflowing blood volume that is ejected in the next systole, whereas retained flow represents the diastolic inflow volume that resides in the ventricle for more than 1 heart beat.

Global Left Ventricular Kinetic Energy Was Not Influenced by Mild Aortic PVL Jet

No major difference in specific kinetic energy measured in the LV cavity was found between NCC, RCC, and control group. The specific kinetic energy within the cavity was dominated by the kinetic energy influx through the mitral valve. Concerning the specific kinetic energy flux from the PVL jet, both NCC and RCC jets carried similar specific kinetic energies: TP1: 46.7 ± 35.6/40.6 ± 41.6 J/m^3, TP2: 43.8 ± 20.8/42.3 ± 49.5 J/m^3, TP3: 34.9 ± 16.7/30.1 ± 20.3 J/m^3, TP4: 15.5 ± 8.0/11.6 ± 7.4 J/m^3, TP5: 15.0 ± 5.8/10.9 ± 14.5 J/m^3, TP6: 17.5 ± 8.0/9.6 ± 9.1 J/m^3, and TP7: 13.2 ± 4.7/9.2 ± 7.5 J/m^3. The largest backflow of kinetic energy through the orifice of the PVL was found during early and peak E-wave.

DISCUSSION

In this work we present a novel, minimally invasive (transcatheter), translational large animal model of mild eccentric aortic regurgitation/PVL—a common complication after TAVR procedure. With the developed model, we are able to simulate PVLs originating from the NCC or the RCC annular region, with a procedural success rate of 93%. The cardiac MRI assessment of regurgitant volume, regurgitant fraction, and back flux of kinetic energy by the PVL jets showed no differences between the NCC and RCC groups, demonstrating a large degree of reproducibility across animals even when targeting different leaflets of the aortic valve.

Although there seems to be some misalignment on the classification of the PVL/AR in past studies and current guide lines (2, 25, 26), regurgitation induced in our study (14% regurgitant fraction) can be described as quite discrete (mild or trace depending on classification). PVLs of similar intensity have been found to have no marked influence on long term mortality in clinical trials (2). Still, PVL/AR jets investigated in our study induced local disturbance of vortex formation. However, portions of the vortex ring medial or lateral from the point of jet-impact were only marginally affected and remained comparable to controls, further demonstrating the discrete nature of the induced changes. By analyzing the acquired velocity vector fields, we could show that NCC jets oriented along the ventricular side of the anterior mitral leaflet got integrated in the naturally occurring diastolic vortex in LVOT. Consequently, NCC jets only marginally affected the vortex size. On the other hand, RCC jets were directed along the septal wall and locally reduced the cross-sectional size of the vortex delaying or even prohibiting vortex formation. Reduced vortex size and delayed vortex formation time was observed in patients and confirmed in models simulating left ventricular hypertrophy (27, 28). These findings were attributed to the reduced LV volume not providing sufficient space for proper vortex development, ultimately resulting in increased kinetic energy dissipation (27, 28). Hence, extrapolating these findings to our study of healthy porcine hearts, it could be argued that RCC regurgitant jets induced a "fluid dynamic" correlate to reduction of space available for proper diastolic vortex development in hypertrophic left ventricle. Translated to TAVR patients with ventricular hypertrophy, such unfavorable PVL jet orientation could display additive effects of anatomical and "fluid dynamic" factors effectively leading to even more pronounced blood flow disturbance and kinetic energy dissipation.

As a direct consequence of mild aortic regurgitant/PVL jet origin and trajectory, regurgitant blood originating from NCC PVL remained mostly in the basal area of the LV and was ejected during the consequent heart beat, whereas RCC jets were reaching the apical sections of the LV leaving, to a large extent, the regurgitant blood in the LV during the subsequent contraction. It has been shown previously that direct passage of blood within a single heart beat is associated with preservation of inflow kinetic energy, whilst prolonged durations of blood remaining within the cavity is associated with reduced preservation of kinetic energy (29). In diseases affecting the entire heart such as dilated cardiomyopathy, a significant increase in the retained flow fraction was found (29, 30). It has been shown that despite having a lower fraction of direct flow the specific kinetic energy of the direct flow component was similar to healthy controls. In contrast, the specific kinetic energy of all remaining flow components was elevated in the DCM cohort. The authors hypothesize that changes in specific kinetic energies may alter the interaction of blood flow and myocardial wall. In our study we investigated the localized phenomenon of PVL. We could not find differences in kinetic energies within the left ventricular blood pool, however a significant increase of retained regurgitant blood volume for RCC PVLs together with a local alteration of vortex formation. This effect may chronically impair the interaction of ventricular wall and blood flow and may ultimately stimulate a remodeling process to provide an optimal geometry for efficient flow (15, 31).

In-silico (simulator) studies showed spatial dependency of PVL jets interaction with the ventricular vortex formation and its effects on kinetic energy (18). However, in this occasion severe aortic PVLs with regurgitant fraction of 41% were studied. In contrast clinical, pre-clinical, and simulator studies of central (or indiscriminate) aortic regurgitation could demonstrate that even mild regurgitant jets can cause relevant disturbances for diastolic flow patterns and increase energy dissipation (17, 32, 33). Despite providing valuable insights, such studies were limited to evaluations of hemodynamic effects in a single plain corresponding to PVL jet trajectory. In our study the use of 4D flow, MRI allowed for re-slicing data along the vortex ring showing that the inhibiting effect of mild eccentric aortic regurgitant/PVL jets on vortex formation does not degrade the entire vortex ring. In accordance with the simulator work we found that the RCC location of PVLs alters the ventricular hemodynamics significantly while NCC PVLs do not, for mild leakages. With the translational model presented here, it is possible to induce different scenarios of vortex formation which can be used to investigate the impact of blood flow disturbances on the ventricle. For example, disturbed vortices have been found in patients suffering from heart failure, LV hypertrophy, or after valvular interventions (29, 34, 35). However, the causative vortex-ventricle relations are not yet fully understood.

In the clinical treatment of PVLs great care is given to the regurgitant volume as therapy thresh-hold and predictor of outcome. Translational data shown here suggest caution when dealing with less-than-severe aortic PVLs. Results presented in this study demonstrate that even mild aortic PVL depending on their origin and flow directionality (i.e., more pronounced in RCC than in NCC jets) can adversely impact LV hemodynamics. Although premature to make statements regarding need for treatment of less-than-severe PVLs, translational insights from this study suggest that analysis of jet origin and trajectory should be investigated in a longitudinal study to assess potential for risk stratification in patients suffering from aortic PVLs.

Although there are some anatomical and physiological differences, porcine cardiac structures and hemodynamic parameters closely resemble that of humans. The translational large animal model of mild eccentric aortic regurgitation/PVL used in this study allows MRI based investigation of blood

flow patterns under controlled and reproducible conditions (i.e., general anesthesia, controlled ventilation, heart rate, and blood pressure). PVLs with standardized regurgitant flow, fraction, and orifice area, induced in a trans-catheter fashion in a native aortic valve of healthy pigs, further helped isolate the effects of regurgitant flow without restraining factors such as comorbidities. The proposed animal model (i.e., without TAVR implant) also greatly facilitates imaging of PVLs as implanted prosthetic valve scaffolding could lead to severe off-resonance artifacts when imaged by MRI. Resulting signal voids appear not only at the site of implantation but also reach into the LVOT. As a consequence, it is very challenging to image PVL jets at their origin in the proximity of the implant by 4D flow MRI. Furthermore, without major manipulations of the TAVR implant itself, it would be challenging to obtain reproducible PVLs (if any) in the healthy porcine model. On the other hand, imaging performed on human-grade scanners ultimately facilitates the translation of study results into patients. Hence, the animal study presented here provides translational insights on effects of mild aortic PVL, for a patient population that would be, otherwise, challenging to investigate.

Study Limitations

This study was performed under general anesthesia, which has an effect on heart rate as well as on blood pressure, consequently affecting the afterload of the heart. Changes in systemic blood pressure may alter regurgitant volume and jet velocities altering the effect of PVL jets on ventricular blood flow patterns. In the *in-vivo* animal model, these physiological parameters may be controlled pharmaceutically. A less challenging control of environmental parameters has been proposed in isolated beating pig hearts with good data quality and reproducibility (20). Further, only healthy animals without prior aortic valve stenosis and respective left ventricular hypertrophy have been used in this study. Hence the effects of prior disease as it would be observed in clinical patients receiving TAVR as well as PVL jets impact on flow patterns within a hypertrophic left ventricle could not be reflected in our study and should be mirrored in future trials. Moreover, invasive hemodynamic assessment (e.g., pressure-volume loop analysis) could have provided more insight of effects of volume overload caused by mild AI/PVL, especially as no differences in kinetic energy were observed between the groups in our study. As they were not implemented in the current trial, such measurements should be considered going forward.

Conclusion

We have established a translational large animal model to create PVLs with a transcatheter technique and assessed their impact on left ventricular hemodynamics by 4D flow MRI.

The origin and trajectory of otherwise comparable mild aortic PVL jets induced different effects on diastolic LV hemodynamics. While regurgitant blood originating from NCC PVL jets got well integrated into the diastolic vortex and was largely contained within the LVOT, RCC jets firstly collided with the vortex, markedly reducing its size, and finally reached the apical region of LV where it resided over the consequent heartbeat.

These translational results suggest that investigating origin and trajectory of mild aortic PVL jets may provide additional information for decision making regarding interventions and potentially play a key role for long-term remodeling in affected patients.

DATA AVAILABILITY STATEMENT

The raw data supporting the conclusions of this article will be made available by the authors, without undue reservation.

ETHICS STATEMENT

The animal study was reviewed and approved by Zurich cantonal Veterinary Office.

AUTHOR CONTRIBUTIONS

NC: conceptualization, study design, development of animal model, surgical procedure, animal handling, data acquisition, data analysis, statistical analysis, and preparation and review of manuscript. MW, MK, and MC: development of animal model, surgical procedure, and animal handling. LG, EP, and SB: data analysis and review of manuscript. VF, SS, SK, and ME: data interpretation and critical review of the manuscript. CS: conceptualization, study design, data acquisition, data reconstruction, data analysis, and preparation and review of manuscript. All authors contributed to the article and approved the submitted version.

FUNDING

This project has been funded in parts by the Swiss national science foundation grant PZ00P2_174144.

REFERENCES

1. Dvir D, Barbash IM, Ben-Dor I, Torguson R, Badr S, Minha S, et al. Paravalvular regurgitation after transcatheter aortic valve replacement: diagnosis, clinical outcome, preventive and therapeutic strategies. *Cardiovasc Revasc Med.* (2013) 14:174-81. doi: 10.1016/j.carrev.2013.02.003
2. Ribeiro HB, Orwat S, Hayek SS, Larose E, Babaliaros V, Dahou A, et al. Cardiovascular magnetic resonance to evaluate aortic regurgitation after transcatheter aortic valve replacement. *J Am Coll Cardiol.* (2016) 68:577-85. doi: 10.1016/j.jacc.2016.05.059
3. Kodali S, Pibarot P, Douglas PS, Williams M, Xu K, Thourani V, et al. Paravalvular regurgitation after transcatheter aortic valve replacement with the Edwards sapien valve in the PARTNER trial: characterizing patients and impact on outcomes. *Eur Heart J.* (2015) 36:449-56. doi: 10.1093/eurheartj/ehu384
4. Hayashida K, Lefevre T, Chevalier B, Hovasse T, Romano M, Garot P, et al. Impact of post-procedural aortic regurgitation on mortality after transcatheter aortic valve implantation. *JACC Cardiovasc Interv.* (2012) 5:1247-56. doi: 10.1016/j.jcin.2012.09.003
5. Kampaktsis PN, Subramayam P, Sherifi I, Vavuranakis M, Siasos G, Tousoulis D, et al. Impact of paravalvular leak on left ventricular remodeling and global

longitudinal strain 1 year after transcatheter aortic valve replacement. *Future Cardiol.* (2021) 17:337-45. doi: 10.2217/fca-2020-0086
6. Tang GHL, Zaid S, Fuchs A, Yamabe T, Yazdchi F, Gupta E, et al. Alignment of Transcatheter Aortic-Valve Neo-Commissures (ALIGN TAVR): impact on final valve orientation and coronary artery overlap. *JACC Cardiovasc Interv.* (2020) 13:1030-42. doi: 10.1016/j.jcin.2020.02.005
7. Mollmann H, Holzhey DM, Hilker M, Toggweiler S, Schafer U, Treede H, et al. The ACURATE neo2 valve system for transcatheter aortic valve implantation: 30-day and 1-year outcomes. *Clin Res Cardiol.* (2021). doi: 10.1007/s00392-021-01882-3. [Epub ahead of print].
8. Popma JJ, Deeb GM, Yakubov SJ, Mumtaz M, Gada H, O'Hair D, et al. Transcatheter aortic-valve replacement with a self-expanding valve in low-risk patients. *N Engl J Med.* (2019) 380:1706-15. doi: 10.1056/NEJMoa1816885
9. Baumgartner H, Falk V, Bax JJ, De Bonis M, Hamm C, Holm PJ, et al. 2017 ESC/EACTS Guidelines for the management of valvular heart disease. *Eur Heart J.* (2017) 38:2739-91. doi: 10.1093/eurheartj/ehx391
10. Jones BM, Tuzcu EM, Krishnaswamy A, Popovic Z, Mick S, Roselli EE, et al. Prognostic significance of mild aortic regurgitation in predicting mortality after transcatheter aortic valve replacement. *J Thorac Cardiovasc Surg.* (2016) 152:783-90. doi: 10.1016/j.jtcvs.2016.05.023
11. Kampaktsis PN, Ullal AV, Minutello RM, Feldman DN, Swaminathan RV, Voudris K, et al. Impact of paravalvular aortic insufficiency on left ventricular remodeling and mortality after transcatheter aortic valve replacement. *J Heart Valve Dis.* (2016) 25:301-8.
12. Arvidsson PM, Kovacs SJ, Toger J, Borgquist R, Heiberg E, Carlsson M, et al. Vortex ring behavior provides the epigenetic blueprint for the human heart. *Sci Rep.* (2016) 6:22021. doi: 10.1038/srep22021
13. Kanski M, Arvidsson PM, Toger J, Borgquist R, Heiberg E, Carlsson M, et al. Left ventricular fluid kinetic energy time curves in heart failure from cardiovascular magnetic resonance 4D flow data. *J Cardiovasc Magn Reson.* (2015) 17:111. doi: 10.1186/s12968-015-0211-4
14. Pedrizzetti G, Sengupta PP. Vortex imaging: new information gain from tracking cardiac energy loss. *Eur Heart J Cardiovasc Imaging.* (2015) 16:719-20. doi: 10.1093/ehjci/jev070
15. Kilner PJ, Yang GZ, Wilkes AJ, Mohiaddin RH, Firmin DN, Yacoub MH. Asymmetric redirection of flow through the heart. *Nature.* (2000) 404:759-61. doi: 10.1038/35008075
16. Hirasawa K, Izumo M, Sasaoka T, Ashikaga T, Suzuki K, Harada T, et al. Effect of aortic regurgitant jet direction on mitral valve leaflet remodeling: a real-time three-dimensional transesophageal echocardiography study. *Sci Rep.* (2017) 7:8884. doi: 10.1038/s41598-017-09252-8
17. Stugaard M, Koriyama H, Katsuki K, Masuda K, Asanuma T, Takeda Y, et al. Energy loss in the left ventricle obtained by vector flow mapping as a new quantitative measure of severity of aortic regurgitation: a combined experimental and clinical study. *Eur Heart J Cardiovasc Imaging.* (2015) 16:723-30. doi: 10.1093/ehjci/jev035
18. Morisawa D, Falahatpisheh A, Avenatti E, Little SH, Kheradvar A. Intraventricular vortex interaction between transmitral flow and paravalvular leak. *Sci Rep.* (2018) 8:15657. doi: 10.1038/s41598-018-33648-9
19. Keshavarz-Motamed Z, Khodaei S, Rikhtegar Nezami F, Amrute JM, Lee SJ, Brown J, et al. Mixed Valvular disease following transcatheter aortic valve replacement: quantification and systematic differentiation using clinical measurements and image-based patient-specific *in silico* modeling. *J Am Heart Assoc.* (2020) 9:e015063. doi: 10.1161/JAHA.119.015063
20. Peper ES, Leopaldi AM, van Tuijl S, Coolen BF, Strijkers GJ, Baan J, Jr., et al. An isolated beating pig heart platform for a comprehensive evaluation of intracardiac blood flow with 4D flow MRI: a feasibility study. *Eur Radiol Exp.* (2019) 3:40. doi: 10.1186/s41747-019-0114-5
21. Cesarovic N, Busch J, Lipiski M, Fuetterer M, Fleischmann T, Born S, et al. Left ventricular blood flow patterns at rest and under dobutamine stress in healthy pigs. *NMR Biomed.* (2019) 32:e4022. doi: 10.1002/nbm.4022
22. Busch J, Giese D, Kozerke S. Image-based background phase error correction in 4D flow MRI revisited. *J Magn Reson Imaging.* (2017) 46:1516-25. doi: 10.1002/jmri.25668
23. von Spiczak J, Crelier G, Giese D, Kozerke S, Maintz D, Bunck AC. Quantitative analysis of vortical blood flow in the thoracic aorta using 4D phase contrast MRI. *PLoS ONE.* (2015) 10:e0139025. doi: 10.1371/journal.pone.0139025
24. Genet M, Stoeck CT, von Deuster C, Lee LC, Kozerke S. Equilibrated warping: finite element image registration with finite strain equilibrium gap regularization. *Med Image Anal.* (2018) 50:1-22. doi: 10.1016/j.media.2018.07.007
25. Lancellotti P, Tribouilloy C, Hagendorff A, Moura L, Popescu BA, Agricola E, et al. European Association of Echocardiography recommendations for the assessment of valvular regurgitation. Part 1: aortic and pulmonary regurgitation (native valve disease). *Eur J Echocardiogr.* (2010) 11:223-44. doi: 10.1093/ejechocard/jeq030
26. Varc-3 Writing C, Genereux P, Piazza N, Alu MC, Nazif T, Hahn RT, et al. Valve Academic Research Consortium 3: updated endpoint definitions for aortic valve clinical research. *Eur Heart J.* (2021) 42:1825-57. doi: 10.1093/eurheartj/ehaa799
27. Samaee M, Nelsen N, Gaddam M, Santhanakrishnan A. Diastolic vortex alterations with reducing left ventricular volume: an *in vitro* study. *J Biomech Eng.* (2020). 142:121006. doi: 10.1115/1.4047663
28. Pagel PS, Hudetz JA. Chronic pressure-overload hypertrophy attenuates vortex formation time in patients with severe aortic stenosis and preserved left ventricular systolic function undergoing aortic valve replacement. *J Cardiothorac Vasc Anesth.* (2013) 27:660-4. doi: 10.1053/j.jvca.2013.01.007
29. Eriksson J, Bolger AF, Ebbers T, Carlhall CJ. Four-dimensional blood flow-specific markers of LV dysfunction in dilated cardiomyopathy. *Eur Heart J Cardiovasc Imaging.* (2013) 14:417-24. doi: 10.1093/ehjci/jes159
30. Svalbring E, Fredriksson A, Eriksson J, Dyverfeldt P, Ebbers T, Bolger AF, et al. Altered diastolic flow patterns and kinetic energy in subtle left ventricular remodeling and dysfunction detected by 4D flow MRI. *PLoS ONE.* (2016) 11:e0161391. doi: 10.1371/journal.pone.0161391
31. Richter Y, Edelman ER. Cardiology is flow. *Circulation.* (2006) 113:2679-82. doi: 10.1161/CIRCULATIONAHA.106.632687
32. Okafor I, Raghav V, Condado JF, Midha PA, Kumar G, Yoganathan AP. Aortic regurgitation generates a kinematic obstruction which hinders left ventricular filling. *Ann Biomed Eng.* (2017) 45:1305-14. doi: 10.1007/s10439-017-1790-z
33. Di Labbio G, Kadem L. Jet collisions and vortex reversal in the human left ventricle. *J Biomech.* (2018) 78:155-60. doi: 10.1016/j.jbiomech.2018.07.023
34. Stoll VM, Hess AT, Rodgers CT, Bissell MM, Dyverfeldt P, Ebbers T, et al. Left ventricular flow analysis. *Circ Cardiovasc Imaging.* (2019) 12:e008130. doi: 10.1161/CIRCIMAGING.118.008130
35. Morichi H, Itatani K, Yamazaki S, Numata S, Nakaji K, Tamaki N, et al. Influences of mitral annuloplasty on left ventricular flow dynamics assessed with 3-dimensional cine phase-contrast flow magnetic resonance imaging. *J Thorac Cardiovasc Surg.* (2020). doi: 10.1016/j.jtcvs.2020.04.127. [Epub ahead of print].

Conflict of Interest: VF has relevant (institutional) financial activities outside the submitted work with following commercial entities: Medtronic GmbH, Biotronik SE & Co., Abbott GmbH & Co. KG, Boston Scientific, Edwards Lifesciences, Berlin Heart, Novartis Pharma GmbH, JOTEC/CryoLife GmbH, Zurich Heart.

The remaining authors declare that the research was conducted in the absence of any commercial or financial relationships that could be construed as a potential conflict of interest.

Publisher's Note: All claims expressed in this article are solely those of the authors and do not necessarily represent those of their affiliated organizations, or those of the publisher, the editors and the reviewers. Any product that may be evaluated in this article, or claim that may be made by its manufacturer, is not guaranteed or endorsed by the publisher.

2.6 Early myocardial damage (EMD) and valvular insufficiency result in impaired cardiac function after multiple trauma in pigs

Weber B, Lackner I, Baur M, Gebhard F, Pfeifer R, Cinelli P, Halvachizadeh S, Teuben M, Pape HC, Imhof A, Lipiski M, Cesarovic N#, Kalbitz M#. Early myocardial damage (EMD) and valvular insufficiency result in impaired cardiac function after multiple trauma in pigs. Sci Rep. 2021 Jan 13;11(1):1151. doi: 10.1038/s41598-020-80409-8. PMID: 33441945; PMCID: PMC7806767.
 # Contributed equally

Valvular heart disease does not only have to be caused by degenerative or infectious processes. Abnormal echocardiographic findings are made in 1/3 of multiple trauma patients with cardiac injury being found in 12% of all blunt trauma fatalities (66, 67). Due to the anatomical location of the heart in the anterior thorax, the right ventricle and atrium are the most frequently injured parts of the heart in trauma patients (68). Moreover, there have been several reports describing severe valvular regurgitations developing following car accidents resulting in blunt chest trauma (69). Therefore, the aim of this study was to conduct a detailed analysis of cardiac function after multiple trauma in pigs in combination with local and systemic detection of cardiac damage. Following ethical approval (ZH 138/2017) 15 male pigs with mean body length of 126 cm and weight of 50 kg were included in the study in either multiple trauma (n=10) or a sham control group (n=5). Multiple trauma was performed in general anesthesia and was defined by a blunt chest trauma, a liver laceration, a haemorrhagic shock and a femur fracture, whereas control sham animals just received anesthesia. Thirty minutes after index event, therapy was initiated, femoral fracture treated, liver packed and lost blood volume replenished. Unsurprisingly data from multiple trauma group revealed an increase in shock index (heart rate / systolic blood pressure). However, analysis of cardiac damage markers revealed an increase of HFABP (Heart fatty acid binding protein) which is known to be a very early marker for cardiac damage after myocardial trauma. Furthermore, following trauma 5/6 animals demonstrated tricuspid and 6/6 pulmonary valve regurgitation, which in some cases worsened over the 6h observation period. This regurgitation coincided with a decrease in left ventricular diastolic pressure, influenced by the volume reaching the left ventricle.

Our study successfully demonstrated multiple levels of damage caused to the heart by blunt chest trauma. One important consequence of cardiac injury, especially in case of direct mechanical impact on the chest, is the impairment of heart valves. However, published case reports of traumatic valvular damage vary widely on observed symptoms: patients are described to be asymptomatic for years or become hemodynamic instable directly after trauma.

We could demonstrate an incidence of immediate tricuspid and pulmonary valvular dysfunction that was much higher than described until now. Which leads to questions regarding potential clinical under-diagnosis in the setting of acute trauma. Despite the fact that in case of traumatic valvular dysfunction, frequently there is a minimal initial valvular regurgitation, that might progress gradually, such long term effects were out of scope of this study.

scientific reports

Check for updates

OPEN

Early myocardial damage (EMD) and valvular insufficiency result in impaired cardiac function after multiple trauma in pigs

Birte Weber[1], Ina Lackner[1], Meike Baur[1], Florian Gebhard[1], Roman Pfeifer[2], Paolo Cinelli[2], Sascha Halvachizadeh[2], Michel Teuben[2], Hans-Christoph Pape[2], Armin Imhof[3], Miriam Lipiski[4], Nikola Cesarovic[4,5,6] & Miriam Kalbitz[1,6]✉

One third of multiple trauma patients present abnormal echocardiographic (ECHO) findings. Therefore, ECHO diagnostic after trauma is indicated in case of hemodynamic instability, shock, after chest trauma and after cardiac arrest. 20 male pigs underwent multiple trauma. Blood samples were collected 4 and 6 h after trauma and concentrations of heart-type fatty acid binding protein (HFABP) as a biomarker for EMD were measured. Myocardial damage was evaluated by scoring Hematoxylin–Eosin stained sections. At baseline, 3 and 6 h after trauma, transesophageal ECHO (TOE) was performed, invasive arterial and left ventricular blood pressure were measured to evaluate the cardiac function after multiple trauma. Systemic HFABP concentrations were elevated, furthermore heart injury score in multiple trauma animals was increased determining EMD. A significant decrease of blood pressure in combination with a consecutive rise of heart frequency was observed. Ongoing depression of mean arterial pressure and diastolic blood pressure were accompanied by changes in ECHO-parameters indicating diastolic and systolic dysfunction. Furthermore, a valvular dysfunction was detected. In this study complex myocardial and valvular impairment after multiple trauma in pigs has been observed. Therefore, detection of EMD and progressive valvular dysfunction might be crucial and therapeutically relevant.

Abbreviations

ATLS	Advanced trauma life support
A-wave	Peak velocity flow in late diastole
BL	Baseline
CI	Contractility index
CO	Cardiac output
Diast.	Diastolic blood pressure
+ dp/dt max	Max positive value of first derivate of pressure during cardiac cycle
-dp/dt min	Max negative value of the first derivate of pressure during cardiac cycle
ECHO	Echocardiography
EDV	End-diastolic volume
EF	Ejection fraction
ELISA	Enzyme-linked immunosorbent assay
EMD	Early myocardial damage
ESV	End-systolic volume
E-wave	Peak velocity blood flow in early diastole

[1]Department of Traumatology, Hand, Plastic and Reconstructive Surgery, Center of Surgery, University of Ulm Medical School, Albert-Einstein-Allee 23, 89081 Ulm, Germany. [2]Department of Trauma, University Hospital of Zurich, Zurich, Switzerland. [3]Department of Internal Medicine II-Cardiology, University of Ulm Medical Centre, Ulm, Germany. [4]Department of Surgical Research, University Hospital of Zurich, Zurich, Switzerland. [5]Department of Health Sciences, Translational Cardiovascular Technologies, Swiss Federal Institute of Technology, Zurich, Switzerland. [6]These authors contributed equally: Nikola Cesarovic and Miriam Kalbitz. ✉email: miriam.kalbitz@uniklinik-ulm.de

FELASA	Federation of European laboratory animal science association
FiO_2	Fraction of inspired oxygen
GV-SOLADES	Society of laboratory animal science
HFABP	Heart-type fatty acid binding protein
HFpEF	Heart failure with preserved ejection fraction
HR	Heart rate
H.E.	Haematoxylin and eosin
IL	Interleukin
ISS	Injury severity score
IVss/d	Intraventricular septal end systole/diastole
LVEDP	Left ventricular end diastolic pressure
LVOT/ RVOT VTI	Left/right ventricular outflow tract velocity time integral
LVP max/min	Max/min left ventricular pressure
MAP	Mean arterial pressure
MV desc time	Mitral desceleration time
SEM	Standard error of the mean
Systole.	Systolic blood pressure
TBI	Traumatic brain injury
TNF	Tumor necrosis factor
TnI	Troponin I
TOE	Transesophageal echocardiography
TTI	Tension-time index

In almost one third of multiple trauma patients hospitalization is due to chest trauma, which is responsible for 20–25% of multiple trauma related deaths[1]. Abnormal echocardiographic (ECHO) findings were detected in 31% of multiple trauma patients, which included 20% patients with ventricular wall motion abnormalities[2]. Therefore, ECHO plays an important role in emergency medicine as a non-invasive method that is universally available and allows therapeutic relevant decisions[3]. The indication for echocardiography after trauma is given in cases of hemodynamic instability, shock, chest trauma, as well as after cardiac arrest with cardiopulmonary resuscitation[3]. In trauma patients, arrhythmias, cardiac murmurs or ongoing hypotension alerts physicians to suspect a cardiovascular trauma, which potentially life-threatening[4–7]. Because of the anterior location of the heart in the thorax, the right ventricle (17–32%) and the atria (8–65%) are the most commonly injured parts of the heart in humans[8,9]. In pigs a reduction of the ejection fraction (EF) as well as an impaired shortening fraction was observed 1.5 h after multiple trauma, which was reported to be reversible after 24 h[10]. During thoracic trauma the heart is susceptible to compression within the bony structures of the thorax, whereas abdominal compression can lead to a rapid increase in blood flow to the heart, which could be responsible for a ventricular rupture, caused by the enormous increase of intracardial pressure[11,12]. Furthermore, after car accidents single case reports of severe valvular regurgitations, rupture of the anterolateral papillary muscle or atypical septum defects were described[13,14].

Because of the high quality of transesophageal ECHO (TOE) measurements[11], in the present study we used this investigation method to evaluate early myocardial damage (EMD) after multiple trauma in pigs. ECHO after trauma is feasible to detect cardiac contusion, because heart contusion is associated with oedematous changes of the myocardium, which lead to an increase of echogenity and thickness[15]. Additionally, injuries of the coronary vessels can be translated in regional wall motion abnormalities of the ventricle detectable by ECHO[15].

In case of blunt chest trauma, troponin I and T were reported as the featured indicator of cardiac damage[16]. Increased systemic troponin levels after multiple trauma in patients have been associated with high injury severity score (ISS), poor outcome and the necessity to administrate additional fluids as well as catecholamines[2,17]. In critically ill patients, elevated cardiac troponin T levels were associated with high in-hospital mortality but did not correlate with long-term survival[18]. Especially the combination of cardiac damage markers such as troponin or HFABP with ECHO findings might ensure an early detection of cardiac complications after trauma[19,20].

Therefore, the aim of this study was to conduct a detailed analysis of cardiac function after multiple trauma in pigs in combination with local and systemic detection of cardiac damage. We hypothesized that multiple trauma in pigs leads to EMD with systolic and diastolic cardiac dysfunction and impaired valvular function.

Results

In order to demonstrate hemodynamic alterations after multiple trauma in pigs, we analyzed the heart rate and the blood pressure after trauma over 6 h. The shock index was increased during the trauma period (Fig. 1) in both groups, whereas the conventional reaming group presented higher values of the shock index during the observation period. 1 h after trauma the shock index was significantly increased in both trauma groups compared to sham.

To describe early myocardial damage in detail, we analyzed parameters of the continuous blood pressure measurement. In the first 6 h after trauma, the contractility parameter dp/dt max as well as the dp/dt min were not influenced by multiple trauma (Fig. 2A,B). However, we measured a decrease of the left ventricular end diastolic pressure (LVEDP) in the combined multiple trauma group after 3 and 6 h (Fig. 2C). Subgroup analysis demonstrated differences in the left ventricular end diastolic pressure between conventional reaming and femoral nailing (Fig. 2D). To get a complete picture of the overall pressure relationships in the heart, we measured the maximal left ventricular pressure (LVPmax) as well as the minimal left ventricular pressure (LVPmin). In the combined multiple trauma group a reduction of the LVPmax was observed after 3 and 6 h (Fig. 2E). This

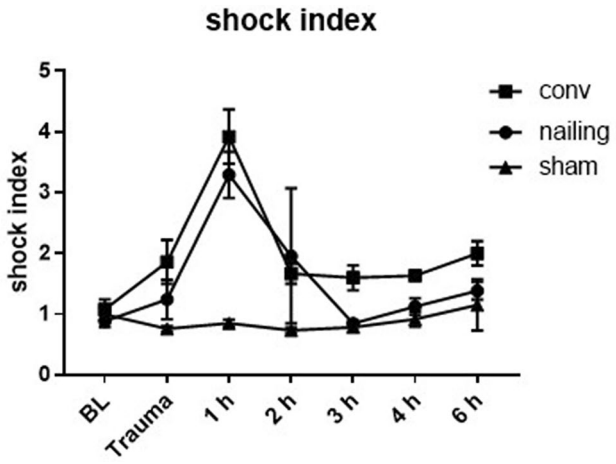

Figure 1. Shock index**.** Shock index calculated as heart rate/systolic blood pressure. Combined multiple trauma group n = 10, femoral nailing n = 5, conventional reaming n = 5, sham = 5. *p < 0.05.

observation was also made in the subgroup analysis of the femoral nailing group (Fig. 2F). LVPmin was not influenced by the multiple trauma with haemorrhage in all conducted groups (Fig. 2G). We did not observe changes in the left ventricular enddiastolic volume compared to baseline. (Fig. 2H), but a significantly reduced value 3 h after trauma compared to sham treated animals.

As standard parameters of systolic cardiac function we measured the cardiac output and the ejection fraction after multiple trauma by transoesophageal echocardiography. We did not detect changes in cardiac output the combined multiple trauma group (Fig. 3A). However, we found an increase of the contractility index 3 and 6 h after trauma in the multiple injured animals (Fig. 3B). As a parameter of diastolic dysfunction of the left ventricle, we measured the mitral valve deceleration time and detected a significant increase in the combined trauma group compared to baseline measurements (Fig. 3C). Baseline values and increased post-traumatic values were measured in the normal range of deceleration (140–240 ms). To determine the diastolic filling of the left ventricle over the mitral valve, we detected the E/A ratio after 3 and 6 h, but did not find any significant changes in the ratio of E wave to A wave (Fig. 3D.). LVOT- and RVOT-VTI were reduced after 6 h in the combined multiple trauma group (Fig. 3E,F). Subgroup analysis presented a reduction of the RVOT-VTI after 3 h in the multiple trauma animals with conventional reaming compared to baseline values (Fig. 3G). Additional ECHO measurements are presented in the supplemental Fig. 1 (Fig. S1).

Furthermore, we assessed the functionality of heart valves to detect potential insufficiencies or stenoses. The aortic valve did not show any functional impairment in the multiple trauma groups (Data not shown). The mitral valve presented an insufficiency grade 1 in 20% of the animals with conventional reaming 6 h after trauma (Fig. 4A). Furthermore, the tricuspid valve was impaired in 5/6 animals after trauma (Fig. 4B). 6 h after trauma the tricuspid valve was sustained impaired in 4/6 animals (Fig. 4B). Interestingly, a pulmonary valve insufficiency grade 1 was found in most of the multiple trauma animals at baseline. During the observation period, we have seen an aggravation of the pulmonary valve insufficiency. 6 h after multiple trauma 6/6 of the animals presented a grade 2 or 3 pulmonary insufficiency. (Fig. 4C). In Fig. 4D a representative image of pulmonary valve impairment measured by echocardiography is shown (Fig. 4D).

In order to determine early myocardial damage after multiple trauma in pigs, we developed a cardiac injury score to evaluate histomorphological changes in H.E. stained sections[21,22]. This score is presented in Fig. 5. There was an increase of histomorphological damage on the surface of the left ventricle (Fig. 5B), whereas an increase of the heart injury score in the luminal layer was only presented as a trend (Fig. 5C). In accordance with this observation we found a significant increase of the heart specific damage marker HFABP (Fig. 5C). Therefore, we assume cardiac injury after multiple trauma with haemorrhagic shock.

Discussion

For the first time to our knowledge, we conducted a detailed analysis of EMD by TOE, diverse blood pressure parameters and valvular function after multiple trauma in pigs. Our analysis of heart rate and blood pressure revealed a reduction of blood pressure while heart rate was increased reactively during haemorrhagic shock period. The shock index (SI), which was calculated as SI = HR/systolic blood pressure, is often described in literature as a valid predictor for mortality, as a useful tool for management of triage of patients with multiple trauma. Furthermore, SI has been described to correlate with the length of intensive care unit (ICU) stay, the days of invasive ventilation, the need for transfusion and the development of septic complications in humans[23–26]. Our results presented in Fig. 1 were in accordance with these manifold investigations of blood pressure and heart rate after trauma with a haemorrhagic component. Hence, our parameters seem valid criteria to evaluate the invasiveness of our multiple trauma model.

Systemic analysis of cardiac damage markers revealed an increase of HFABP which is known to be a very early marker for cardiac damage after myocardial infarction and after trauma[10]. Especially, in the combination

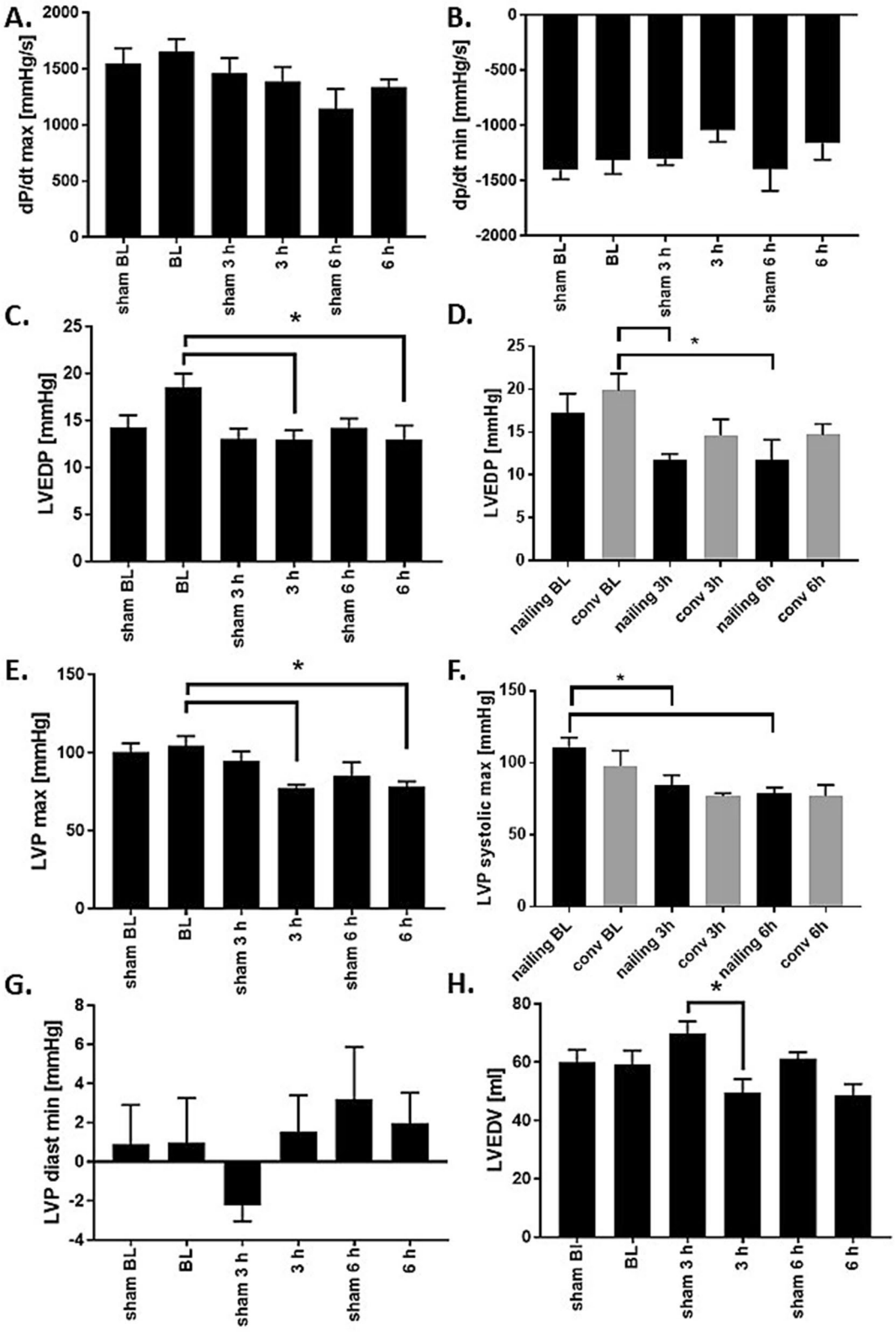
A.
dP/dt max [mmHg/s]
2000
1500
1000
500
0
sham BL
BL
sham 3 h
3 h
sham 6 h
6 h
B.
dp/dt min [mmHg/s]
0
-500
-1000
-1500
-2000
sham BL
BL
sham 3 h
3 h
sham 6 h
6 h
C.
LVEDP [mmHg]
25
20
15
10
5
0
*
sham BL
BL
sham 3 h
3 h
sham 6 h
6 h
D.
LVEDP [mmHg]
25
20
15
10
5
0
*
nailing BL
conv BL
nailing 3h
conv 3h
nailing 6h
conv 6h
E.
LVP max [mmHg]
150
100
50
0
*
sham BL
BL
sham 3 h
3 h
sham 6 h
6 h
F.
LVP systolic max [mmHg]
150
100
50
0
*
nailing BL
conv BL
nailing 3h
conv 3h
* nailing 6h
conv 6h
G.
LVP diast min [mmHg]
8
6
4
2
0
-2
-4
sham BL
BL
sham 3 h
3 h
sham 6 h
6 h
H.
LVEDV [ml]
80
60
40
20
0
sham Bl
BL
sham 3 h
3 h
sham 6 h
6 h

◂**Figure 2.** Cardiac function after multiple trauma—blood pressure. (**A**) dp/dt max in mmHg/s at baseline (BL), 3 and 6 h after multiple trauma (femur fracture, liver laceration, chest trauma and hemorrhagic shock) in pigs, presented as a combined trauma group consisting of femoral nailing and conventional reaming as treatment. (**B**) dp/dt min in mmHg/s at baseline (BL), 3 and 6 h after trauma in pigs. (**C**) Left ventricular end diastolic pressure (LVEDP) in mmHg at BL, 3 and 6 h after multiple trauma in pigs, $p^* < 0.05$ compared to baseline. (**D**) Subgroup analysis of left ventricular end diastolic pressure in mmHg in animals with femoral nailing (nailing, black) or conventional reaming (conv, gray) at BL, 3 h and 6 h after multiple trauma, $^*p > 0.05$ compared to baseline. (**E**) Maximal left ventricular pressure (LVP max) in mmHg at BL, 3 and 6 h after multiple trauma, $^*p < 0.05$. (**F**) Subgroup analysis of maximal left ventricular pressure (LVP max) in mmHg in animals with femoral nailing (nailing, black) or conventional reaming (conv, gray) at BL, 3 and 6 h after multiple trauma, $^*p > 0.05$ compared to baseline. (**G**) Minimal left ventricular pressure (LVP min) in mmHg at BL, 3 and 6 h after multiple trauma, $^*p < 0.05$. (**H**) Left ventricular enddiastolic volume in ml. Combined multiple trauma group n = 10, femoral nailing n = 5, conventional reaming n = 5, sham n = 5.

with ECHO measurements, the systemic increase of cardiac damage markers such as HFABP demonstrates EMD after trauma.

The present results are based on a broad analysis of cardiac functional impairment after trauma. One important consequence of cardiac injury, especially in case of direct mechanical impact on the chest, is the impairment of heart valves. The literature describes that traumatic rupture of the chordae tendineae leads to acute severe mitral regurgitation, in case of motor vehicle accidents[27]. Furthermore, different case reports described trauma associated with severe tricuspid regurgitation[28,29]. However, published case reports of traumatic valvular damage vary widely on observed symptoms: patients are described to be asymptomatic for years or become hemodynamic instable directly after trauma. Most of the reported patients developed symptoms within the first 7 days[30,31]. Valvular lesions resulted from high-energetic direct trauma on the chest such as car accidents or falls from great heights. The most likely mechanism is the sudden deceleration or compression of the blood column in the heart during the vulnerable phase of the cardiac cycle[30]. Pre-existing valvular diseases are associated with an increased risk of developing a valvular disorders after blunt chest trauma and penetrating thoracic trauma[32–35]. The most susceptible valves seem to be the atrioventricular ones[20,36]. Frequently in case of traumatic valvular dysfunction, there is a minimal initial valvular regurgitation, that might progress gradually, until cardiovascular surgery is necessary[1,37]. In contrast to atrioventricular valves, aortic valve regurgitation results from sudden increase in intrathoracic pressure against the closed valve and is associated in multiple trauma patients with a sternum or multiple rib fractures[20,38,39]. In contrast to the literature, in the present model of multiple trauma there was no evidence of any aortic valve participation. Traumatic valvular lesions and their consequences might be currently underestimated due to a wide variation of symptoms and the considerable diagnostic effort. In the present study, we observed mitral valve insufficiency in the pigs 6 h after multiple trauma and conventional reaming (Fig. 4A). Mitral valve injury typically manifested as pulmonary edema and hypotension[40]. Furthermore, we reported a high incidence of trauma-induced tricuspid impairment in Fig. 4B.

Tricuspid valve regurgitation was described as the most common cardiac complication after blunt chest trauma[41], with a rising incidence in the last decade, caused by improved diagnostic tools[42]. The common lesion is a subvalvular rupture of the anterior papillary muscle[43]. Causes of delayed tricuspid regurgitation are papillary muscle contusion (with hemorrhage), inflammation or necrosis[44]. Therefore, in future studies of chest trauma-related cardiac injuries papillary muscle biopsies should be taken into consideration.

Next to the alterations in valvular function after multiple trauma, we further observed changes in the diastolic function of the heart. Diastolic dysfunction can occur isolated without a compromise of the systolic function, which is called heart failure with preserved ejection fraction (HFpEF). Diastolic parameters, which are accessible by cardiac catheterization and echocardiography, are the left ventricular end diastolic pressure (LVEDP) and volume (LVEDV). It is considered as an important measurement of ventricular compliance, intravascular volume as well as pressure and further could help to identify patients with an increased risk of a clinical manifestation of heart failure[45]. This value is elevated (> 15 mmHg) in patients with coronary heart disease or myocardial ischemia[45,46]. Diastolic function measured by increased LVEDP is a parameter of asynchronous myocardial relaxation and therefore of cardiac stiffness[46]. In the present study, we observed a reduction of the LVEDP in the multiple trauma group compared to baseline (Fig. 2C). The fact that LVEDP decreased can be the result of hypovolemia as demonstrated by decreased LVEDV. Another factor that might point to this is the decrease of the diastolic blood pressure as presented in Fig. 1F. Furthermore, general decrease of LV pre-load caused by fusion of tricuspid and pulmonary valve regurgitation. Another parameter of diastolic function is the ratio between E and A wave as measured by TEE among the mitral valve. As presented in Fig. 3E, no changes in the E/A ratio occurred in the pigs with multiple trauma in the present observation period. We measured an increase of the mitral valve deceleration time (Fig. 3C), which is also associated with diastolic dysfunction in the literature. The E/A ratio is described to depend heavily on multiple interrelated factors and is therefore not useful for detect diastolic function without taking other parameters into account[46]. Diastolic dysfunction was shown to be promoted by cardiac macrophages and their increased production and release of IL-10[47]. An increase of cardiac macrophages after chest trauma has been detected previously[48].

In the present multiple trauma model, we failed to detect changes in cardiac output or ejection fraction in any of the investigated groups 6 h after multiple trauma. These results are in contrast to earlier transthoracic measurements after multiple trauma in pigs[10]. Measurement of cardiac output especially in hypovolemic conditions is time consuming and depends on the investigators experience[15]. Therefore, cardiac output does not seem to be the ideal parameter for cardiac function assessment after trauma. One limitation of the study is that it is rather difficult to ensure the use of TOE as a diagnostic procedure in multiple trauma in the emergency room

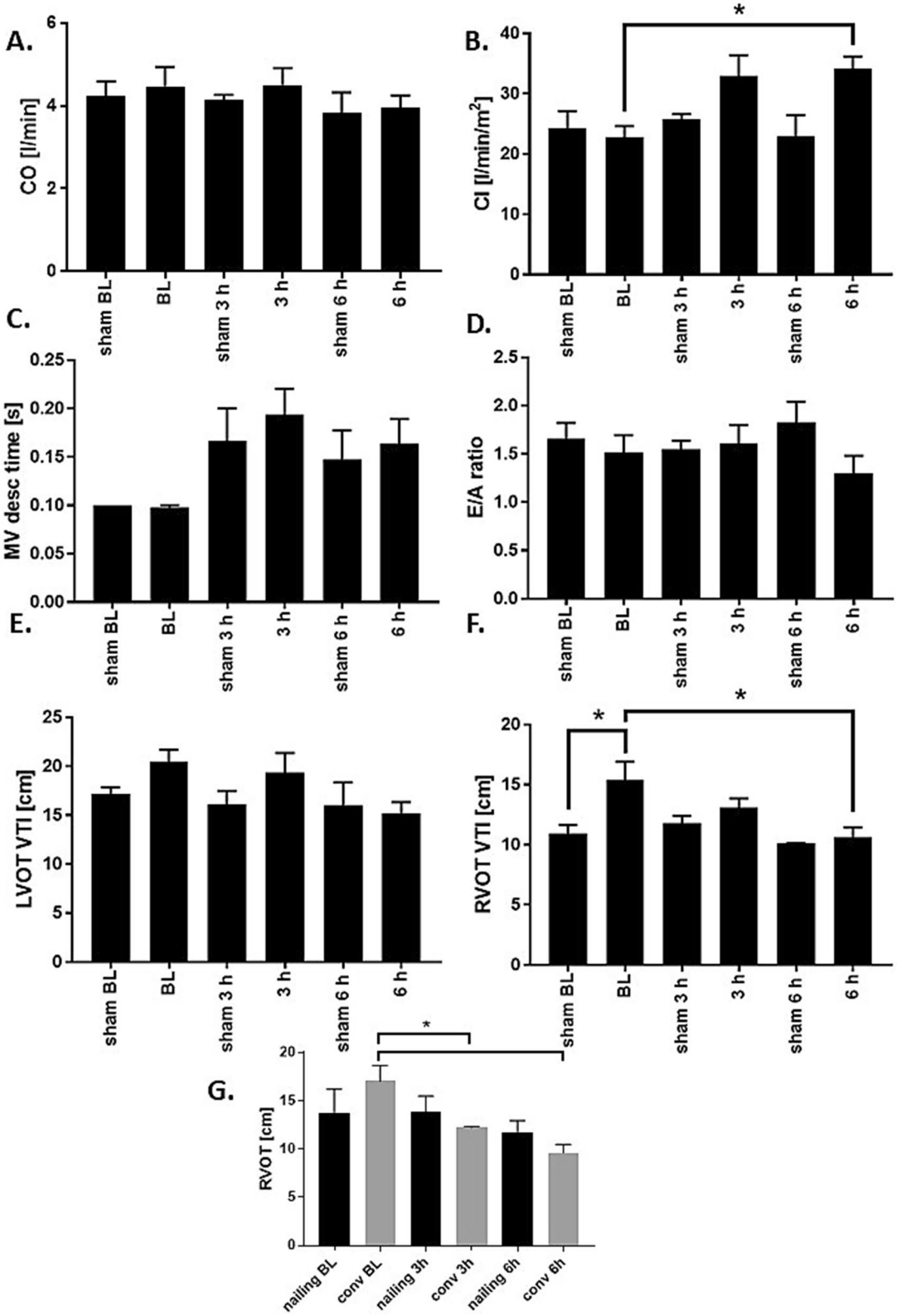
A.
CO [l/min]
B.
CI [l/min/m²]
C.
MV desc time [s]
D.
E/A ratio
E.
LVOT VTI [cm]
F.
RVOT VTI [cm]
G.
RVOT [cm]
sham BL
BL
sham 3 h
3 h
sham 6 h
6 h
nailing BL
conv BL
nailing 3h
conv 3h
nailing 6h
conv 6h
*

◂ **Figure 3.** Cardiac function—echocardiography—parameters. (**A**) Cardiac output (CO) in l/min at baseline (BL), 3 and 6 h after multiple trauma in pigs (femur fracture, liver laceration, chest trauma and hemorrhagic shock) presented as a combined trauma group containing femoral nailing and conventional reaming as therapeutic treatment. (**B**) Contractility index (CI) in l/min/m^2 measured at BL, 3 and 6 h after multiple trauma, *$p < 0.05$ compared to baseline. (**C**) Mitral valve deceleration time (MV desc time) in sec detected at BL, 3 and 6 h after trauma in pigs, *$p < 0.05$ compared to baseline. (**D**) Ratio of E wave and A wave (E/A) measured at BL, 3 and 6 h after multiple trauma with hemorrhagic shock. (**E**) Left ventricular tract velocity time integral (LVOT VTI) in cm at BL, 3 and 6 h after trauma, *$p = 0.06$ compared to baseline. (**F**) Right ventricular outflow tract velocity time integral (RVOT VTI) in cm measured at BL, 3 and 6 h after multiple trauma, *$p < 0.05$ compared to baseline. (**G**) Subgroup analysis of right ventricular outflow tract velocity time integral (RVOT VTI) in cm at BL, 3 and 6 h after trauma and either conventional reaming (conv, gray) or femoral nailing (nailing, black), * $p < 0.05$ compared to baseline. Combined multiple trauma group n = 10, femoral nailing n = 5, conventional reaming n = 5, sham n = 5.

(ER). Here, transthoracic echocardiography or ECG triggered CT are the more realistic methods to evaluate cardiac function. In the clinical setting TOE is more often used in order to access cardiac function additionally in anesthetized patients in the OR or for follow-up measurements on the intensive care unit.

In patients with previously diagnosed hypertension and left ventricular hypertrophy, traumatic bleeding can lead to dynamic obstruction of the left ventricular outflow tract[15]. In the present study we detected a reduction of the LVOT VTI 6 h after multiple trauma in pigs (Fig. 3F). A reduction of the LVOT VTI has been described as a predictor of heart failure and increased mortality[49]. LVOT VTI is a sensitive systolic marker low cardiac output, cardiogenic shock and impaired ability to keep up the systemic tissue perfusion and metabolic demands[49]. Additionally, a hyperdynamic left ventricle might also be a sign of traumatic hypovolemia. This condition is well-reported in cases of low peripheral resistance after sepsis or as expression of post-traumatic inflammation[50]. Furthermore, traumatic lesions far away from the thorax were to influence the systolic function of the heart: 22% of patients after a traumatic brain injury (TBI) developed systolic dysfunction, caused by a maladaptive catecholamine excess state[51].

Conclusion

Taken together, this study observed complex EMD and valvular impairment after multiple trauma in pigs as accessed by TOE. These results were accompanied by systemic release of the cardiac damage marker HFABP. Translating these findings into clinical medicine, detection of EMD and progressive valvular dysfunction might be crucial and therapeutically relevant and therefore may improve treatment of patients after multiple trauma.

Materials and methods

Animals. This study is a part of a large porcine multiple trauma project, which was conducted by the TREAT research consortium. This model and the animal experiments were described previously by Lackner et al.[52].

The animal housing and experimental protocols were approved by the Cantonal Veterinary Department, Zurich, Switzerland, under the licence number: ZH 138/2017 (approval for the study was given to the Department of Trauma, University Hospital of Zurich, Zurich, Switzerland). This study was conducted in in accordance with the Swiss Animal Protection Law. Housing and experimental procedures also conformed to European Directive 2010/63/EU of the European Parliament and of the Council on the Protection of Animals used for scientific purpose and to the Guide for the Care and Use of Laboratory Animals (Institute of Laboratory Animal Resources, National Research Council, National Academy of Sciences, 2011). We included 15 male pigs (Sus scrofa domestica) in the present study. The animals had a mean body length of 123.6 cm and a mean weighting of 50 ± 5 kg. Pigs underwent either multiple trauma (n = 10) or sham-procedure (n = 5). The pig model was described previously by Horst et al. [53]. The animals received a premedication with ketamine (20 mg/kg body weight), azaperone (1–2 mg/kg body weight) and atropine (0.1.0.2 mg/kg body weight) by intramuscular injection. Furthermore, the continuous anesthesia was performed by propofol infusion (1–2 mg/kg body weight). The anesthesia was maintained during the observation period of 6 h by continuous propofol application (5–10 mg/kg/h) furthermore as pain medication sufentanyl was given as perfusion over the whole experimental period (1 µg/kg/h).

Multiple trauma in pigs. The conducted, well-standardized multiple trauma model is defined by a penetrating chest trauma, a liver laceration, a haemorrhagic shock and a femur fracture. All in All, an Injury severity score (ISS) > 16 was guaranteed. Femur fracture was induced by a bolt gun (Blitz-Kernen, turbocut JOBB GmbH, Germany) loaded with cattle-killing cartridges (9 × 17; DynamitNobel AG, Troisdorf, Germany). The chest trauma was also induced by the shock wave of the bolt gun. Therefore, a pair of panels (0.8 cm, lead 1.0 cm thickness) was placed on the right dorsal lower chest as described previously[53,54]. The abdominal trauma was simulated by a penetrating hepatic injury, which was induced by cross-like incision halfway through the liver tissue. After a short period of uncontrolled bleeding (30 s), liver package was performed. The multiple trauma was completed by a pressure-controlled haemorrhagic shock (MAP of 25 ± 5 mmHg, max. 45% of total blood volume). After 60 min of shock, animals were resuscitated according to established trauma guidelines (ATLS, AWMF-S3 guideline on Treatment of Patients with Severe and Multiple Injuries) by adjusting FiO_2 and infusing additional fluids (Ringerfundin, 2 ml/kg body weight/h).

Sham procedure (n = 5) included instrumentation and anaesthesia without any trauma. We randomized the multiple trauma group in two therapy arms: pigs received either femoral nailing without reaming (n = 5) or standard reaming (n = 5). In both groups a shortened conventional tibia nail was introduced. The conventional reaming

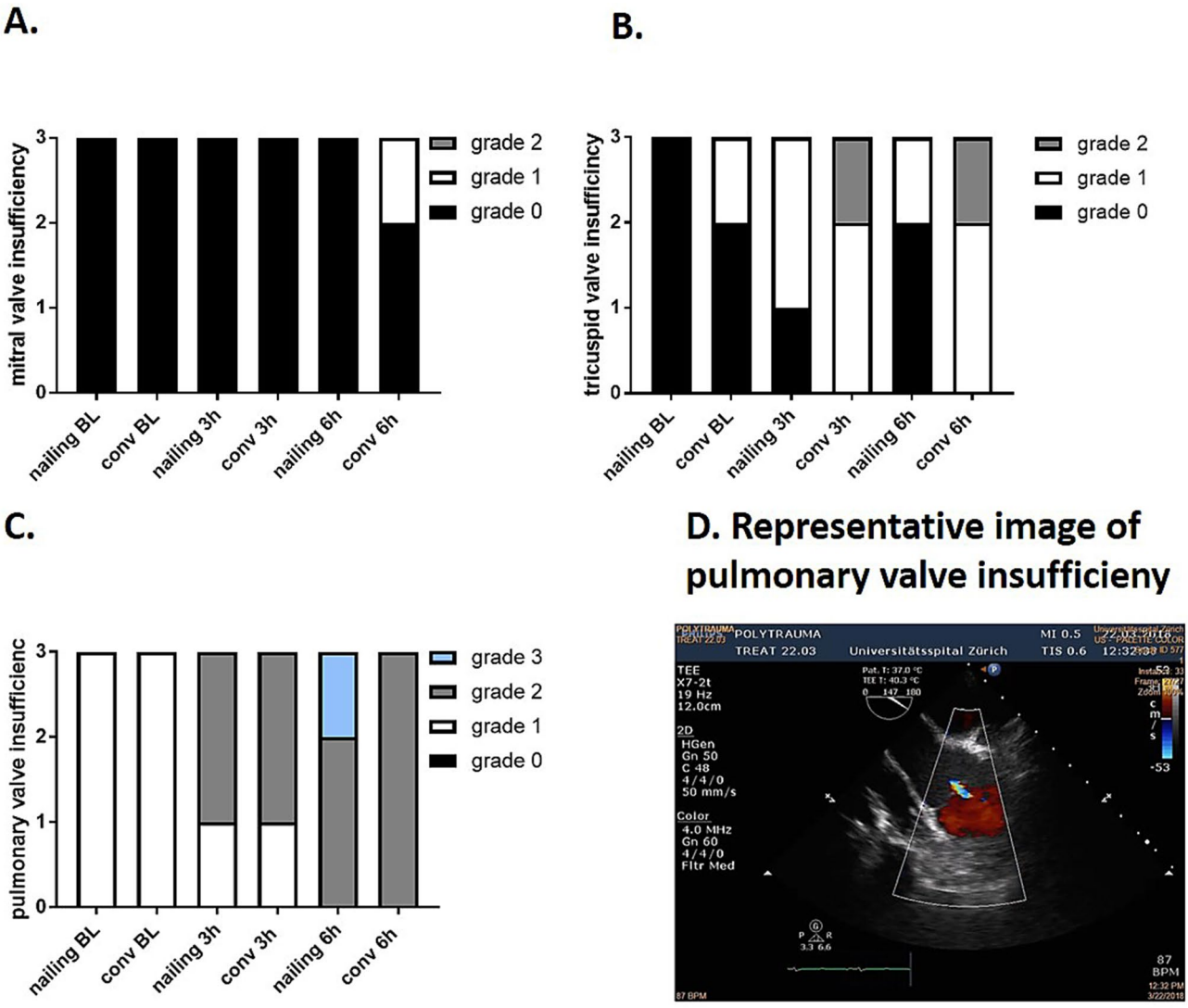

Figure 4. Heart valve insufficiency. (**A**) Subgroup analysis of mitral valve insufficiency at baseline (BL), 3 h and 6 h after multiple trauma (femur fracture, liver laceration, chest trauma and hemorrhagic shock) in pigs with either femoral nailing or conventional reaming as therapeutic treatment. (**B**) Subgroup analysis of tricuspid valve insufficiency in at BL, 3 and 6 h after trauma. (**C**) Subgroup analysis of pulmonary valve insufficiency determined at BL, 3 h and 6 h after trauma after femoral nailing and conventional reaming detected by transesophageal echocardiography. (**D**) Representative image of pulmonary valve insufficiency. Femoral nailing group n = 3, conventional reaming n = 3.

is conducted by a standard drill without irrigation and suction of the intramedullary contents. The present study contains data from both treatment groups summarized as a multiple trauma group, as well as subgroup analysis.

Hemodynamic parameters were continuously monitored for 6 h (DataScience International Ponemah V5.1 New Brighton, MN, US). At the end of the experiment, the animals were euthanized under deep, general anaesthesia by intravenous Na-Pentobarbital overdose. We collected serum and plasma samples at the following timepoints: baseline, 4 h and 6 h after trauma. After centrifugation (1500*g* for 12 min at 4 °C), serum and EDTA-plasma were removed and stored at − 80 °C. Tissue samples of the left ventricle were obtained 6 h after trauma. To ensure a detailed analysis, we separated the superficial and the luminal layers of the ventricle and fixed the tissue with 4% formalin, followed by embedding in paraffin. Moreover, tissue was quick-frozen in liquid nitrogen to further analyse gene expression by PCR. This animal experiment was also the base of the study, described by Lackner et al.[52].

Transesophageal echocardiography (TOE) in pigs. Imaging was performed according to the recommendations using a standard cardiac ultrasound machine (Cx50 xMATRIX, Phillips Healthcare, Germany with the X7-2t probe and the S5-1 ultrasound probe for additional transthoracic measurements). Serial imaging was performed before trauma, 3 and 6 h after trauma by an experienced investigator for echocardiography in pigs. The following parameters were measured: cardiac output (CO) in l/min, the ratio (A/E) of peak velocity blood

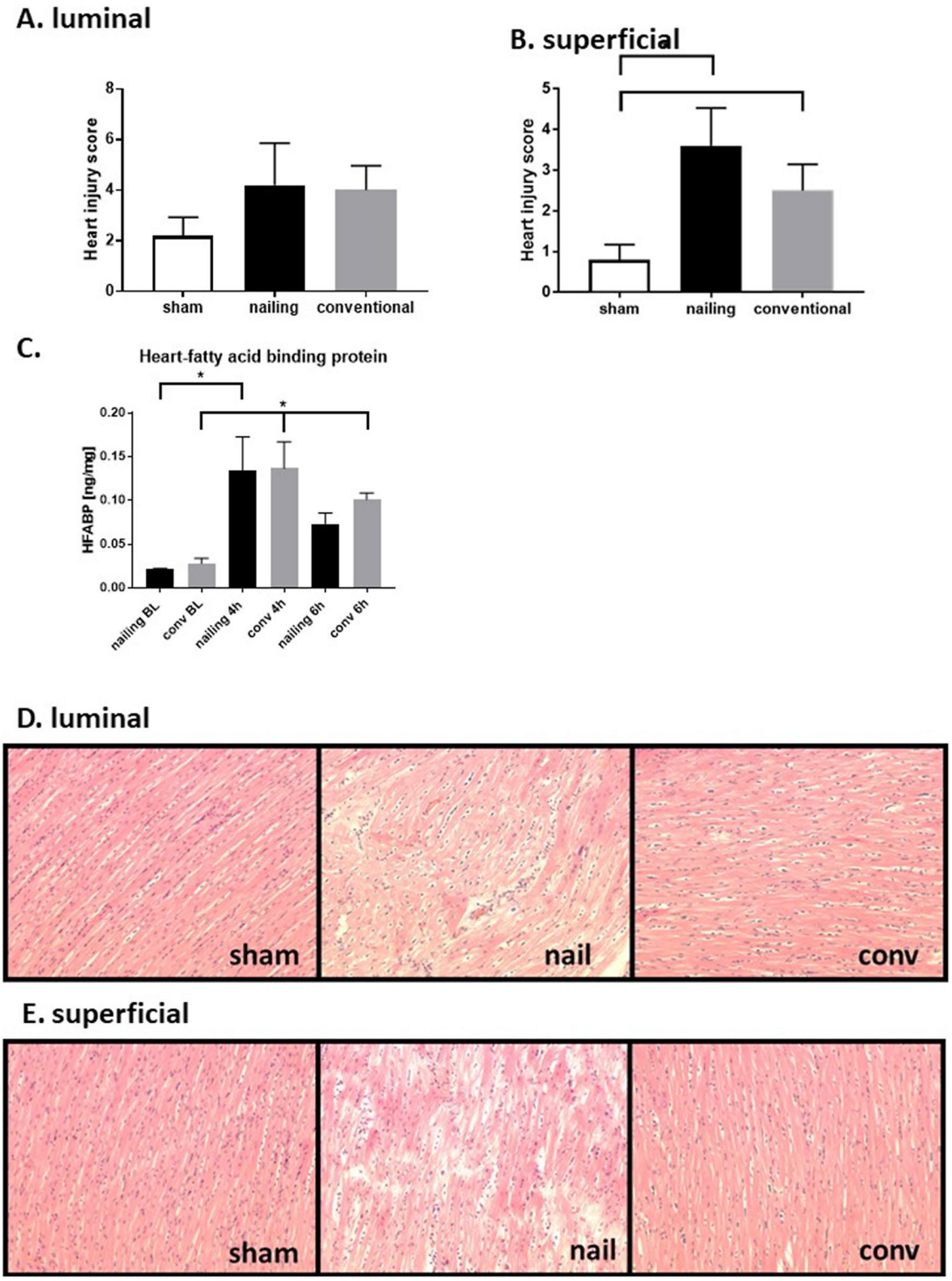

Figure 5. Cardiac damage after multiple trauma in pigs measured by echocardiography. (**A**,**B**) Heart injury score reflecting histomorphological sections of H.E. stained sections of the left ventricle 6 h after trauma, scored for apoptosis, contraction band necrosis, neutrophilic infiltration, intramuscular bleeding, rupture, edema and ischemia, *$p < 0.05$, $n = 5$ in each group compared to sham treated animals. (**C**) Heart-fatty acid binding protein (HFABP) in ng/ml detected in both subgroups at BL, 4 h and 6 h after multiple trauma. (**D**) Representative images of H.E: stained sections from the luminal left ventricle. (**E**) Representative Images of the superficial issue layers stained by H.E. *$p < 0.05$ compared to baseline, $n = 5$ in each group.

flow in early diastole (the E wave) to peak velocity flow in late diastole caused by atrial contraction (A wave), mitral deceleration time (MV desc time) in s, left ventricular outflow tract velocity time integral (LVOT VTI) in cm, right ventricular outflow tract velocity time integral (RVOT VTI) in cm, intraventricular septum thickness in end systole (IVSs) and end diastole (IVSd) in cm, right ventricular outflow tract diameter (RVOT diameter) in cm and left ventricular outflow tract diameter (LVOT diameter) in cm. Additionally, an experienced investigator evaluated the heart valve function by means of color Doppler echocardiography imaging. The observed insufficiencies were rated from grade 0 (no insufficiency) to grade 3 (massive insufficiency). We measured insufficiencies in the aortic, the pulmonary, mitral and tricuspid valve at Baseline, 3 h and 6 h after trauma.

In addition, we analyzed the continuously measured arterial blood pressure curves over 6 h and detected the following parameters: heart rate (HR) in beats per minute (bpm) (actually: pulse wave), arterial systolic and diastolic blood pressure and MAP in mmHg at baseline, trauma, 1, 2, 3, 4 and 6 h after trauma. Furthermore, at specific timepoints (BL, 3 h and 6 h) the following parameters were measured: left ventricular end-diastolic pressure (LVEDP) in mmHg, maximal left ventricular/systolic pressure (LVP max) in mmHg, minimal left ventricular/diastolic pressure (LVP min) in mmHg, contractility index (CI) in l/min/m^2, maximum positive value of the first derivative of the pressure that occurs during cardiac cycle (+ dp/dt max) in mmHg/s, maximum negative value of the first derivative of the pressure that occurs during the cardiac cycle (-dp/dt min) in mmHg/s and tension-time index (TTI = integration between the LVEDP point and -dp/dt max) by placing a pig tail catheter 5Fr.) in the left ventricle as previously published[55], the shock index during the observation period was calculated as heart rate/systolic pressure.

Heart-fatty acid binding protein (HFABP)-ELISA in pigs. Plasma samples were analyzed by using ELISA kits according to the manufacturer instructions. Heart fatty acid binding protein concentrations were detected by a pig cardiac fatty acid binding protein ELISA kit (life diagnostics, West Chester, PA, USA). We decided to use HFABP for systemic cardiac damage analysis instead of troponin, since HFABP is known to increase early after cardiac contusion.

Heart injury score. To evaluate the cardiac damage a fast H.E. staining-kit (Morphisto, Frankfurt am Main, Germany) was used to stain the left ventricle 6 h after trauma. To evaluate histomorphological changes, H.E. stained sections were scored for (1) apoptosis, (2) contraction band necrosis, (3) neutrophilic infiltration, (4) intramuscular bleeding, (5) rupture, (6) edema and (7) ischemia. This score was previously established by our working group[21,22]. For each animal, 4 fields of vision (magnification: 100 ×) were summarized in one mean score per section.

Statistical procedures. Mean values were analysed by one-way ANOVA followed Dunnett's or Tukey's multiple comparison test. Therefore, changes were defined as statistically significant with a $p \leq 0.05$. Statistical analysis and graphical presentation were conducted by using the GraphPad Prism 7.0 software (GraphPad Software, Incorporated, San Diego, CA, USA). The values were presented as mean ± SEM in all graphs.

Received: 21 October 2019; Accepted: 20 October 2020
Published online: 13 January 2021

References

1. Parmley, L. F., Manion, W. C. & Mattingly, T. W. Nonpenetrating traumatic injury of the heart. *Circulation* **18**, 371–396 (1958).
2. Karakus, A., Kekec, Z., Akcan, R. & Seydaoglu, G. The relationship of trauma severity and mortality with cardiac enzymes and cytokines at multiple trauma patients. *Turk. J. Trauma Emerg. Surg.* **18**, 289–295. https://doi.org/10.5505/tjtes.2012.81488 (2012).
3. Hagendorff, A. Echocardiography in emergency diagnostics. *Herz* **37**, 675–686. https://doi.org/10.1007/s00059-012-3646-5 (2012).
4. Saranteas, T. *et al.* Cardiovascular ultrasonography detection of embolic sources in trauma. *J. Crit. Care* **45**, 215–219. https://doi.org/10.1016/j.jcrc.2018.03.017 (2018).
5. Wolbrom, D. H., Rahman, A. & Tschabrunn, C. M. Mechanisms and clinical management of ventricular arrhythmias following blunt chest trauma. *Cardiol. Res. Pract.* **1**, 7270247. https://doi.org/10.1155/2016/7270247 (2016).
6. de Biasi, A. R., Seastedt, K. P., Eachempati, S. R. & Salemi, A. Common cause of mortality in trauma but manageable nonetheless. *Circulation* **132**, 537–545. https://doi.org/10.1161/CIRCULATIONAHA.115.016061 (2015).
7. Roy-Shapira, A., Levi, I. & Khoda, J. Sternal fractures: A red flag or a red herring?. *J. Trauma* **37**, 59–61 (1994).
8. Schultz, J. M. & Trunkey, D. D. Blunt cardiac injury. *Crit. Care Clin.* **20**, 57–70 (2004).
9. Mattox, K. L. *et al.* Blunt cardiac injury. *J. Trauma* **33**, 649–650 (1992).
10. Kalbitz, M. *et al.* Cardiac depression in pigs after multiple trauma: Characterization of posttraumatic structural and functional alterations. *Sci. Rep.* **7**, 17861. https://doi.org/10.1038/s41598-017-18088-1 (2017).
11. Chirillo, F. *et al.* Usefulness of transthoracic and transoesophageal echocardiography in recognition and management of cardiovascular injuries after blunt chest trauma. *Heart (British Cardiac Society)* **75**, 301–306 (1996).
12. Sybrandy, K. C., Cramer, M. J. M. & Burgersdijk, C. Diagnosing cardiac contusion: Old wisdom and new insights. *Heart (British Cardiac Society)* **89**, 485–489 (2003).
13. Hammerstingl, C., Nickenig, G., Weber, S. & Knuefermann, P. A "small" defect with malignant effect. *J. Am. Coll. Cardiol.* **58**, e23. https://doi.org/10.1016/j.jacc.2010.10.075 (2011).
14. Marras, E., Cukon-Buttignoni, S., Berton, G. & Tamari, W. Cardiac injury as a rare cause of cardiogenic shock following polytrauma. *Eur. Heart J.* **35**, 3231. https://doi.org/10.1093/eurheartj/ehu260 (2014).
15. Saranteas, T., Mavrogenis, A. F., Mandila, C., Poularas, J. & Panou, F. Ultrasound in cardiac trauma. *J. Crit. Care* **38**, 144–151. https://doi.org/10.1016/j.jcrc.2016.10.032 (2017).
16. Bertinchant, J. P. *et al.* Evaluation of incidence, clinical significance, and prognostic value of circulating cardiac troponin I and T elevation in hemodynamically stable patients with suspected myocardial contusion after blunt chest trauma. *J. Trauma* **48**, 924–931 (2000).

17. Kalbitz, M. *et al.* The role of troponin in blunt cardiac injury after multiple trauma in humans. *World J. Surg.* **41**, 162–169. https://doi.org/10.1007/s00268-016-3650-7 (2017).
18. Vasile, V. C., Chai, H.-S., Abdeldayem, D., Afessa, B. & Jaffe, A. S. Elevated cardiac troponin T levels in critically ill patients with sepsis. *Am. J. Med.* **126**, 1114–1121. https://doi.org/10.1016/j.amjmed.2013.06.029 (2013).
19. Korff, S., Katus, H. A. & Giannitsis, E. Differential diagnosis of elevated troponins. *Heart (British Cardiac Society)* **92**, 987–993. https://doi.org/10.1136/hrt.2005.071282 (2006).
20. Bock, J. S. & Benitez, R. M. Blunt cardiac injury. *Cardiol. Clin.* **30**, 545–555. https://doi.org/10.1016/j.ccl.2012.07.001 (2012).
21. Weber, B. *et al.* Tissue damage in the heart after cardiac arrest induced by asphyxia and hemorrhage in newborn pigs. *Pediatr. Res.* https://doi.org/10.1038/s41390-019-0505-6 (2019).
22. Braun, C. K. *et al.* Early structural changes of the heart after experimental polytrauma and hemorrhagic shock. *PLoS ONE* **12**, e0187327. https://doi.org/10.1371/journal.pone.0187327 (2017).
23. Toccaceli, A. *et al.* The role of shock index as a predictor of multiple-trauma patients' pathways. *Nurs. Crit. Care* **21**, e12–e19. https://doi.org/10.1111/nicc.12152 (2016).
24. Berger, T. *et al.* Shock index and early recognition of sepsis in the emergency department. Pilot study. *West. J. Emerg. Med.* **14**, 168–174. https://doi.org/10.5811/westjem.2012.8.11546 (2013).
25. Bruijns, S. R., Guly, H. R., Bouamra, O., Lecky, F. & Lee, W. A. The value of traditional vital signs, shock index, and age-based markers in predicting trauma mortality. *J. Trauma Acute Care Surg.* **74**, 1432–1437. https://doi.org/10.1097/TA.0b013e31829246c7 (2013).
26. McNab, A., Burns, B., Bhullar, I., Chesire, D. & Kerwin, A. A prehospital shock index for trauma correlates with measures of hospital resource use and mortality. *Surgery* **152**, 473–476. https://doi.org/10.1016/j.surg.2012.07.010 (2012).
27. Saric, P., Ravaee, B. D., Patel, T. R. & Hoit, B. D. Acute severe mitral regurgitation after blunt chest trauma. *Echocardiography* **35**, 272–274. https://doi.org/10.1111/echo.13775 (2018).
28. Hasdemir, H. *et al.* Severe tricuspid regurgitation and atrioventicular block caused by blunt thoracic trauma in an elderly woman. *J. Emerg. Med.* **43**, 445–447. https://doi.org/10.1016/j.jemermed.2010.05.069 (2012).
29. Tutun, U., Aksoyek, A., Parlar, A. I. & Cobanoglu, A. Post-traumatic tricuspid insufficiency: A case report. *TJTES* **17**, 563–566. https://doi.org/10.5505/tjtes.2011.02212 (2011).
30. Driessen, R., Doodeman, I., Bogaard, K. & Reichert, S. Contusio cordis, not an innocent diagnosis. *BMJ Case Rep.* https://doi.org/10.1136/bcr-2014-204139 (2014).
31. Li, W., Ni, Y., Chen, X. & Ma, L. Aortic valve tear with severe aortic regurgitation following blunt chest trauma. *J. Cardiothorac. Surg.* **6**, 84. https://doi.org/10.1186/1749-8090-6-84 (2011).
32. Yousaf, H., Ammar, K. A. & Tajik, A. J. Traumatic pulmonary valve injury following blunt chest trauma. *Eur. Heart J. Cardiovasc. Imaging* **16**, 1206. https://doi.org/10.1093/ehjci/jev193 (2015).
33. Kim, S. *et al.* Traumatic aortic regurgitation combined with descending aortic pseudoaneurysm secondary to blunt chest trauma. *Cardiovasc. J. Afr.* **25**, e5. https://doi.org/10.5830/CVJA-2014-039 (2014).
34. Pasquier, M., Sierro, C., Yersin, B., Delay, D. & Carron, P.-N. Traumatic mitral valve injury after blunt chest trauma: A case report and review of the literature. *J. Trauma* **68**, 243–246. https://doi.org/10.1097/TA.0b013e3181bb881e (2010).
35. Repossini, A. *et al.* Chest blunt trauma: An uncommon cause of aortic stentless bioprosthesis dysfunction. *Ann. Thorac. Surg.* **100**, 1094–1096. https://doi.org/10.1016/j.athoracsur.2014.11.014 (2015).
36. Simmers, T. A., Meijburg, H. W. & La Riviere, A. B. Traumatic papillary muscle rupture. *Ann. Thorac. Surg.* **72**, 257–259 (2001).
37. Rywik, T., Sitkowski, W., Cichocki, J., Rajecka, A. & Suwalski, K. Acute mitral regurgitation caused by penetrating chest injury. *J. Heart Valve Dis.* **4**, 293–295 (1995).
38. Pretre, R. & Faidutti, B. Surgical management of aortic valve injury after nonpenetrating trauma. *Ann. Thorac. Surg.* **56**, 1426–1431 (1993).
39. Parry, G. W. & Wilkinson, G. A. Traumatic aortic regurgitation. *Injury* **28**, 679–680 (1997).
40. Marcolini, E. G. & Keegan, J. Blunt cardiac injury. *Emerg. Med. Clin. North Am.* **33**, 519–527. https://doi.org/10.1016/j.emc.2015.04.003 (2015).
41. Schuster, I. *et al.* Heterogeneity of traumatic injury of the tricuspid valve: A report of four cases. *Wien. Klin. Wochenschr.* **120**, 499–503. https://doi.org/10.1007/s00508-008-1012-7 (2008).
42. Lin, S.-J. *et al.* Traumatic tricuspid insufficiency with chordae tendinae rupture: A case report and literature review. *Kaohsiung J. Med. Sci.* **22**, 626–629. https://doi.org/10.1016/S1607-551X(09)70363-8 (2006).
43. Richard, P., Vayre, F., Sabouret, P., Gandjbakhch, I. & Ollivier, J. P. Outcome of traumatic tricuspid insufficiency, treated surgically: Apropos of 9 cases. *Arch. Mal. Coeur Vaiss.* **90**, 451–456 (1997).
44. Banning, A. P. & Pillai, R. Non-penetrating cardiac and aortic trauma. *Heart (British Cardiac Society)* **78**, 226–229 (1997).
45. Mielniczuk, L. M. *et al.* Left ventricular end-diastolic pressure and risk of subsequent heart failure in patients following an acute myocardial infarction. *Congestive Heart Failure* **13**, 209–214 (2007).
46. Du, L.-J. *et al.* Association between left ventricular end-diastolic pressure and coronary artery disease as well as its extent and severity. *Int. J. Clin. Exp. Med.* **8**, 18673–18680 (2015).
47. Hulsmans, M. *et al.* Cardiac macrophages promote diastolic dysfunction. *J. Exp. Med.* **215**, 423–440. https://doi.org/10.1084/jem.20171274 (2018).
48. Kalbitz, M. *et al.* Experimental blunt chest trauma-induced myocardial inflammation and alteration of gap-junction protein connexin 43. *PLoS ONE* **12**, e0187270. https://doi.org/10.1371/journal.pone.0187270 (2017).
49. Tan, C. *et al.* Left ventricular outflow tract velocity time integral outperforms ejection fraction and Doppler-derived cardiac output for predicting outcomes in a select advanced heart failure cohort. *Cardiovasc. Ultrasound* **15**, 18. https://doi.org/10.1186/s12947-017-0109-4 (2017).
50. Armstrong, W. F. & Ryan T. *Feigenbaum's Echocardiography.* 7th ed. (2009).
51. Krishnamoorthy, V. *et al.* Association of early hemodynamic profile and the development of systolic dysfunction following traumatic brain injury. *Neurocrit. Care* **26**, 379–387. https://doi.org/10.1007/s12028-016-0335-x (2017).
52. Lackner, I. *et al.* Midkine is elevated after multiple trauma and acts directly on human cardiomyocytes by altering their functionality and metabolism. *Front. Immunol.* **10**, 1920. https://doi.org/10.3389/fimmu.2019.01920 (2019).
53. Horst, K. *et al.* Characterization of blunt chest trauma in a long-term porcine model of severe multiple trauma. *Sci. Rep.* **6**, 39659. https://doi.org/10.1038/srep39659 (2016).
54. Horst, K. *et al.* Local inflammation in fracture hematoma: Results from a combined trauma model in pigs. *Mediat. Inflamm.* https://doi.org/10.1155/2015/126060 (2015).
55. Leite-Moreira, A. F. *et al.* Diastolic tolerance to systolic pressures closely reflects systolic performance in patients with coronary heart disease. *Basic research in cardiology* **107,** 251. Doi: https://doi.org/10.1007/s00395-012-0251-y (2012).

Acknowledgements

We kindly acknowledge the TREAT research consortium. This work was conducted in the framework of the CRC 1149 funded by the Deutsche Forschungsgemeinschaft (DFG, German Research Foundation)—Project

number 251293561. This work was also funded by the AO Grant S-16-133T: effects of standard reaming an RIA techniques on local soft tissue and systemic homeostasis in a porcine trauma model.

Author contributions

B.W., I.L., M.B., S.H., M.T., M.L, N.C. performed the experiments including animal experiments, ECHO measurements and ELISAs. B.W., M.K., A.I. primarily wrote the paper. F.G, H.C.P, R.P., P.C., N.C. and M.K. contributed to experimental design and data analysis and coordinated the study and supervised financial support for the studies. All authors made substantial contributions to conception and design of the study and participated in drafting the article. All authors gave final approval of the version to be published. Please note that M.Kalbitz and N.Cesarovic were equally contributed last authors.

Funding

Open Access funding enabled and organized by Projekt DEAL.

Competing interests

The authors declare no competing interests.

Additional information

Supplementary information is available for this paper at https://doi.org/10.1038/s41598-020-80409-8.

Correspondence and requests for materials should be addressed to M.K.

Reprints and permissions information is available at www.nature.com/reprints.

Publisher's note Springer Nature remains neutral with regard to jurisdictional claims in published maps and institutional affiliations.

3. Discussion

3.1. Pigs are veritable models of human cardiac system – anatomical and fluid-dynamic considerations

Depending on the cardiovascular process being studied, the choice of the experimental model needs to be considered carefully since it affects experimental outcomes and whether findings of the study can be reasonably translated to humans. Some models like computational fluid-dynamics, organs-on-a-chip or even zebrafish are more suitable for answering fundamental questions of mechanical influences, the genetic background or molecular pathways underlying the specific disease. Furthermore, such models are exceptionally well suited for screening studies, where either a multitude of mechanical and/or environmental parameters can be investigated (like in computational models) or a whole palette of specific gene mutation can be individually assessed for their impact on cardiac health (like in many zebrafish studies).

The translational value of such models lays in the fact that they either present a small human population bearing a certain genetic defect or are actually using patient specific data (based on anatomical CT scans or physiological / hemodynamic measurements) to perform computation modelling. However, it is still challenging to extrapolate such experimental data to humans, as cardiac health conditions are rarely a sole result of a single gene malfunction, and cardiac morphology and function of zebrafish heart is quite distinct from that of a human (16, 20).

Moreover, computer systems of today are still struggling with precision and granularity necessary to perform multi-parametric calculations and predictions. Computational fluid dynamics, fluid-structure interactions and finite element analysis play an important role in the development of valvular replacement devices, where they are an important engineering tool used to advise implant design and suitable materials (45, 70). Recently developed systems are even capable of making predictions on patients specific tissue-implant interactions (71). Such computational simulations have swiftly found their way into the clinic and are used for procedural planning, displaying some benefits especially in patients with challenging or borderline-acceptable anatomy (72). However, due to the varying mechanical characteristics of multiple tissue types present in native valves, their complex anatomy and fluid dynamic environment constantly changing with every heartbeat, computer systems of today are still largely struggling with precisely modelling native cardiac structures (45).

On the other hand, small mammals (like rodents) display high similarity in cardiac anatomy compared to humans. Their valvular structures bare only discreet differences like smaller papillary muscles and thinner chords. Due to the abundance of genetically modified mouse strains, fully sequenced mouse genome and well-established experimental protocols, these little rodents have been the cornerstone

of understanding molecular pathways underlaying valvular disease development and progression in humans (25).

In order to study the hallmarks of advanced calcific aortic valve stenosis such as accumulation of amorphous or bone-like calcium and the excessive production and accrual of collagen and extracellular matrix proteins, mouse models of hypercholesterolemia have been the predominant model of choice (73). Once the disease pathways have been illuminated, mice have also been used to study the therapeutic effects of pharmacological agents aimed at reducing osteogenic and non-osteogenic calcification as well as inflammation and fibrosis of the aortic valve. Despite the fact that rodent heart beats approx. 10 times faster than human, that the aortic valve is only 1 mm in diameter and that the heart weights less than 1 gram, a vast variety of experimental techniques and non-invasive imaging modalities have been developed to support studies of valvular disease and to take advantage of the plethora of genetically modified or even humanized mouse strains. Taken together, mice will continue to contribute to our understanding of pathological processes and uncover molecular targets essential for future prevention and treatment of valvular disease. However, aside from a few experimental attempts, mice and other rodents are not suitable for the development of surgical nor interventional therapies.

Other models, such as large animal translational models, are designated to bridge the gap between the basic science and the sick patient in need of a device based treatment (implant or prosthesis). As a simple rule, the closer the heart or body weight of the animal model to human heart or body weight, the more similar are the hearts (74).

To bare the title of a translational model, a large animal experimental model needs to fulfil several criteria. Good availability, reasonable cost and socio-emotional acceptance are only a few factors that are generally considered when deciding on the animal species to be used in an academic project. However, many other factors need to be addressed depending on the specific area of research. In the field of heart valve research, anatomical, physiological and fluid-dynamic resemblance to human patients plays an immensely important role (35). From the past studies using explanted hearts and ex-vivo specimens, it was well known that porcine valve morphology as well as valvular tissue structure shows great similarities with its human counterparts (65).

The aortic valve, one of the best studied valves, displays a distinct 3-layer structure in both, humans and porcine. On the aortic side, the fibrosa layer is an arrangement of collagen sheets and large collagen fibre bundles. On the ventricular side, there is the thin ventricularis layer. Between these outer layers is the spongiosa, a layer rich in proteoglycans. Such layered structure represents an adaptation to the multiple functional requirements posed on the cardiac valves such as for frequent flexion cycle, durability, high shear compliance, and high resistance to pressure forces. As in humans,

porcine aortic valves even display similar heterogeneity in size and surface area of the leaflets, however not necessary in the same anatomical order as in pigs the right-coronary cusp appears to be the largest, slightly tilting the coaptation centre-point towards the non-coronary area (37). Nevertheless, the similarities are so pronounced that whole porcine valves have been extensively used for production of surgically implantable valvular prosthesis used in clinic (38).

However, in contrast to surgical implants, in developing of modern transcatheter valvular therapies not only the valvular prosthesis but also the delivery devices as well as deployment technique need to be tested (75). For an animal model to accommodate such procedures, anatomical and physiological similarities to humans need to go beyond the valvular constitution itself and to include the surrounding atrio-ventricular structures and great vessels. With porcine in-vivo computer tomography study of cardiac structures, presented in this manuscript, we could demonstrate that the anatomical landmarks important for valvular interventions bare great similarities with humans, and hence can allow the use of human-grade delivery systems and procedures, with certain limitations admittedly.

For example, height of the coronary artery ostia from the annular plane of the aortic valve in pigs is usually at the lower level of values that would be accepted in a case of a clinical TAVI procedure, indicating a higher risk of coronary artery occlusions and narrower landing zone in pigs compared to humans. Such information is essential to keep in mind when planning and evaluating results of novel aortic valve replacement devices, as some negative results (like occlusion of the right coronary artery) might be caused by the porcine specific anatomy rather than being an implant design-issue, per se.

On the other hand, the large, opened angle between the porcine mitral and aortic valve makes dynamic left ventricular outflow tract (LVOT) obstruction during transcatheter mitral valve replacements, a dreaded procedural complication in humans, much less likely to occur in pigs. Hence, in contrast to the aortic valve where device unrelated issues might hamper development, in testing of mitral valve replacement devices care needs to be taken not to over-estimate the safety of a particular device in regard to LVOT obstruction.

Another important anatomical aspect in transcatheter mitral valve interventions is the left atrium. Such devices are usually introduced via the femoral vein and can access the mitral valve only over a trans-septal route. Therefore, the final stage of the device navigation and delivery is happening in the left atrium, which needs to be large enough to accommodate for such manipulations. In patients suffering from the mitral valve disease, left atria are often markedly enlarged as a result of long-standing regurgitation. However, due to ethical issues as well as time and budget constraints, in animal trials almost as a rule healthy animals used. Hence, the size of the left atria appears to be an additional screening parameter that needs to be considered when choosing the animals for a particular study.

Further, in contrast to clinical use, in pre-clinical testing the animal needs to be selected to fit the size of the device as more often than not, only one implant size is available for testing. This fact renders proper subject selection vitally important for the success of a pre-clinical testing and development trials. As farm pigs are bred to quickly gain weight and develop muscle mass, during their development process the size of cardiac structures is not linearly following weight progression. It is a well-known fact that smaller, juvenile farm pigs have a cardiac weight / body weight index that is very similar to adult, non- obese humans (36).

However, as they grow, farm pigs tend to put on weight much faster than the growth of the cardiac muscle can follow. Hence, by the adulthood, the relative cardiac mass has decreased from 5gr/kg to just 2.3-2.9gr/kg of body weight. Thus, great care must be taken when choosing the weight category of the animals that should enter a trial, especially when limited choices of test-item sizes can be expected.

With our study we were able to demonstrate that pigs of 90 ± 5 kg provide the best match of diameters, perimeters and areas of all four heart valves in grown-up healthy humans. Furthermore, even though cardiac growth does not linearly correlate with the body weight of growing farm pigs, we could demonstrate that by knowing the weight of the animal the cardiac dimensions such as valvular size and diameter as well as aortic and pulmonary length could be predicted with a high level of accuracy. This finding will enable researchers to precisely select the animals suitable for their study, reducing the overall number of animals in a sense of the good reduce-replace-refine practice (3Rs).

On the other hand, it is not only the anatomy that renders pigs as a good translational model for valvular interventions. Cardiac valves are functioning in a complex fluid-dynamic environment that is determined by pressures, pressure gradients and flows constantly oscillating with every heartbeat. Despite such repetitive changes in the blood flow and pressures, cardiac valves experience fairly constant cyclical loads. Such loads are one of the predetermining factors of valvular prosthesis durability and are closely linked to the intra-cardiac blood flow patterns and pressure gradients. Hence, the component of fluid movement and behaviour in the atrias, ventricles and great vessels plays a significant role in translational suitability of a particular animal model.

By using clinical-grade magnetic resonance imaging, we were able to study the blood movement in the chambers of the porcine heart in detail. It was interesting to observe that blood flow patterns described in humans could readily be observed in pigs as well. Particularly important in development and treatment of valvular disease are diastolic vortices developing both at the sinuses of the aortic valve and within the ventricles.

Blood swirls (vortices) observed in the sinuses of the aortic valve play an important role in sinus-washout as well as in supplying the coronary arteries with fresh, non-stagnant blood. Furthermore, disturbance of such aortic vortices (as suggested with some aortic valve replacement implants) might be the contributing factor to early valve thrombosis (76). On the other hand, diastolic vortical ring appearing in the left ventricle has been attributed with kinetic energy preservation and smooth redirection of blood as in moves from the inflow to the outflow track (58). Moreover, healthy ventricular diastolic vortex plays an important role in timely closure of the mitral valve in early systole.

In our study, we could demonstrate that all fluid-dynamic structures showed very similar development, progression and resolution during the cardiac cycle between humans and pigs. Porcine, as human, diastolic vortex ring formed in early diastole and was markedly asymmetric with a larger cross-section formed behind the anterior mitral leaflet (i.e. in the left ventricular out-flow track). It reached its maximum cross-sectional size during late E wave however often resolved during the diastasis. Furthermore, in our study it could be shown that these flow structures remain stable even at higher hearts rates, although their form and size changes. Similar changes have also been observed in humans.

Taken together, the findings stated above provide scientific basis for the claims of porcine as a reliable and reproducible translational model for valvular disease and therapy development. Porcine cardiac dimensions are quite comparable with human and can accommodate most of the human-grade valvular implants and delivery devices, if the animals of appropriate size are chosen. Moreover, healthy porcine display intra-cardiac blood flow profile very similar to the one of healthy humans, providing human-like fluid-dynamic framework for valvular testing and development.

However, due to the lack of readily available disease models and subsequent anatomical changes, some procedures remain constrained by the anatomy of the healthy porcine hearts. Transseptal mitral procedures exemplify this issue as the catheter navigation is significantly impeded by the small height and volume of the healthy porcine left atrium.

3.2. Adaptation of Echocardiographic Imaging and Operative Procedures for the Use in Experimental Heart Valve Procedures

Development and testing of modern trans-catheter heart valve therapies goes beyond mere testing of the implant. Implant delivery devices as well as implantation procedures have become an integral part of the therapy and need to be developed together with the prosthesis itself. Transcatheter heart valve repair or replacement procedures usually are guided by cardiac ultrasound imaging (77). Imaging quality is one of the most important factors that determine safety and success of such procedures and

could sometimes be the limiting factor or even render patient untreatable. During development and testing of valvular implants and procedures, good imaging quality is of paramount importance not only to successfully guide the novel procedure but also to closely monitor the behaviour of the delivery system and implant device, hence provide input to engineering teams for further improvement. Although this imaging method is well established in humans, its application has some major challenges in pigs. We could demonstrate that clinical grade echocardiographic equipment could readily be used in pigs without any additional adaptations. Transesophageal ultrasound imaging (TEE) of the heart relies on close contact of the ultrasound probe lying in the oesophagus, with the cardiac structures. In humans, this is the case as oesophagus runs closely to the atria and the posterior face of the heart.

However, there are marked differences regarding intra-thoracal anatomy relevant for transesophageal ultrasound imaging (TEE) of the heart. Unlike humans, where thorax has ellipsoid cross section with esophagus running in close proximity to the heart, in most quadruped species (pigs included), thorax is rather triangular and the heart is positioned centrally in close contact with the sternum rather than the esophagus (65, 78).

Subsequently, echo-windows (i.e. place with good echocardiographic view of the heart) available for TEE are rather limited in pigs. Nonetheless, by adapting the imaging technique to the anatomical features, we were able to demonstrate that with TEE all heart structures relevant for valvular interventions can be reliably and reproducibly depicted in pigs. In contrast to the clinical use in humans, by strong ante- and left-flexion at the depth of approx. 55 cm from the snout, aortic mitral and tricuspid valve could be readily shown in both 2- and 3-dimensional fashion. By slight movements of the TEE probe and angles landmarks important for navigation of the transcatheter procedures, such as anterior/posterior leaflets and lateral/medial commissures of the mitral valve as well as sub-valvular apparatus, could be imaged in projections and quality that is comparable with clinic.

However, animal models will always remain exactly that: a comparable but not identical representation of humans. Some limitations could be overcome by simply adapting the technique of use, as case for TEE imaging demonstrates. Other might require changes of the animal's structure itself. The so called 'humanization' procedures as widely used in immunology and cancer research, where animals (mostly rodent) natural immune system is replaced with human derived cells (79). However, such approaches have not been widely used in large animal models.

For testing of novel transcatheter interventions of the mitral valve, the device is usually introduced via the femoral vein and can access the mitral valve only over a trans-septal route. Presence of a very sharp angle between the inferior vena-cava, atrial septum and the mitral valve in pigs, poses a huge challenge for the delivery devices developed for human use where access angles are much flatter. If not corrected, the sharp cavo-mitral angle puts tremendous strain on the devices, impedes their proper

function and can even lead to malfunction and failure. To overcome such anatomical limitations of domestic pigs, we developed a surgical procedure to create human-like anatomy necessary for successful deployment and testing of transcatheter mitral therapies.

By suturing a graft conduit at an oblique angle to the latero-posterior side of the right atrium at the confluence of inferior vena cava, a 'neo-cava' was created. This extra-anatomical vessel was not relevant for the blood flow, as still both native caval veins were open, and was solely used as an access point for the tested devices. Such approach made access to the intra-atrial septum and subsequently to the mitral valve possible at angles that closely mimic ones in humans. By using this technique, a human-grade mitral annuloplasty device could be successfully tested and further developed in pigs (80). Moreover, rate of successful procedures dramatically increased and procedural as well as fluoroscopy time decreased, demonstrating that 'humanization' of porcine models had strongly beneficial effects on experimental animal welfare (by decreasing the number of animals with unsuccessful procedure) and occupational health of the researchers by decreasing radiation exposure. Finally, transcatheter annuloplasty devices require great dexterity and precise navigation of their delivery systems in order to reach all target areas around the mitral valve. Hence, human-like anatomy of the access points and delivery trajectories are very important not only for development of such devices but also for physician training prior to entry in the clinical trial.

Based on these findings presented here, it can be concluded that trans-oesophageal echocardiography (TEE) provides a useful tool to assist testing of valvular procedures in pigs, providing data that could be reliably translated to clinical patients in the next stage of development. For guidance and navigation of transcatheter systems in pigs, standard clinical echocardiography equipment can be used, but the imaging protocols and handling needs to be adapted to echo windows available in porcine. However, for complex procedures requiring intricate navigation with human-grade devices sometimes surgical adaptations of porcine anatomy are needed to provide routes closely mimicking clinical patients. Further, one should not neglect the fact that novel valvular procedures at the stage of preclinical testing usually do not have standardized access, imaging and implantation protocols in place. Hence, we advocate that the development of procedure-specific imaging standards and treatment protocols should be considered an integral part of preclinical development of novel heart valve therapies.

3.3. Porcine Models of Mitral, Tricuspid and Aortic Valve Disease and Therapy

Apart from preclinical device testing and development, translational animal models are used for study of valvular diseases whose investigation would be cumbersome, inefficient or even unethical in clinical patients. This is particularly true in valvular disfunction following heart valve disease, as it is often a part of a complex disorder rather than being an isolated phenomenon by itself. It is usually accompanied or even caused by ischemic heart disease, hypertension or metabolic disorders. But sometimes it can suddenly occur following blunt chest trauma, as observed after car accidents of falls from height (67). Because of its position in the anterior thorax and proximity to the chest wall, right ventricular structures are the most commonly injured portion of the heart in chest trauma patients (68). In order to create a translational model that could closely reflect the complex interplay of blunt chest trauma and cardiac injury, it was important to recreate the direction of force vector across the heart in an animal species whose thorax wall had similar thickness and stiffens whereas abdominal organs similar weight and composition as in humans.

By redirecting the chest trauma force vector from antero-posterior (as usually occurring in car accidents) to latero-lateral one to account for the triangular shape of porcine thorax, blunt cardiac injury could reliably be reproduced. Factors indicating myocardial damage (such as heart-type fatty acid binding protein) and tricuspid valve regurgitation was readily observed. Surprisingly, valvular regurgitation worsened during the observation period, indicating a progressive disorder with cardiac injury as initiating event. Due to the fact that such injuries are relatively rare and, when occur, render patients critically ill and highly unstable, clinical studies of trauma associated valvular disfunction are exceptionally challenging. Translational animal models as described in our study are essential tools enabling investigations of such clinical complexes. Further, under laboratory setting a batch of animals could receive precisely titrated chest trauma and standardized response therapy. Hence, by using translational animal models, it is possible to timely produce data on number of individuals that in clinical setting of varying injury and therapy protocols would take multiple years or even decades to recruit.

Further, translational animal models are often used to provide standardization and narrow-down the variability when studying disease that occur in heterogenous manner and plethora of clinical presentations. This is especially true when looking for subtle changes, that display their deleterious effects on the patient's health only when summarized over longer periods of time. Such is the case when investigating fluid dynamic properties of aortic insufficiency and paravalvular leakage. Movement of the blood, its flow patterns and resulting energy loss are not only influenced by blood pressure differences across the valve at the time of investigation, but also by patient specific anatomy

of the left ventricle, position of the regurgitant orifice and current blood composition. Further, the changes are so discrete that could be studied only if the model is highly standardize and all parameters could be controlled and held within quite narrow margins.

Moreover, detailed investigations of blood flow require long MRI scanning sequences that are very sensitive to movement artifacts. Such procedures are often not well tolerated by patients suffering from heart valve disease. However, these goals are achievable with the proper use of an animal model. With our study we were able to demonstrate that, with proper methodology, aortic insufficiency jets that are clinically considered to be of minor importance actually have clear effects on left ventricular flow dynamics and display features (such as decreased diastolic vortex size and increased proportion of blood that is not ejected in the subsequent heart beat) and that are readily observed in serious heart disease with poor prognosis (81). Particularly interesting was the fact that, depending of the place of origin and trajectory within the left ventricle, aortic regurgitant and paravalvular leak jets had different impact to the fluid dynamic homeostasis of the heart. If confirmed in future studies, such findings could lead to re-evaluation of therapeutic strategies currently used for clinical treatment of AI and PVL.

Another area where large animal models play an important role is the development of novel transcatheter therapies for valvular heart disease. Nowadays, transcatheter aortic valve interventions are widely used in clinical practice world-wide. However, in treatment of mitral valve disease, there is still large need for development, improvement and testing of such devices. With their high degree of similarities to human anatomy and physiology, good availability and acceptable socio-emotional value (as demonstrated before), farm pigs are uniquely positioned to accommodate these experiments, as animal model (35).

Dimensions of the mitral valve area, septo-lateral and commissure-commissure distances as well as circumference of the posterior annulus in 90-100 kg pigs, closely resemble those in healthy adult humans. Hence, in recent years pigs have been extensively used for development of transcatheter mitral valve repair and replacement devices (40, 82, 83). However, there are some important differences between porcine and human anatomy relevant for such procedures. Many of these differences are the result of a quadruped compared with biped stance as well as the exclusively human feature of dorsoventrally compressed thorax, compared with the thorax of other mammals, which typically is laterally compressed (78). Consequently, the major cardiac axis of the porcine heart is tipped forwards, forms a steeper angle and makes the heart appear like it is hanging by its major vessels. Arising from this difference between the two species (pigs and humans), one important limitation was hampering translational development of trans-venous trans-septal mitral valve therapeutical approaches. That was the anatomical mismatch of cavo-mitral angles between pigs and humans, rendering the use of human-grade devices very challenging for trans-septal access in pigs.

By implementing a ‘pig model humanization’ step in the procedure, where an artificial vascular graft could be sutured to the right atrium and be used for device access, hence correcting the cavo-mitral angle from pig to human-like, reaching the mitral valve in transseptal manner was greatly facilitated. Once mastering the initial learning curve, such approach greatly increased successful testing of mitral annuloplasty device and their translation into clinical use (84).

4. Summary

Valvular disease and successful therapy is dependent on a complex interplay of metabolic, hemodynamic / fluid dynamic, neuro-hormonal and immunologic processes (Sutton 2000). In order to grasp the mechanism of a disease or evaluate novel therapies, biological systems are needed that are capable of mimicking this fascinating complexity. Due to the closely resembling anatomical landmarks of the valvular apparatus and ventricular cavities as well as intra-ventricular and intra-aortic fluid dynamic behavior of blood flow, farm pigs should be considered when there is a need for translational large animal model in the field of heart valve research. The use of 90-100 kg pigs enables usage of human grade devices as cardiac dimensions in this weight-class of animals closely resembles one of adult patients. Further, clinical-grade echocardiography imaging equipment with minimal adaptations of the application technique can be routinely used for TEE guidance of valvular procedures in experimental projects using this animal species. For navigationally challenging procedures, such as transseptal interventions on the mitral valve, porcine animal model could be humanized by relatively simple surgical intervention. Besides proving researchers with robust, human-like platform for valvular implant testing and development, porcine models provide exceptional value in investigations of diseases where clinical studies are either impractical, time consuming or unethical. Such being studies of cardiac injury in poly-trauma or precise hemodynamic effects of valvular regurgitation. In such studies, clinical grade medical equipment (such as standard CT and MRI machines and anesthesia equipment) can routinely be used and novel protocols developed and tested, which can then rapidly be adapted for human use, further closing the translation gap.

Finally, experience gathered during preclinical testing and learning curve achieved with translational animal models could and should be used to provide practitioners with a solid starting point when novel valve therapies finally find their way to clinical use. Yet, a certain translational gap still remains.

5. Outlook

In recent years translational research experienced strong bi-directional development. Not only that the clinical application of research results grew, also clinical input into animal modelling of heart valve disease rapidly progressed. Anatomical ‘humanization’ of large animal models stands at the very beginning of a process that aims at creating more precise models of human disease. Efforts to create readily attainable and affordable animal models of rapidly developing valvular stenosis and annular calcification for testing of valvular implants relying of radial force for anchoring, stand exemplary for this scientific process. Moreover, the use of novel intra-procedural imaging techniques such as 2D and 3D intra-cardiac echocardiography is finding it’s way into preclinical use and needs to be rapidly

adapted for application in large animals used for research purposes. It is our opinion that the future of translational heart valve research lies in close collaboration between researchers, clinicians engineers and veterinarians that are able to deeply understand each other needs and goal and not only translate preclinical information into patients benefits, but also clinical experience into improvement of animal experimentation.

6. Literature

1. Timmis A, Townsend N, Gale C, Grobbee R, Maniadakis N, Flather M, et al. European Society of Cardiology: Cardiovascular Disease Statistics 2017. Eur Heart J. 2018;39(7):508-79.
2. Maganti K, Rigolin VH, Sarano ME, Bonow RO. Valvular heart disease: diagnosis and management. Mayo Clin Proc. 2010;85(5):483-500.
3. Chen J, Li W, Xiang M. Burden of valvular heart disease, 1990-2017: Results from the Global Burden of Disease Study 2017. J Glob Health. 2020;10(2):020404.
4. Disease GBD, Injury I, Prevalence C. Global, regional, and national incidence, prevalence, and years lived with disability for 354 diseases and injuries for 195 countries and territories, 1990-2017: a systematic analysis for the Global Burden of Disease Study 2017. Lancet. 2018;392(10159):1789-858.
5. Nkomo VT, Gardin JM, Skelton TN, Gottdiener JS, Scott CG, Enriquez-Sarano M. Burden of valvular heart diseases: a population-based study. Lancet. 2006;368(9540):1005-11.
6. Misfeld M, Sievers HH. Heart valve macro- and microstructure. Philos Trans R Soc Lond B Biol Sci. 2007;362(1484):1421-36.
7. McCarthy KP, Ring L, Rana BS. Anatomy of the mitral valve: understanding the mitral valve complex in mitral regurgitation. Eur J Echocardiogr. 2010;11(10):I3-I9.
8. Adamczyk MM, Lee TC, Vesely I. Biaxial strain properties of elastase-digested porcine aortic valves. J Heart Valve Dis. 2000;9(3):445-53.
9. Mrsic Z, Hopkins SP, Antevil JL, Mullenix PS. Valvular Heart Disease. Prim Care. 2018;45(1):81-94.
10. Rahimtoola SH, Frye RL. Valvular heart disease. Circulation. 2000;102(20 Suppl 4):IV24-33.
11. Attia RQ, Raja SG. Surgical pericardial heart valves: 50 Years of evolution. Int J Surg. 2021;94.
12. Prendergast BD, Baumgartner H, Delgado V, Gerard O, Haude M, Himmelmann A, et al. Transcatheter heart valve interventions: where are we? Where are we going? European Heart Journal. 2019;40(5):422-40.
13. Roy D, Mazumder O, Sinha A, Khandelwal S. Multimodal cardiovascular model for hemodynamic analysis: Simulation study on mitral valve disorders. PLoS One. 2021;16(3):e0247921.
14. Verberkmoes NJ, Verberkmoes-Broeders EM. A novel low-fidelity simulator for both mitral valve and tricuspid valve surgery: the surgical skills trainer for classic open and minimally invasive techniques. Interact Cardiovasc Thorac Surg. 2013;16(2):97-101.
15. Kalogirou S, Malissovas N, Moro E, Argenton F, Stainier DY, Beis D. Intracardiac flow dynamics regulate atrioventricular valve morphogenesis. Cardiovasc Res. 2014;104(1):49-60.
16. Poon KL, Brand T. The zebrafish model system in cardiovascular research: A tiny fish with mighty prospects. Glob Cardiol Sci Pract. 2013;2013(1):9-28.
17. Beis D, Stainier DY. In vivo cell biology: following the zebrafish trend. Trends Cell Biol. 2006;16(2):105-12.
18. Hove JR, Koster RW, Forouhar AS, Acevedo-Bolton G, Fraser SE, Gharib M. Intracardiac fluid forces are an essential epigenetic factor for embryonic cardiogenesis. Nature. 2003;421(6919):172-7.
19. Bensimon-Brito A, Ramkumar S, Boezio GLM, Guenther S, Kuenne C, Helker CSM, et al. TGF-beta Signaling Promotes Tissue Formation during Cardiac Valve Regeneration in Adult Zebrafish. Dev Cell. 2020;52(1):9-20 e7.
20. Hu N, Clark EB, Yost HJ. Cardiac morphology and blood pressure in the adult zebrafish. Faseb J. 2001;15(5):A1231-A.
21. Postlethwait JH, Yan YL, Gates MA, Horne S, Amores A, Brownlie A, et al. Vertebrate genome evolution and the zebrafish gene map. Nat Genet. 1998;18(4):345-9.
22. Webb S, Brown NA, Anderson RH. The structure of the mouse heart in late fetal stages. Anat Embryol (Berl). 1996;194(1):37-47.
23. Papadimitriou D, Xanthos T, Dontas I, Lelovas P, Perrea D. The use of mice and rats as animal models for cardiopulmonary resuscitation research. Lab Anim-Uk. 2008;42(3):265-76.

24. Wessels A, Sedmera D. Developmental anatomy of the heart: a tale of mice and man. Physiol Genomics. 2003;15(3):165-76.
25. Cripps RM, Olson EN. Control of cardiac development by an evolutionarily conserved transcriptional network. Dev Biol. 2002;246(1):14-28.
26. Yoshioka M, Yuasa S, Matsumura K, Kimura K, Shiomi T, Kimura N, et al. Chondromodulin-I maintains cardiac valvular function by preventing angiogenesis. Nat Med. 2006;12(10):1151-9.
27. Dina C, Bouatia-Naji N, Tucker N, Delling FN, Toomer K, Durst R, et al. Genetic association analyses highlight biological pathways underlying mitral valve prolapse. Nat Genet. 2015;47(10):1206-+.
28. Weiss RM, Ohashi M, Miller JD, Young SG, Heistad DD. Calcific aortic valve stenosis in old hypercholesterolemic mice. Circulation. 2006;114(19):2065-9.
29. Phoon CK, Ji RP, Aristizabal O, Worrad DM, Zhou B, Baldwin HS, et al. Embryonic heart failure in NFATc1-/- mice: novel mechanistic insights from in utero ultrasound biomicroscopy. Circ Res. 2004;95(1):92-9.
30. Honda S, Miyamoto T, Watanabe T, Narumi T, Kadowaki S, Honda Y, et al. A novel mouse model of aortic valve stenosis induced by direct wire injury. Arterioscler Thromb Vasc Biol. 2014;34(2):270-8.
31. Ksiazek AA, Mitchell KJ, Cesarovic N, Schwarzwald CC, Hoerstrup SP, Weber B. PGA (polyglycolic acid)-P4HB (poly-4-hydroxybutyrate)-Based Bioengineered Valves in the Rat Aortic Circulation. J Heart Valve Dis. 2016;25(3):380-8.
32. Lee YU, Yi T, James I, Tara S, Stuber AJ, Shah KV, et al. Transplantation of Pulmonary Valve Using a Mouse Model of Heterotopic Heart Transplantation. Jove-J Vis Exp. 2014(89).
33. Gao S, Ho D, Vatner DE, Vatner SF. Echocardiography in Mice. Curr Protoc Mouse Biol. 2011;1:71-83.
34. Kusunose K, Penn MS, Zhang Y, Cheng Y, Thomas JD, Marwick TH, et al. How similar are the mice to men? Between-species comparison of left ventricular mechanics using strain imaging. PLoS One. 2012;7(6):e40061.
35. Kheradvar A, Zareian R, Kawauchi S, Goodwin RL, Rugonyi S. Animal Models for Heart Valve Research and Development. Drug Discov Today Dis Models. 2017;24:55-62.
36. Hughes HC. Swine in cardiovascular research. Lab Anim Sci. 1986;36(4):348-50.
37. Rock CA, Han L, Doehring TC. Complex collagen fiber and membrane morphologies of the whole porcine aortic valve. PLoS One. 2014;9(1):e86087.
38. David TE, Ropchan GC, Butany JW. Aortic valve replacement with stentless porcine bioprostheses. J Card Surg. 1988;3(4):501-5.
39. Bergmeister KD, Aman M, Kramer A, Schenck TL, Riedl O, Daeschler SC, et al. Simulating Surgical Skills in Animals: Systematic Review, Costs & Acceptance Analyses. Front Vet Sci. 2020;7:570852.
40. Sundermann SH, Gessat M, Cesarovic N, Frauenfelder T, Biaggi P, Bettex D, et al. Implantation of personalized, biocompatible mitral annuloplasty rings: feasibility study in an animal model. Interact Cardiovasc Thorac Surg. 2013;16(4):417-22.
41. Hasiwa N, Bailey J, Clausing P, Daneshian M, Eileraas M, Farkas S, et al. Critical Evaluation of the Use of Dogs in Biomedical Research and Testing in Europe. Altex-Altern Anim Ex. 2011;28(4):326-40.
42. Lopez-Perez A, Sebastian R, Ferrero JM. Three-dimensional cardiac computational modelling: methods, features and applications. Biomed Eng Online. 2015;14:35.
43. Mittal R, Seo JH, Vedula V, Choi YJ, Liu H, Huang HHW, et al. Computational modeling of cardiac hemodynamics: Current status and future outlook. J Comput Phys. 2016;305:1065-82.
44. de Tullio MD, Nam J, Pascazio G, Balaras E, Verzicco R. Computational prediction of mechanical hemolysis in aortic valved prostheses. Eur J Mech B-Fluid. 2012;35:47-53.
45. Sun W, Mao WB, Griffith BE. Computer modeling and simulation of heart valve function and intervention. Principles of Heart Valve Engineering. 2019:177-211.
46. Niederer SA, Lumens J, Trayanova NA. Computational models in cardiology. Nat Rev Cardiol. 2019;16(2):100-11.

47. Emmert MY, Schmitt BA, Loerakker S, Sanders B, Spriestersbach H, Fioretta ES, et al. Computational modeling guides tissue-engineered heart valve design for long-term in vivo performance in a translational sheep model. Sci Transl Med. 2018;10(440).
48. Jorba I, Mostert D, Hermans LHL, van der Pol A, Kurniawan NA, Bouten CVC. In Vitro Methods to Model Cardiac Mechanobiology in Health and Disease. Tissue Eng Part C-Me. 2021;27(3):139-51.
49. Filippo Buono M, von Boehmer L, Strang J, Hoerstrup SP, Emmert MY, Nugraha B. Human Cardiac Organoids for Modeling Genetic Cardiomyopathy. Cells. 2020;9(7).
50. Saini H, Navaei A, Van Putten A, Nikkhah M. 3D cardiac microtissues encapsulated with the co-culture of cardiomyocytes and cardiac fibroblasts. Adv Healthc Mater. 2015;4(13):1961-71.
51. Bohula May EA, Faxon D. Transcatheter aortic valve replacement: history and current status. Trends Cardiovasc Med. 2013;23(5):172-8.
52. Salenger R, Gammie JS, Collins JA. Minimally Invasive Aortic Valve Replacement. J Card Surg. 2016;31(1):38-50.
53. Koruth JS, Schneider C, Avitall B, Ribeiro L, Dukkipati S, Walcott GP, et al. Pre-Clinical Investigation of a Low-Intensity Collimated Ultrasound System for Pulmonary Vein Isolation in a Porcine Model. JACC Clin Electrophysiol. 2015;1(4):306-14.
54. Smerup M, Pedersen TF, Nyboe C, Funder JA, Christensen TD, Nielsen SL, et al. A long-term porcine model for evaluation of prosthetic heart valves. Heart Surg Forum. 2004;7(4):E259-E64.
55. Choo SJ, Kim KI, Park NH, Song JM, Choi IC, Shim JY, et al. Development of an animal experimental model for a bileaflet mechanical heart valve prosthesis. J Korean Med Sci. 2004;19(1):37-41.
56. Worlein JM, Baker K, Bloomsmith M, Coleman K, Koban TL. The Eighth Edition of the Guide for the Care and Use of Laboratory Animals (2011); Implications for Behavioral Management. Am J Primatol. 2011;73:98-.
57. Gharib M, Kremers D, Koochesfahani MM, Kemp M. Leonardo's vision of flow visualization. Exp Fluids. 2002;33(1):219-23.
58. Faludi R, Szulik M, D'hooge J, Herijgers P, Rademakers F, Pedrizzetti G, et al. Left ventricular flow patterns in healthy subjects and patients with prosthetic mitral valves: An in vivo study using echocardiographic particle image velocimetry. J Thorac Cardiov Sur. 2010;139(6):1501-10.
59. Akiyama K, Nakamura N, Itatani K, Naito Y, Kinoshita M, Shimizu M, et al. Flow-dynamics assessment of mitral-valve surgery by intraoperative vector flow mapping. Interact Cardiov Th. 2017;24(6):869-75.
60. Crandon S, Westenberg JJM, Swoboda PP, Fent GJ, Foley JRJ, Chew PG, et al. Impact of Age and Diastolic Function on Novel, 4D flow CMR Biomarkers of Left Ventricular Blood Flow Kinetic Energy. Sci Rep-Uk. 2018;8.
61. Mehrotra P, Labib SB, Schick EC. Differential Effects of Dobutamine Versus Treadmill Exercise on Left Ventricular Volume and Wall Stress. J Am Soc Echocardiog. 2012;25(8):911-8.
62. Gallegos RP, Nockel PJ, Rivard AL, Bianco RW. The current state of in-vivo pre-clinical animal models for heart valve evaluation. J Heart Valve Dis. 2005;14(3):423-32.
63. Lang RM, Bierig M, Devereux RB, Flachskampf FA, Foster E, Pellikka PA, et al. Recommendations for chamber quantification. Eur J Echocardiogr. 2006;7(2):79-108.
64. Evangelista A, Flachskampf FA, Erbel R, Antonini-Canterin F, Vlachopoulos C, Rocchi G, et al. Echocardiography in aortic diseases: EAE recommendations for clinical practice. Eur J Echocardiogr. 2010;11(8):645-58.
65. Crick SJ, Sheppard MN, Ho SY, Gepstein L, Anderson RH. Anatomy of the pig heart: comparisons with normal human cardiac structure. J Anat. 1998;193:105-19.
66. Karakus A, Kekec Z, Akcan R, Seydaoglu G. The relationship of trauma severity and mortality with cardiac enzymes and cytokines at multiple trauma patients. Ulus Travma Acil Cer. 2012;18(4):289-95.
67. de Biasi AR, Seastedt KP, Eachempati SR, Salemi A. Common Cause of Mortality in Trauma but Manageable Nonetheless. Circulation. 2015;132(6):537-45.
68. Schultz JM, Trunkey DD. Blunt cardiac injury. Crit Care Clin. 2004;20(1):57-70.

69. Marras E, Cukon-Buttignoni S, Berton G, Tamari W. Cardiac injury as a rare cause of cardiogenic shock following polytrauma. European Heart Journal. 2014;35(45):3231-.
70. Sun W, Martin C, Pham T. Computational modeling of cardiac valve function and intervention. Annu Rev Biomed Eng. 2014;16:53-76.
71. Han Y, Ribeiro JM, de Jaegere PPT, Zhang G. TAVR in a Patient With Quadricuspid Aortic Stenosis: The Role of Patient-Specific Computer Simulation in Treatment Planning and Outcome Prediction. JACC Cardiovasc Interv. 2021;14(9):e93-e5.
72. El Faquir N, De Backer O, Bosmans J, Rudolph T, Buzzatti N, Bieliauskas G, et al. Patient-Specific Computer Simulation in TAVR With the Self-Expanding Evolut R Valve. JACC Cardiovasc Interv. 2020;13(15):1803-12.
73. Cheek JD, Wirrig EE, Alfieri CM, James JF, Yutzey KE. Differential activation of valvulogenic, chondrogenic, and osteogenic pathways in mouse models of myxomatous and calcific aortic valve disease. J Mol Cell Cardiol. 2012;52(3):689-700.
74. Milani-Nejad N, Janssen PM. Small and large animal models in cardiac contraction research: advantages and disadvantages. Pharmacol Ther. 2014;141(3):235-49.
75. Taramasso M, Emmert MY, Reser D, Guidotti A, Cesarovic N, Campagnol M, et al. Pre-clinical In Vitro and In Vivo Models for Heart Valve Therapies. J Cardiovasc Transl Res. 2015;8(5):319-27.
76. Sengupta PP, Narula J. TAVR-Related Complications Why Did We Forget the Design of a Normal Aortic Valve? Jacc-Cardiovasc Imag. 2017;10(1):100-3.
77. Zamorano JL, Badano LP, Bruce C, Chan KL, Goncalves A, Hahn RT, et al. EAE/ASE recommendations for the use of echocardiography in new transcatheter interventions for valvular heart disease. European Heart Journal. 2011;32(17):2189-U145.
78. Lelovas PP, Kostomitsopoulos NG, Xanthos TT. A comparative anatomic and physiologic overview of the porcine heart. J Am Assoc Lab Anim Sci. 2014;53(5):432-8.
79. Shultz LD, Brehm MA, Garcia-Martinez JV, Greiner DL. Humanized mice for immune system investigation: progress, promise and challenges. Nat Rev Immunol. 2012;12(11):786-98.
80. Maisano F, Reser D, Pavicevic J, Guidotti A, Denti P, Taramasso M, et al. A translational "humanised" porcine model for transcatheter mitral valve interventions: the neo inferior vena cava approach. EuroIntervention. 2015;11(1):92-5.
81. Bolger AF, Heiberg E, Karlsson M, Wigstrom L, Engvall J, Sigfridsson A, et al. Transit of blood flow through the human left ventricle mapped by cardiovascular magnetic resonance. J Cardiovasc Magn Reson. 2007;9(5):741-7.
82. Ge Z, Pan W, Pan C, Zhou D, Li W, Wei L, et al. The Effect of a Novel Transcatheter Edge-to-Edge Mitral Valve Repair Device in a Porcine Model of Mitral Regurgitation. Acta Cardiol Sin. 2020;36(6):620-5.
83. Vu TD, Oo MZ, Nguyen DV, Ocampo EM, Ong Y, Cheyyatraivendran-Arularasu S, et al. Transapical cardioscopic mitral annuloplasty: a short-term survival study in a porcine model. Interact Cardiovasc Thorac Surg. 2018;26(1):131-8.
84. Taramasso M, Guidotti A, Cesarovic N, Denti P, Addis A, Candreva A, et al. Transcatheter direct mitral annuloplasty with Cardioband: feasibility and efficacy trial in an acute preclinical model. EuroIntervention. 2016;12(11):e1428-e34.

7. Acknowledgements

First and foremost, I would like to thank to Prof. Dr. med. Volkmar Falk, Medical Director of German Heart Center Berlin and Director of Department of Cardiothoracic and Vascular Surgery on his unwavering support and encouragement throughout my academic journey. I'm fortunate and extremely grateful for the opportunity to have him as my mentor and boss, first in Zurich, and then in Berlin. His guidance and expertise have been invaluable to me, and I'm deeply thankful for all his time and dedication he has put into helping me to successfully complete my postdoctoral thesis.

I would also like to thank to my mentor Prof. Dr. med. Maximilian Y. Emmert from Institute for Regenerative Medicine of the University of Zurich and Cardiosurgical Research at the Charite Berlin and the German Heart Center Berlin for providing guidance and insights throughout my work. I am grateful for his untiring support, and especially his careful attention to detail. With his help my postdoctoral thesis matured from multiple perspectives owing this particularly to his valuable knowledge and skills he has shared with me.

I wish to extend my special thanks to Dr. med. vet. Miriam Weisskopf, Head of Experimental OR Facilities at the University Hospital of Zurich. I am grateful for her willingness to impart her knowledge and to provide suggestions and advice throughout the various stages of completing and reaching this milestone. I must also thank to the whole team from Department of Experimental OR Facilities at the University Hospital of Zurich as well for their helpful suggestions and support during the research process.

Special thanks have to go to my colleagues and valued friends PD Dr. med. Simon Sündermann, PD Dr. med. Héctor Rodriguez, PD Dr. med. Markus Kofler and Dr. med. Timo Nazari for challenging and furthering my thinking through this entire process each in their own unique way. They have shown me what it means to work hard and to be committed entirely to a specific cause, which kept me motivated and inspired throughout my journey.

I'm thankful for and I would like to acknowledge many others who helped me along the way, too many to name individually, for moral support, help and kindness.

From the beginning of this journey up until its closure I had an ongoing support from Ursi Wacker. I owe a debt of gratitude for her enthusiasm and willingness always to go above and beyond. Together with the office team at German Heart Center Berlin, she has been instrumental in keeping my project running smoothly regarding all administrative and organizational matters.

Finally, I would like to thank my caring and patient family, my parents, and my wife Milica for their constant supply of positive encouragement and enthusiasm during this past intense several years. I am also deeply grateful to my daughter Draga and my son Mihailo. Their unconditional love and support have been my constant source of joy and main force to keep me going even when things were tough.

Erklärung

§ 4 Abs. 3 (k) der HabOMed der Charité

Hiermit erkläre ich, dass

- weder früher noch gleichzeitig ein Habilitationsverfahren durchgeführt oder angemeldet wurde,
- die vorgelegte Habilitationsschrift ohne fremde Hilfe verfasst, die beschriebenen Ergebnisse selbst gewonnen sowie die verwendeten Hilfsmittel, die Zusammenarbeit mit anderen Wissenschaftlern/Wissenschaftlerinnen und mit technischen Hilfskräften sowie die verwendete Literatur vollständig in der Habilitationsschrift angegeben wurden,
- mir die geltende Habilitationsordnung bekannt ist.

Ich erkläre ferner, dass mir die Satzung der Charité – Universitätsmedizin Berlin zur Sicherung Guter Wissenschaftlicher Praxis bekannt ist und ich mich zur Einhaltung dieser Satzung verpflichte.

06.01.2022 ……..

Datum Unterschrift